

## Star Forming Regions in Cepheus

Mária Kun

*Konkoly Observatory, H-1525 Budapest, P.O. Box 67, Hungary*

Zoltán T. Kiss

*Baja Astronomical Observatory, P.O. Box 766, H-6500 Baja, Hungary*

Zoltán Balog<sup>1</sup>

*Steward Observatory, University of Arizona, 933 N. Cherry Av., Tucson AZ  
85721, USA*

**Abstract.** The northern Milky Way in the constellation of Cepheus ( $100^\circ \leq l \leq 120^\circ$ ;  $0^\circ \leq b \leq 20^\circ$ ) contains several star forming regions. The molecular clouds of the Cepheus Flare region at  $b > 10^\circ$ , are sites of low and intermediate mass star formation located between 200 and 450 pc from the Sun. Three nearby OB associations, Cep OB2, Cep OB3, Cep OB4, located at 600–800 pc, are each involved in forming stars, like the well known high mass star forming region S 140 at 900 pc. The reflection nebula NGC 7129 around 1 kpc harbors young, compact clusters of low and intermediate mass stars. The giant star forming complex NGC 7538 and the young open cluster NGC 7380, associated with the Perseus arm, are located at  $d > 2$  kpc.

### 1. Overview

In this chapter we describe the star forming regions of the constellation of Cepheus. A large scale map of the constellation, with the boundaries defined by IAU overlaid, and the most prominent star forming regions indicated, is shown in Fig. 1. This huge area of the sky, stretching between the Galactic latitudes of about  $0^\circ$  and  $+30^\circ$ , contains several giant star forming molecular cloud complexes located at various distances from the Sun. According to their distance they can be ranged into three large groups:

- (1) Clouds nearer than 500 pc located mainly at  $b \geq 10^\circ$ , in the Cepheus Flare.
- (2) Three OB associations, Cep OB 2, Cep OB 3 and Cep OB 4 between 600–900 pc.
- (3) Star forming regions associated with the Perseus spiral arm at 2–3 kpc.

In the following we discuss the first two of these groups.

Fig. 2 shows the distribution of dark clouds perpendicular to the Galactic plane (Dobashi et al. 2005), with the outlines of the major star forming complexes overplotted.

The large-scale  $^{13}\text{CO}$  observations performed by Yonekura et al. (1997) led to a refinement of division of the clouds into complexes. The groups listed in Table 2,

---

<sup>1</sup>on leave from Dept. of Optics and Quantum Electronics, University of Szeged, Dóm tér 9, Szeged, H-6720, Hungary

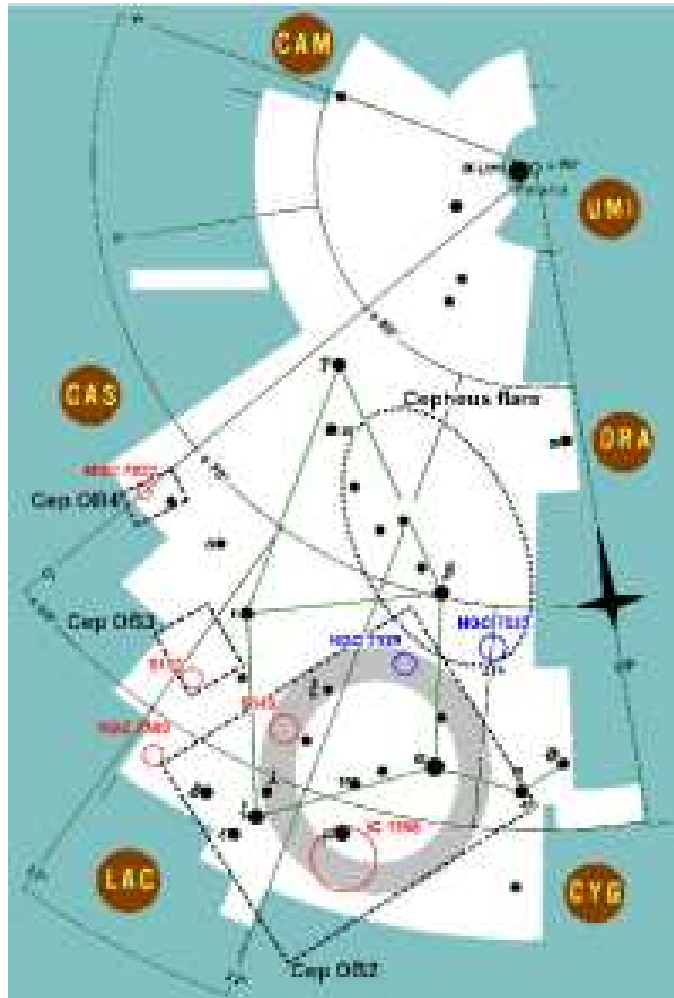


Figure 1. Positions of the major star forming regions of Cepheus, overplotted on a schematic drawing of the constellation.

adopted from Yonekura et al. (1997), were defined on the basis of their positions, radial velocities, and distances, where distance data were available.

Table 1 lists the dark clouds identified in the Cepheus region from Barnard (1927) to the Tokyo Gakugei University (TGU) Survey (Dobashi et al. 2005), and the molecular clouds, mostly revealed by the millimeter emission by various isotopes of the carbon monoxide (Dobashi et al. 1994; Yonekura et al. 1997). The cloud name in the first column is the LDN (Lynds 1962) name where it exists, otherwise the first appearance of the cloud in the literature. Equatorial (J2000) and Galactic coordinates are listed in columns (2)–(5), and the area of the cloud in square degrees in column (6). Column (7) shows the radial velocity of the cloud with respect to the Local Standard of Rest. The number of associated young stellar objects is given in column (8), and the alternative names, following the system of designations by *SIMBAD*, are listed in column (9). We

note that the LDN coordinates, derived from visual examination of the POSS plates, may be uncertain in several cases.

Figure 3 shows the distribution of the pre-main sequence stars and candidates over the whole Cepheus region.

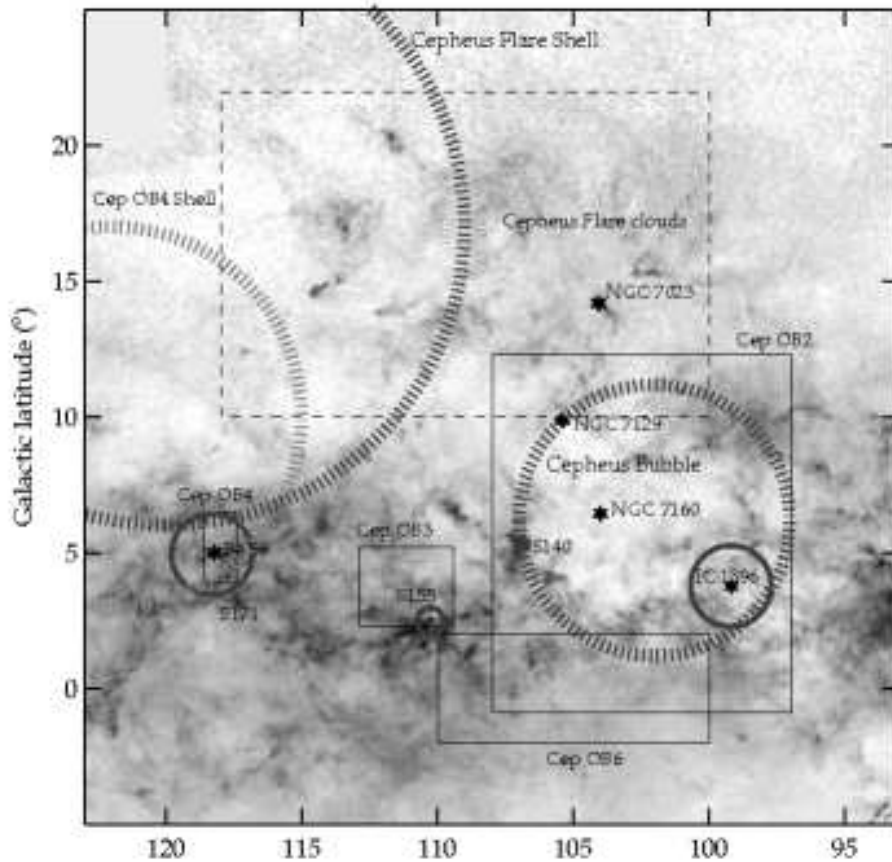


Figure 2. Distribution of the visual extinction in the Cepheus region in the  $[l, b]$  plane (Dobashi et al. 2005) with outlines of the major star forming regions, discussed in this chapter, overplotted. Solid rectangles indicate the nominal boundaries of the OB associations (Humphreys 1978; de Zeeuw et al. 1999), and the dashed rectangle shows the Cepheus Flare cloud complex; giant HII regions are marked by solid grey circles, and star symbols indicate young open clusters. Three large circles, drawn by radial dashes, show giant shell-like structures in the interstellar medium. The Cepheus Flare Shell (Olano et al. 2006) belongs to the nearby Cepheus Flare complex, and the Cepheus Bubble (Kun et al. 1987) is associated with the association Cep OB2, and the Cepheus OB4 Shell (Olano et al. 2006) is associated with Cep OB4.

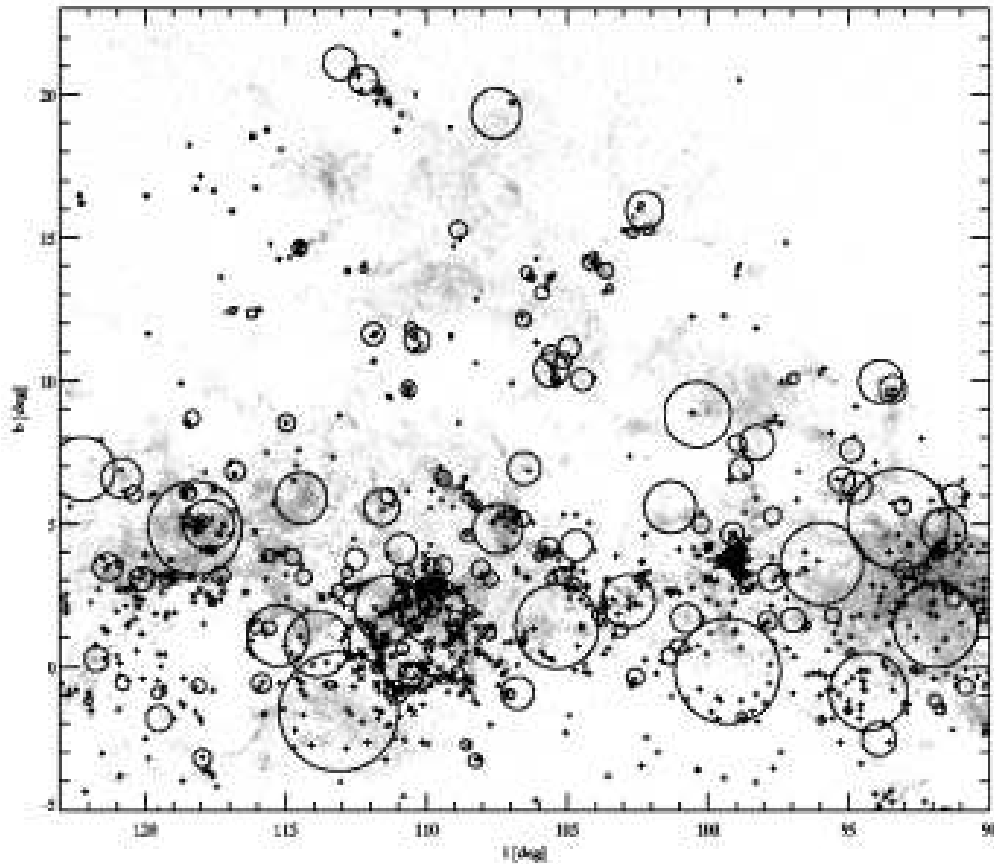


Figure 3. Pre-main sequence stars and candidates in the Cepheus region overlaid on the map of visual extinction obtained from 2MASS data based on interstellar reddening using the NICER method (Lombardi & Alves 2001). Large circles denote those clouds from Table 1 which have been associated with young stars. The meaning of different symbols are as follows: Filled triangles - T Tauri stars; Filled squares - Herbig Ae/Be stars; Filled circles - Weak-line T Tauri stars; Diamonds - Tr 37 ROSAT X-ray sources; Open triangles - PMS members of Tr 37; Open squares - Candidate and possible PMS members of Cep OB3b; X -  $H\alpha$  emission stars; + - T Tauri candidates selected from a 2MASS color-color diagram.

Table 1.: List of clouds catalogued in Cepheus.

Cloud name	RA(2000) (h m)	Dec(2000) ( $^{\circ}$ $'$ )	l ( $^{\circ}$ )	b ( $^{\circ}$ )	Area (sq.deg.)	$v_{LSR}$ ( $\text{km s}^{-1}$ )	$n_{star}$	Alternative names
LDN 1122	20 32.7	+65 20.3	99.97	+14.81	0.041	4.8	0	YMD CO 1, TGU 597
LDN 1089	20 32.8	+63 30.3	98.40	+13.78	0.244	-2.4	0	TDS 366, TGU 586
LDN 1094	20 32.8	+64 00.3	98.83	+14.06	0.002	0.1	1	CB 222
TGU 667	20 33.9	+73 51.6	107.53	+19.33	2.460		1	[KTK2006] G107.1+19.3, [KTK2006] G107.5+19.8, [KTK2006] G107.9+18.9
LDN 1152	20 34.4	+68 00.4	102.37	+16.14	0.025	2.9	0	YMD CO 8
CB 223	20 34.7	+64 10.7	99.10	+13.98	0.003	-2.7	0	
LDN 1100	20 34.8	+64 00.4	98.96	+13.88	0.007	-2.7	1	CB 224
LDN 1033	20 37.2	+57 10.5	93.44	+9.69	0.714	-2.4	0	TDS 343, TDS 345, TDS 346, TGU 549, DBY 093.1+09.6, DBY 093.5+09.4
LDN 1036	20 38.2	+57 10.6	93.52	+9.58	0.088	-2.1	1	DBY 093.5+09.4
LDN 1041	20 38.2	+57 30.6	93.79	+9.78	0.022	-2.1	0	DBY 093.5+09.4
LDN 1157	20 39.5	+68 00.7	102.65	+15.75	0.005	2.9	1	[DE95] LDN 1157 A1, YMD CO 8, TGU 619
LDN 1147	20 40.5	+67 20.8	102.14	+15.29	0.127	2.9	0	YMD CO 8, TDS 379, TGU 619, JWT Core 36, [LM99] 340, [BM89] 1-99, [LM99] 344
LDN 1148	20 40.5	+67 20.8	102.14	+15.29	0.015	2.9	1	YMD CO 8, TGU 619
LDN 1044	20 41.2	+57 20.8	93.90	+9.35	0.006	-2.1	0	DBY 093.5+09.4
LDN 1049	20 42.2	+57 30.8	94.12	+9.35	0.005	0.6	0	DBY 094.1+09.4
LDN 1039	20 42.3	+56 50.8	93.58	+8.94	0.079	-2.1	0	DBY 093.5+09.4
LDN 1051	20 42.7	+57 30.9	94.16	+9.29	0.010	0.6	0	DBY 094.1+09.4
LDN 1155	20 43.5	+67 40.9	102.60	+15.25	0.006	2.9	0	YMD CO 8, TGU 619
LDN 1158	20 44.5	+67 41.0	102.66	+15.17	0.111	0.9	0	TDS 388, [BM89] 1-100, [LM99] 346, TGU 619 [BM89] 1-102, [BM89] 1-103, [LM99] 348 [BM89] 1-104, DBY 093.5+09.4
LDN 1038	20 46.3	+56 21.0	93.53	+8.20	0.660	-2.1	0	DBY 096.8+10.2
LDN 1076	20 49.3	+59 51.2	96.57	+10.04	0.008	-2.2	0	
LDN 1082	20 51.1	+60 11.3	96.98	+10.07	0.111	-2.6	8	Barnard 150, GF 9, TDS 362, [LM99] 350, DBY 097.1+10.1, [BM89] 1-105, [LM99] 351
LDN 1171	20 53.5	+68 19.5	103.71	+14.88	0.002	3.4	0	CB 229
LDN 1037	20 54.4	+55 26.5	93.53	+6.75	0.591		0	TGU 551
LDN 1168	20 56.6	+67 36.6	103.31	+14.21	0.003		0	

Table 1.: Continued.

Cloud name	RA(2000) (h m)	Dec(2000) ( $^{\circ}$ $'$ )	l ( $^{\circ}$ )	b ( $^{\circ}$ )	Area (sq.deg.)	$v_{\text{LSR}}$ ( $\text{km s}^{-1}$ )	$n_{\text{star}}$	Alternative names
LDN 1061	20 58.3	+57 21.7	95.36	+7.56	0.618	-2.1	0	DBY 095.2+07.4, DBY 095.2+07.4
LDN 1071	20 58.3	+58 11.7	96.00	+8.10	0.092	-0.4	0	Barnard 354, DBY 096.0+08.1, TGU 569
LDN 1056	20 58.4	+56 01.7	94.35	+6.69	0.036		0	
TGU 730	20 58.8	+78 11.8	112.23	+20.50	0.803	-8.0	3	[BM89] 1-108, [BM89] 1-109, [B77] 48, [BM89] 1-112, GN 21.00.4, RNO 129
LDN 1228	20 59.0	+77 31.8	111.67	+20.10	0.086	-7.6	4	YMD CO 66, MBM 162, TGU 718
LDN 1170	21 01.7	+67 36.9	103.63	+13.84	0.215	2.8	0	TDS 392, TGU 629, GSH 093+07+9 [LM99] 359, [LM99] 361
LDN 1058	21 02.4	+56 01.9	94.72	+6.27	0.869	-1.1	1	TDS 354, TGU 558
LDN 1174	21 02.6	+68 11.9	104.15	+14.14	0.294	2.8	$\gtrsim 15$	TDS 393, [LM99] 358, [BM89] 1-110, [B77] 39, [BM89] 1-113, [LM99] 360, [BM89] 1-114, [BM89] 3B- 9, [BM89] 1-111, PP 100, [BM89] 1-115 Ced 187, GN 21.01.0, YMD CO 14
LDN 1172	21 02.7	+67 41.9	103.76	+13.82	0.010	2.7	$\gtrsim 4$	YMD CO 14, TGU 629
LDN 1167	21 03.7	+67 02.0	103.30	+13.32	0.062	2.8	0	YMD CO 11
LDN 1173	21 04.7	+67 42.0	103.88	+13.67	0.006	2.7	0	YMD CO 14
LDN 1068	21 06.3	+57 07.1	95.89	+6.59	0.027	0.2	0	Barnard 359, DBY 095.9+06.6, TGU 570
LDN 1063	21 07.4	+56 22.2	95.44	+5.97	0.025	0.3	0	Barnard 151, Barnard 360, DBY 095.5+06.5, TGU 561
LDN 1065	21 07.4	+56 32.2	95.56	+6.09	0.023	0.3	0	DBY 095.5+06.5, TGU 568
LDN 1069	21 08.4	+56 52.2	95.90	+6.21	0.018	0.3	0	DBY 095.5+06.5
LDN 1067	21 09.4	+56 42.3	95.87	+6.00	0.012	0.3	0	DBY 095.5+06.5, TGU 568
Sh 2-129	21 11.3	+59 42.3	98.26	+7.84	1.190	3.7	2	DBY 097.3+08.5, BFS 9
LDN 1060	21 11.5	+55 17.4	95.02	+4.82	0.031	-0.9	0	DBY 090.5+02.4
LDN 1119	21 13.2	+61 42.4	99.91	+9.03	0.010	2.5	0	DBY 100.1+09.3, TGU 598
LDN 1062	21 13.5	+55 32.4	95.40	+4.79	0.003	-0.9	0	DBY 090.5+02.4
LDN 1064	21 13.5	+55 37.4	95.46	+4.85	0.001	-0.9	0	DBY 090.5+02.4
LDN 1125	21 14.7	+61 42.5	100.04	+8.90	0.010	2.5	1	Barnard 152, TDS 376, [LM99] 365, DBY 100.1+09.3, TGU 598
LDN 1072	21 16.5	+56 12.6	96.18	+4.95	1.510	-0.6	0	Barnard 153, TDS 358, TGU 574, DBY 096.3+05.2
LDN 1177	21 18.8	+68 15.7	105.22	+13.06	0.005	2.9	2	CB 230, TGU 641

Table 1.: Continued.

Cloud name	RA(2000) (h m)	Dec(2000) ( $^{\circ}$ $'$ )	l ( $^{\circ}$ )	b ( $^{\circ}$ )	Area (sq.deg.)	$v_{\text{LSR}}$ ( $\text{km s}^{-1}$ )	$n_{\text{star}}$	Alternative names
TGU 589	21 19.7	+59 27.7	98.83	+6.90	0.560		2	
LDN 1162	21 20.0	+65 02.8	102.92	+10.76	0.004		0	
LDN 1080	21 21.5	+56 32.8	96.91	+4.69	0.001		0	Barnard 154
YMD CO 23	21 22.2	+69 22.6	106.27	+13.60	0.056	-9.4	2	TGU 656
LDN 1108	21 26.4	+59 33.1	99.49	+6.37	0.046		0	
DBY 098.4+05.2	21 26.8	+57 55.9	98.40	+5.17	0.107	1.0	0	
LDN 1086	21 28.5	+57 33.2	98.30	+4.74	0.095	-4.6	18	DBY 098.8+04.2, TGU 584, [PGS95] 2, IC 1396 W, FSE 1
LDN 1176	21 31.0	+66 43.3	104.93	+11.15	0.446	-10.4	0	YMD CO 17, TGU 634, JWT Core 44, GAL 104.9+11.2
LDN 1145	21 31.3	+62 43.3	102.14	+8.24	0.183		0	TGU 622, [PGH98b] Cloud 11
LDN 1146	21 31.3	+62 43.3	102.14	+8.24	0.183		0	
LDN 1096	21 31.5	+58 03.3	98.93	+4.83	0.001		0	TGU 590
LDN 1102	21 32.5	+58 03.3	99.03	+4.74	0.008		0	
LDN 1085	21 33.3	+56 44.6	98.23	+3.69	0.010	3.4	0	WWC 156
LDN 1093	21 33.5	+57 38.4	98.85	+4.34	0.034	-4.6	20	DBY 098.8+04.2, TGU 587, FSE 3 [PGS95] 8
LDN 1083	21 33.6	+55 58.0	97.72	+3.11	0.761	8.7		WCC 178-179
LDN 1098	21 34.5	+57 38.0	98.95	+4.25	0.025	-4.6	20	DBY 098.8+04.2, FSE 3
Barnard 365	21 34.9	+56 43.0	98.36	+3.53	0.010	7.6		WWC 140
TGU 639	21 35.5	+66 32.0	105.13	+10.70	0.280		1	[KTK2006] G105.0+10.7
LDN 1087	21 35.6	+56 33.5	98.32	+3.35	0.013	7.4	2	TDS 364
LDN 1090	21 35.6	+56 43.5	98.43	+3.48	0.028		0	Barnard 365
LDN 1199	21 35.9	+68 33.5	106.57	+12.15	0.235	-11.5	1	TDS 398, TGU 653 [KTK2006] G106.4+12.0, [KTK2006] G106.7+12.3
LDN 1099	21 36.5	+57 23.5	98.98	+3.88	0.008	-8.0	22	DBY 099.1+04.0, FSE 5
LDN 1116	21 36.5	+58 33.5	99.76	+4.75	0.034		3	[IS94] 7, [PGS95] 16, [IS94] 14, SFO 35, [G85] 5, [PGS95] 17, [PGS95] 19, FSE 6
LDN 1105	21 37.1	+57 33.5	99.15	+3.95	0.008	-8.0	22	TDS 369, [B77] 37, DBY 099.1+04.0, FSE 5
YMD CO 19	21 37.3	+67 01.2	105.60	+10.93	0.279	-10.2	1	TGU 642, [KTK2006] G105.5+10.8, [KTK2006] G105.7+10.8
LDN 1092	21 37.6	+56 58.5	98.81	+3.48	0.014		1	

Table 1.: Continued.

∞

Cloud name	RA(2000) (h m)	Dec(2000) ( $^{\circ}$ $'$ )	l ( $^{\circ}$ )	b ( $^{\circ}$ )	Area (sq.deg.)	$v_{\text{LSR}}$ ( $\text{km s}^{-1}$ )	$n_{\text{star}}$	Alternative names
LDN 1112	21 38.5	+58 03.6	99.63	+4.20	0.013	-0.3	0	DBY 099.7+04.1
LDN 1117	21 38.5	+58 18.6	99.79	+4.39	0.004	-0.7	0	WWC 114-116
LDN 1088	21 38.6	+56 13.6	98.41	+2.83	0.019	7.2	2	Barnard 160, TGU 585, DBY 098.4+02.9
LDN 1135	21 39.4	+60 38.6	101.44	+6.06	0.054		0	
LDN 1110	21 39.5	+57 53.6	99.62	+3.99	0.007	-0.3	2	DBY 099.7+04.1
LDN 1111	21 39.5	+57 53.6	99.62	+3.99	0.002	-0.3	2	Barnard 161, DBY 099.7+04.1, CB 233
LDN 1123	21 39.5	+58 28.6	100.00	+4.43	0.003		0	
LDN 1126	21 39.5	+58 33.6	100.06	+4.49	0.006		0	
LDN 1101	21 39.6	+56 58.6	99.01	+3.30	0.095		0	
LDN 1131	21 40.0	+59 33.7	100.77	+5.20	0.046	-0.4	0	Barnard 366, TDS 378, DBY 100.9+05.3, TGU 609
LDN 1140	21 40.4	+60 53.7	101.70	+6.16	0.240		0	
LDN 1121	21 40.5	+58 16.7	99.97	+4.19	0.008	-0.2	$\gtrsim 25$	DBY 100.0+04.2, [IS94] 5, [G85] 14, [LM99] 379, [IS94] 17, IC 1396 N, SFO 38, [PGS95] 24, FSE 19, TGU 599
CB 234	21 40.5	+70 18.6	108.09	+13.15	0.044	-5.0	0	
LDN 1127	21 40.9	+58 33.7	100.20	+4.37	0.004		0	TGU 599
TDS 395	21 40.9	+66 35.7	105.57	+10.38	0.161	-10.8	1	[KTK2006] G105.5+10.3, YMD CO 18
LDN 1124	21 41.5	+58 13.7	100.04	+4.07	0.015	-0.2	20	DBY 100.0+4.2, IC 1396 N
LDN 1128	21 41.5	+58 33.7	100.26	+4.32	0.015	1.2	0	TGU 599, WWC 117
LDN 1134	21 41.5	+60 13.7	101.35	+5.58	2.630	-0.4	0	[PGH98b] Cloud 19, DBY 100.9+05.3, [PGH98b] Cloud 21, DBY 101.7+05.0
LDN 1103	21 41.7	+56 43.7	99.07	+2.92	0.003		0	
LDN 1104	21 42.1	+56 43.7	99.11	+2.89	0.006	4.1	2	Barnard 163, TDS 371, WWC 184, [G85] 17, [LM99] 381
LDN 1181	21 42.1	+66 08.7	105.36	+9.97	0.008	-9.9	0	YMD CO 18, TGU 645
LDN 1183	21 42.1	+66 13.7	105.42	+10.03	0.090	-9.9	$>84$	Ced 196, GM 1-57, [B77] 40, TDS 395, [FMS2001] NGC 7129, [MPR2003] HI Ring, [MPR2003] HI Knot, BFS 11, JWT Core 46
LDN 1095	21 42.6	+56 18.8	98.89	+2.52	0.012		0	



Table 1.: Continued.

Cloud name	RA(2000) (h m)	Dec(2000) ( $^{\circ}$ $'$ )	l ( $^{\circ}$ )	b ( $^{\circ}$ )	Area (sq.deg.)	$v_{\text{LSR}}$ ( $\text{km s}^{-1}$ )	$n_{\text{star}}$	Alternative names
LDN 1106	21 42.6	+56 53.8	99.27	+2.97	0.009	-0.4	0	[PGS95] 28
LDN 1113	21 44.6	+57 11.8	99.67	+3.02	0.002	4.5	1	Barnard 367, WWC 186
LDN 1130	21 44.6	+58 18.8	100.40	+3.87	0.012	-3.0	8	TGU 604, [PGS95] 32, FSE 8
LDN 1136	21 45.5	+59 58.9	101.57	+5.06	0.012	-2.9	0	DBY 101.7+05.0
DBY 100.0+03.0	21 46.3	+57 25.1	100.00	+3.03	0.015	-1.9	16	IC 1396 E,SFO 39, FSE 9
LDN 1115	21 46.6	+56 58.9	99.74	+2.68	0.002		0	
LDN 1118	21 46.6	+57 12.9	99.89	+2.86	0.001	-2.1	0	SFO 42, [PGS95] 38
LDN 1129	21 46.6	+57 53.9	100.33	+3.38	0.041	-2.1	0	[PGS95] 36, DBY 100.4+03.4, WWC 40-42
LDN 1132	21 46.6	+58 43.9	100.87	+4.02	0.003		0	
LDN 1120	21 47.6	+57 09.0	99.96	+2.72	0.001		0	
LDN 1114	21 49.7	+56 24.0	99.69	+1.96	0.016	-1.8	0	TDS 375, DBY 099.9+01.8
LDN 1241	21 50.0	+76 44.1	113.08	+17.48	1.380	-3.7	0	YMD CO 72, YMD CO 75, TGU 728, TGU 739
LDN 1144	21 50.5	+60 07.1	102.14	+4.77	0.027	-2.2	1	Barnard 166, DBY 102.1+04.8
LDN 1137	21 51.6	+59 04.1	101.58	+3.87	0.018	-10.5	0	[G85] 31, DBY 101.5+03.8
LDN 1138	21 51.6	+59 04.1	101.58	+3.87	0.018	-10.5	0	DBY 101.5+03.8
LDN 1109	21 51.7	+55 49.1	99.55	+1.33	0.150	-1.5	0	DBY 099.5+01.2
Barnard 167	21 52.0	+60 04.0	102.25	+4.61	0.005		1	
LDN 1139	21 55.6	+58 34.3	101.68	+3.15	0.015	0.1	15	Barnard 169, DBY 101.3+03.00, TGU 620, [LM99] 386, [PGH98b] Cloud 27, FSE 10
LDN 1141	21 55.6	+58 44.3	101.78	+3.28	0.010	0.1	0	Barnard 171, DBY 101.3+03.00,
LDN 1142	21 56.6	+59 04.3	102.09	+3.47	0.002	0.1	0	CB 235, DBY 101.3+03.00
LDN 1143	21 57.6	+58 59.3	102.14	+3.32	0.020	0.1	1	Barnard 170, TDS 380, DBY 101.3+03.00
LDN 1149	21 57.6	+59 07.3	102.22	+3.43	0.015	0.1	0	DBY 101.3+03.00
LDN 1151	21 59.6	+59 04.4	102.40	+3.23	0.027	0.1	0	DBY 101.3+03.00
LDN 1153	22 00.6	+58 59.5	102.45	+3.09	0.079	0.1	0	TDS 383, DBY 101.3+03.00
LDN 1133	22 02.7	+56 14.5	101.02	+0.72	0.248		0	
LDN 1160	22 04.7	+58 59.6	102.87	+2.78	0.019	0.1	0	DBY 101.3+03.00
LDN 1166	22 05.7	+59 34.6	103.32	+3.18	0.001	-3.0	0	CB 236
LDN 1159	22 06.7	+58 34.7	102.84	+2.29	2.790	-1.0	17	Barnard 174, TDS 384, TDS 391, [LM99] 389, [GA90] 3-36, DSH J2206.2+5819, DBY 102.9+02.4, [G85] 32, DBY 102.8+02.1, DBY 103.3+02.8,

Table 1.: Continued.

Cloud name	RA(2000) (h m)	Dec(2000) ( $^{\circ}$ $'$ )	l ( $^{\circ}$ )	b ( $^{\circ}$ )	Area (sq.deg.)	$v_{\text{LSR}}$ ( $\text{km s}^{-1}$ )	$n_{\text{star}}$	Alternative names
								DBY 103.2+01.8, [PGH98b] Cloud 30, DBY 103.5+02.0, GSH 103+02-66
LDN 1164	22 06.7	+59 09.7	103.18	+2.76	0.019	-2.2	36	DBY 103.3+02.8, FSE 11
LDN 1165	22 07.2	+59 04.7	103.18	+2.66	0.019	-2.2	1	DBY 103.3+02.8
LDN 1169	22 07.2	+59 44.7	103.57	+3.20	0.004	-3.2	0	CB 237
TGU 659	22 09.0	+64 29.7	106.53	+6.93	1.070		1	[KTK2006] G106.9+07.1
LDN 1178	22 09.1	+62 19.8	105.27	+5.16	0.005		0	
LDN 1243	22 10.6	+75 20.0	113.16	+15.61	0.081	-2.9	0	YMD C0 74
LDN 1219	22 11.6	+70 59.9	110.58	+12.06	0.003	-4.6	1	Barnard 175, TDS 414, YMD CO 57
LDN 1182	22 13.1	+61 54.9	105.42	+4.55	0.004		0	
LDN 1217	22 13.1	+70 44.9	110.54	+11.79	0.186	-4.6	1	Ced 201, YMD CO 57, TDS 414, TGU 696
LDN 1186	22 13.6	+62 07.9	105.59	+4.70	0.005		0	TGU 649
LDN 1175	22 13.7	+60 44.9	104.81	+3.55	0.015		0	TGU 635
LDN 1191	22 14.1	+62 24.9	105.80	+4.90	0.004		0	
LDN 1193	22 14.6	+62 24.9	105.85	+4.87	0.002		0	
LDN 1235	22 14.9	+73 25.0	112.24	+13.88	0.037	-4.0	4	YMD CO 69, TDS 426, HCL 1F, TGU725, [BM89] 1-117, [LM99] 390
TGU 627	22 15.2	+58 47.6	103.87	+1.83	0.210		3	
LDN 1150	22 15.8	+56 00.0	102.37	-0.53	0.007	-6.9	0	Barnard 369, TDS 385, TGU 621
LDN 1188	22 16.7	+61 45.0	105.67	+4.18	0.398	-10.6	$\gtrsim 20$	YMD CO 21, TGU 652, [PGH98b] Cloud 33, [ADM95] 3, [ADM95] 4, [ADM95] 5, [ADM95] 7, [ADM95] 13, [ADM95] 8, GN 22.15.0
LDN 1154	22 16.8	+56 13.0	102.61	-0.43	0.007		0	
TGU 636	22 16.9	+60 11.6	104.83	+2.87	0.240		2	
TGU 640	22 17.6	+60 36.5	105.13	+3.17	0.330		2	DG 181, DG 182, GN 22.14.9
LDN 1156	22 19.9	+55 45.1	102.71	-1.05	0.043		0	
LDN 1161	22 19.9	+56 08.1	102.92	-0.73	0.006		0	[KC97c] G102.9-00.7
YMD CO 29	22 20.2	+63 53.1	107.20	+5.73	0.018	-11.0	13	Sh2-145, SFO 44
LDN 1184	22 20.7	+60 45.1	105.53	+3.08	0.124		0	TGU 643, TGU 644
LDN 1247	22 20.8	+75 15.2	113.66	+15.17	0.167	-5.1	0	TDS 430, TGU 742
LDN 1163	22 20.9	+56 10.1	103.05	-0.78	0.007		0	
LDN 1201	22 23.6	+63 30.2	107.31	+5.21	0.009		0	TGU 661

Table 1.: Continued.

Cloud name	RA(2000) (h m)	Dec(2000) ( $^{\circ}$ $'$ )	l ( $^{\circ}$ )	b ( $^{\circ}$ )	Area (sq.deg.)	$v_{\text{LSR}}$ ( $\text{km s}^{-1}$ )	$n_{\text{star}}$	Alternative names
LDN 1202	22 26.7	+63 05.3	107.38	+4.67	0.004		0	TGU 661
LDN 1204	22 26.7	+63 15.3	107.47	+4.82	2.500	-7.6	$\gtrsim 100$	YMD CO 27, TDS 399, TDS 401, TDS 403, TDS 404, TDS 405, [KC97c], [PGH98b] Cloud 32, [PGH98b] Cloud 37, [PGH98b] Cloud 38, [G84b] 12, DG 185, [PGH98b] Cloud 36, Sh2-140, GSH 108+05-46, GN 22.21.5, TGU 661
LDN 1180	22 26.8	+59 15.3	105.37	+1.41	7.000	-3.6	19	YMD CO 20, YMD CO 24, TDS 396, TDS 397, CB 240, TGU 631, TGU 638, TGU 655, TGU 658, Min 2-72, [PGH98b] Cloud 34, [KC97c] G104.6+01.4, KR 47, [LM99] 394, [KC97c] G105.6+00.4, Sh 2-138, [GSL2002] 109, [GSL2002] 110, [P85b] 18, [LM99] 396, DSH J2222.5+5918B, TGU 657, [B77] 42, [LM99] 391, GN 22.24.9
LDN 1195	22 26.8	+61 15.3	106.42	+3.11	0.017		1	
LDN 1196	22 26.8	+61 15.3	106.42	+3.11	0.029		1	
LDN 1179	22 27.3	+59 02.3	105.31	+1.19	0.002		0	
LDN 1203	22 27.7	+63 00.3	107.43	+4.54	0.016		0	TGU 661
TGU 719	22 27.8	+71 21.4	111.90	+11.63	0.510		3	
LDN 1221	22 28.4	+69 00.4	110.67	+9.61	0.020	-4.9	3	TDS 416, [KTK2006] G110.6+09.6, [LM99] 392, TGU 702
LDN 1206	22 28.7	+64 25.4	108.27	+5.70	0.083		0	TGU 673, [PGH98b] Cloud 35
LDN 1185	22 29.3	+59 05.4	105.56	+1.10	0.006		0	
LDN 1207	22 29.7	+64 25.4	108.36	+5.64	0.047		0	
LDN 1209	22 29.7	+64 45.4	108.53	+5.93	0.111	-8.8	3	Sh2-150, TGU 680
LDN 1208	22 30.7	+64 25.4	108.46	+5.58	0.018		0	
LDN 1190	22 30.9	+59 08.4	105.75	+1.04	0.004		0	
LDN 1242	22 31.2	+73 15.4	113.15	+13.11	0.793		0	
LDN 1213	22 31.6	+65 25.5	109.06	+6.39	0.006	-9.2	0	YMD CO 48, TGU 686, Sh2-150
LDN 1194	22 32.9	+59 05.5	105.95	+0.87	0.009		0	
LDN 1214	22 33.6	+65 45.5	109.41	+6.57	0.256	-8.5	1	TDS 407, YMD CO 48, Sh2-150
LDN 1192	22 33.9	+58 35.5	105.81	+0.37	0.007	-3.6	0	CB 240

Table 1.: Continued.

Cloud name	RA(2000) (h m)	Dec(2000) ( $^{\circ}$ $'$ )	l ( $^{\circ}$ )	b ( $^{\circ}$ )	Area (sq.deg.)	$v_{\text{LSR}}$ ( $\text{km s}^{-1}$ )	$n_{\text{star}}$	Alternative names
TDS 417	22 35.5	+69 13.1	111.33	+9.47	0.014	-7.2	1	YMD CO 65, [B77] 46, GN 22.33.6 [KTK2006] G101.9+15.8
TGU 679	22 35.9	+63 35.2	108.53	+4.57	0.170		1	
LDN 1251	22 36.1	+75 15.6	114.51	+14.65	0.195	-3.8	$\gtrsim 20$	YMD CO 79, TGU 750, [SMN94] B, HCL 1A, [SMN94] C, [SMN94] D, [LM99] 397, [NJH2003] 5, [TW96] H2, [SMN94] E, [TW96] H1, [KTK2006] G114.4+14.6
LDN 1198	22 36.9	+59 25.6	106.57	+0.90	0.054	-11.91	2	
TGU 672	22 37.5	+62 20.6	108.07	+3.40	0.360		1	
LDN 1197	22 37.9	+58 55.6	106.43	+0.40	0.009		0	
LDN 1187	22 38.0	+57 15.6	105.62	-1.06	0.145		0	
LDN 1189	22 39.0	+57 15.6	105.74	-1.12	0.473		0	
TGU 671	22 44.1	+60 16.1	107.77	+1.20	0.200		2	
LDN 1210	22 44.9	+62 05.8	108.70	+2.77	0.011	-10.0	0	YMD CO 40, TGU 699
Sh 2-142	22 45.0	+57 55.8	106.76	-0.92	1.063	-41.0	14	Ced 206, GM 2-42, TGU 663, SFO 43, [KC97c] G107.2-01.0, [KC97c] G107.3-00.9
LDN 1205	22 45.9	+60 25.8	108.04	+1.24	0.095		0	
LDN 1200	22 46.0	+58 45.8	107.27	-0.24	0.020	-3.7	3	YMD CO 28, TDS 402, TGU 665
TGU 678	22 46.5	+61 12.8	108.47	+1.90	0.170		1	
LDN 1211	22 46.9	+62 10.8	108.95	+2.74	0.011	-11.1	4	YMD CO 40, TGU 699
LDN 1212	22 47.9	+62 12.9	109.07	+2.71	0.014	-10.0	0	YMD CO 40, TGU 699
TGU 689	22 50.2	+62 51.5	109.60	+3.17	0.160		2	
TGU 692	22 50.7	+63 15.4	109.83	+3.50	0.240		2	
YMD CO 38	22 51.1	+60 51.6	108.80	+1.33	0.028	-8.5	1	TGU 606, [KTK2006] G100.6+16.2
YMD CO 49	22 51.1	+62 38.9	109.60	+2.93	0.014	-9.6	1	TGU 690
LDN 1215	22 51.9	+62 06.0	109.44	+2.40	0.021		0	TGU 699
LDN 1216	22 51.9	+62 16.0	109.52	+2.55	0.142	-9.5	11	Cep F, TDS 408, GN 22.51.3, TGU 699
LDN 1236	22 52.7	+68 56.0	112.56	+8.49	0.044	-5.0	0	YMD CO 73, TGU 729
YMD CO 51	22 56.2	+62 02.7	109.87	+2.13	0.489	-10.2	$\gtrsim 15$	Cep A
LDN 1223	22 56.9	+64 16.1	110.89	+4.11	1.010		1	TGU 703, [BKP2003] 455 GN 22.58.2, GSH 111+04-105

Table 1.: Continued.

Cloud name	RA(2000) (h m)	Dec(2000) ( $^{\circ}$ $'$ )	l ( $^{\circ}$ )	b ( $^{\circ}$ )	Area (sq.deg.)	$v_{\text{LSR}}$ ( $\text{km s}^{-1}$ )	$n_{\text{star}}$	Alternative names
TGU 715	22 57.0	+65 53.5	111.60	+5.57	1.280		0	
TGU 684	22 57.4	+59 27.5	108.90	-0.27	0.230	-47.0	6	[KC97c] G109.1-00.3, [G82a] 13
TGU 705	22 59.5	+63 26.0	110.80	+3.23	0.410		2	
LDN 1218	23 02.0	+62 16.2	110.58	+2.05	1.590	-5.1	>400	YMD CO 53, YMD CO 51 YMD CO 56, YMD CO 58, YMD CO 59, YMD CO 62, YMD CO 63, TDS 418, Cep A, Cep A west, [THR85] Cep A-3, GAL 109.88+02.11, [HW84] 7d, [B77] 44, [TOH95] Ridge, [TOH95] C, [TOH95] B, [TOH95] A, Cep B, GN 22.55.2, [KC97c] G110.2+02.5, Cep E, Cep E South, Cep E North, [YNF96] a, [YNF96] b, TGU 699
YMD CO 55	23 02.1	+61 29.2	110.27	+1.33	0.056	-7.3	2	
LDN 1224	23 04.0	+63 46.2	111.39	+3.33	0.016		0	
LDN 1220	23 04.1	+61 51.2	110.63	+1.57	0.006	-10.1	1	YMD CO 58, Cep E
LDN 1222	23 05.1	+61 46.2	110.70	+1.45	0.002	-10.1	0	YMD CO 58, Cep E, TGU 699
TGU 707	23 09.0	+61 04.8	110.87	+0.63	0.160		1	
TGU 700	23 09.7	+60 06.4	110.57	-0.30	0.650	-52.8	10	BFS 18
LDN 1226	23 10.1	+62 16.3	111.44	+1.68	0.009	-10.7	0	YMD CO 63, TGU 699
LDN 1227	23 10.1	+62 19.3	111.46	+1.73	0.008	-10.7	0	YMD CO 63, TGU 699
LDN 1240	23 11.0	+66 26.3	113.12	+5.50	0.126		0	
LDN 1225	23 12.1	+61 36.3	111.41	+0.97	0.036	-10.9	4	TDS 419, CB 242, TGU 699
LDN 1239	23 12.3	+66 04.3	113.11	+5.11	0.005	-7.6	0	CB 241
NGC 7538	23 14.1	+61 29.4	111.58	+0.77	0.011	-57.0	$\sim$ 2000	[KSH92] CS 5, [KSH92] CS 4, [M73] C, [KSH92] CS 3, Ced 209, [WAM82] 111.543+0.7, [M73] B, [M73] A, [KSH92] CS 2, Sh2-158 GAL 111.53+00.82, [WC89] 111.54+0.78, [KSH92] CS 1
LDN 1229	23 14.1	+61 59.4	111.78	+1.24	0.004	-10.0	0	Cep D, TGU 699
LDN 1230	23 14.1	+62 01.4	111.79	+1.27	0.002	-10.0	0	Cep D, TGU 699
LDN 1233	23 16.5	+62 20.4	112.15	+1.47	0.001	-10.0	0	Cep D
LDN 1232	23 17.2	+61 46.4	112.03	+0.91	0.004	-10.6	0	YMD CO 68, TGU 699
LDN 1234	23 17.2	+62 24.4	112.25	+1.51	0.004		0	
TGU 717	23 17.3	+60 48.1	111.70	0.00	0.200	-30.1	$\gtrsim$ 9	

Table 1.: Continued.

Cloud name	RA(2000) (h m)	Dec(2000) ( $^{\circ}$ $'$ )	l ( $^{\circ}$ )	b ( $^{\circ}$ )	Area (sq.deg.)	$v_{\text{LSR}}$ ( $\text{km s}^{-1}$ )	$n_{\text{star}}$	Alternative names
TGU 757	23 17.3	+69 56.0	114.97	+8.53	0.270		1	
LDN 1231	23 18.2	+61 16.4	111.97	+0.40	0.013	-11.2	0	TDS 424
LDN 1250	23 22.1	+67 16.5	114.45	+5.89	2.630	-8.6	1	YMD CO 78, YMD CO 80, TDS 432, TGU 747 GSH 114+06-47
LDN 1259	23 22.9	+74 16.5	116.93	+12.44	0.035	3.9	0	YMD CO 101, TGU 772
LDN 1244	23 25.2	+62 46.5	113.25	+1.53	0.007		0	
LDN 1246	23 25.2	+63 36.5	113.52	+2.32	0.002	-11.1	0	CB 243, [GA90] 3-40, [LM99] 400
LDN 1261	23 27.0	+74 16.5	117.20	+12.35	0.030	3.9	2	YMD CO 101, TDS 447, TGU 772, TDS 448, CB 244, [LM99] 401
LDN 1262	23 27.0	+74 16.5	117.20	+12.35	0.066	3.9	2	[BM89] 3B-10, [BM89] 1-119, TGU 772
YMD CO 85	23 32.6	+67 02.0	115.33	+5.33	0.084	-5.4	0	
YMD CO 86	23 35.8	+66 26.2	115.47	+4.67	0.056	-7.0	0	
YMD CO 87	23 39.3	+65 42.4	115.60	+3.87	0.168	-25.3	2	
TGU 767	23 42.9	+68 52.9	116.80	+6.83	0.400		2	
LDN 1264	23 52.5	+68 16.7	117.50	+6.03	0.102		0	
LDN 1266	23 57.5	+67 16.7	117.75	+4.95	2.540	-6.8	14	YMD CO 103, YMD CO 104, YMD CO 105, YMD CO 108, YMD CO 111, TDS 449, TDS 451, TGU 774, [LM99] 404, [YF92] C1, [LM99] 405, [YF92] C2, GN 23.56.1, [KC97c] G118.1+05.0, [LM99] 406, [GA90] 1-1, [GA90] 1-1a, [LM99] 1, [KC97c] G118.4+04.7, DG 1, [GA90] 3-41, [GA90] 3-42, SFO 1, SFO 3, DSH J2359.6+6741
LDN 1274	23 57.5	+70 56.7	118.52	+8.54	0.032	-2.5	0	YMD CO 109
LDN 1268	23 59.5	+67 26.7	117.97	+5.07	0.158	-6.2	3	Sh2-171, YMD CO 104, TGU 774
LDN 1269	00 00.6	+67 09.7	118.01	+4.78	0.025		0	TGU 774
LDN 1270	00 01.6	+67 09.7	118.11	+4.76	0.009		2	TGU 774
LDN 1271	00 01.6	+67 16.7	118.13	+4.87	0.010	-15.1	0	YMD CO 108, TGU 774
LDN 1272	00 02.6	+67 16.7	118.23	+4.85	8.690	-6.3	23	YMD CO 97, YMD CO 98, YMD CO 110, YMD CO 112, YMD CO 113, YMD CO 114, YMD CO 116, TGU 779, SFO 2, [GA90] 3-1, [GA90] 1-1b, GSH 119+05-74

Table 1.: Continued.

Cloud name	RA(2000) (h m)	Dec(2000) (° ′)	l (°)	b (°)	Area (sq.deg.)	$v_{\text{LSR}}$ (km s <sup>-1</sup> )	$n_{\text{star}}$	Alternative names
LDN 1273	00 02.6	+68 31.7	118.46	+6.08	0.199	-8.8	4	YMD CO 114
LDN 1275	00 06.6	+67 26.7	118.64	+4.95	0.020		0	TGU 781

References: [ADM95] – Abraham et al. (1995); Barnard – Barnard (1927); [B77] – Bernes (1977); [BKP2003] – Brunt et al. (2003); [BM89] – Benson & Myers (1989); BFS – Blitz et al. (1982); CB – Clemens & Barvainis (1988); Ced – Cederblad (1946) DBY – Dobashi et al. (1994); [DE95] – Davis & Eislöffel (1995); DG – Dorschner & Gürtler (1964); DSH – Kronberger et al. (2006); [ETM94] – Eiroa et al. (1994); [FMS2001] – Font et al. (2001); FSE – Froebrich et al. (2005); [G82a] – Gyulbudaghian (1982) [G85] – Gyulbudaghian (1985); [GA90] – Gyulbudaghian & Akopyan (1990); GAL – Kerber et al. (1996); GF – Schneider & Elmegreen (1979); GM – Magakian (2003); GN – Magakian (2003); GSH – Ehlerova & Palous (2005); [GSL2002] – Giveon et al. (2002) HCL – Heiles (1967); [HW84] – Hughes & Wouterloot (1984); [IS94] – Indrani & Sridharan (1994); JWT Core – Jessop & Ward-Thompson (2000); [KC97c] – Kuchar & Clark (1997); KR – Kallas & Reich (1980); [KSH92] – Kawabe et al. (1992); [KTK2006] – Kiss et al. (2006); LDN – Lynds (1962); [LM99] – Lee & Myers (1999); [M73] – Martin (1973); MBM – Magnani et al. (1985); Min – Minkowski (1947); [MPR2003] – Matthews et al. (2003); [NJH2003] – Nikolić et al. (2003); [P85b] – Petrossian (1985) [PGH98b] Cloud – Patel et al. (1998); [PGS95] – Patel et al. (1995); PP – Parsamian & Petrosian (1979); RNO – Cohen (1980) SFO – Sugitani et al. (1991); Sh2- – Sharpless (1959); [SMN94] – Sato et al. (1994); TDS – Taylor et al. (1987); TGU – Dobashi et al. (2005); [THR85] – Torrelles et al. (1985); [TOH95] – Testi et al. (1995); [TW96] – Tóth & Walmsley (1996); [WAM82] – Wink, Altenhoff & Mezger (1982); [WC89] – Wood & Churchwell (1989); WWC – Weikard et al. (1996); YMD CO – Yonekura et al. (1997); [YF92] – Yang & Fukui (1992); [YNF96] – Yu et al. (1996).

## 2. The Cepheus Flare

### 2.1. Large-scale Studies of the Cepheus Flare

The term ‘Cepheus flare’ was first used by Hubble (1934) who recognized that the zone of avoidance of external galaxies, confined to the Galactic plane, extended to higher latitudes at certain segments of the plane, suggesting significant obscuration outside the main Galactic belt. He called these wide segments for Galactic disk *flares*. The Cepheus Flare can be found at  $100^\circ \leq l \leq 120^\circ$ : there is a large amount of dense ISM above  $b \geq 10^\circ$  (Lynds 1962; Taylor, Dickman & Scoville 1987; Clemens & Barvainis 1988; Dobashi et al. 2005).

Heiles’ (1967) study of the HI distribution in the region revealed two kinematically separate sheets of interstellar gas in the Galactic latitude interval  $+13^\circ \leq b \leq +17^\circ$ , moving at a velocity of  $\sim 15 \text{ km s}^{-1}$  relative to each other. Heiles speculated that the two sheets probably represent an expanding or colliding system at a distance interval of 300–500 pc. Berkhuijsen (1973) found a giant radio continuum region *Loop III* centered on  $l=124 \pm 2^\circ$ ,  $b=+15.5 \pm 3^\circ$  and stretching across  $65^\circ$ , and suggested that it was a result of multiple supernova explosions. The HI shell reported by Hu (1981) at  $l=105^\circ$ ,  $b=+17^\circ$  and  $v_{centr}=+3 \text{ km s}^{-1}$  also indicates that the interstellar medium in this region is in a state of energetic motion. The wide range in the velocity thus may reflect disturbances from various shocks.

Lebrun’s (1986) low-resolution CO survey revealed that, in this region, the clouds constitute a coherent giant molecular cloud complex. Based on Racine’s (1968) study of reflection nebulae, Lebrun placed the Cepheus Flare molecular clouds between 300 and 500 pc. Grenier et al. (1989) extended the CO survey to a region of  $490 \text{ deg}^2$  in Cepheus–Cassiopeia above  $b=+10^\circ$ . They found that the clouds could be divided into two kinematically well separated subsystems around the radial velocities of  $v_{LSR} \sim 0 \text{ km s}^{-1}$  and  $-10 \text{ km s}^{-1}$ , respectively. They also detected CO emission around  $v_{LSR} \sim 0 \text{ km s}^{-1}$  at higher longitudes ( $124^\circ < l < 140^\circ$ ) in Cassiopeia, and found an area free of CO emission at  $118^\circ < l < 124^\circ$ . They suggested that the void between the Cepheus and Cassiopeia clouds is a supernova bubble. They estimated the age of the bubble as  $4 \times 10^4$  years, and proposed that it may result from a Type I supernova.

Yonekura et al. (1997) conducted a large-scale  $^{13}\text{CO}$  survey of the Cepheus–Cassiopeia region at an 8-arcmin grid spacing and with  $2.7$  beam size. Out of the 188 molecular clouds found in the whole surveyed region 51 fall in the Cepheus Flare region. Their surface distribution, adopted from Yonekura et al. (1997), is shown in Fig. 4.

These clouds, distributed over the velocity interval of  $(-15, +6) \text{ km s}^{-1}$ , were classified into three kinematically different components by Yonekura et al. (see Table 2). The high latitude part of the molecular complex is included in Magnani et al.’s (1985) catalog of high latitude molecular clouds. Ammonia observations of dense cores have been reported by Benson & Myers (1989) and Tóth & Walmsley (1996). In addition to the two major catalogs of dark clouds (Lynds 1962; Dobashi et al. 2005), dark cloud cores were catalogued by Lee & Myers (1999).

Kun (1998) determined cloud distances using Wolf diagrams, and presented a list of candidate YSOs found during an objective prism  $\text{H}\alpha$  survey, and selected from the IRAS Catalogs.

Kiss et al. (2006) performed a complex study of the visual and infrared properties of the ISM in the Cepheus Flare region using USNO, 2MASS, DIRBE, IRAS, and ISO data. Based on the distribution of visual extinction they identified 208 clouds,



Table 2. Cloud groups in Cepheus, classified by Yonekura et al. (1997).

N	Longitude		Latitude		$V_{LSR}$		D (pc)	M ( $M_{\odot}$ )	Associated objects	Ref.
	$l_l$ ( $^{\circ}$ )	$l_u$ ( $^{\circ}$ )	$b_l$ ( $^{\circ}$ )	$b_u$ ( $^{\circ}$ )	$V_l$ ( $\text{km s}^{-1}$ )	$V_u$ ( $\text{km s}^{-1}$ )				
Close Group										
1	99	105	13	18	1	5	440	3900	NGC 7023, L1157	1, 2
2	102	104	16	18	-4	-1	300	90		3
3	105	110	-1	1	-4	-1	300	110	L1200	3
4	106	116	13	19	-8	-1	300	3600	Cepheus Flare	4
5	110	116	4	12	-9	-3	300	730	L1221, L1250	3
6	110	117	19	21	-9	-4	300	680	L1228	3
7	115	117	-4	-1	-4	-1	140	20	L1253, L1257	5
8	116	118	12	13	3	5	200	26	L1262	6
9	117	124	6	10	-3	-1	300	200	L1304	3
Distant Group										
10*	95	99	3	7	-8	2	624	4000	IC 1396	17
13	103	111	9	15	-21	-8	1000	12000	NGC 7129	7, 8
14	105	110	0	7	-14	-6	910	11000	S 140	9
15	108	117	0	4	-17	-4	730	15000	Cep OB3	10
16	115	116	3	5	-26	-23	1000	1400	M115.5+4.0	11
17	116	124	-2	7	-22	-2	850	27000	Cep OB4	12
Clouds in Perseus Arm										
22	111	112	-1	1	-31	-30	2200	2500	MWC1080	13, 14
23	112	113	-3	-2	-37	-34	3000	5400	Cas A	15
24	123	124	-7	-6	-32	-30	2100	2000	NGC 281	16

References. (1) Viotti (1969); (2) Shevchenko et al. (1989); (3) Grenier et al. (1989); (4) Kun & Prusti (1993); (5) Snell (1981); (6) Myers & Benson (1983); (7) Racine (1968); (8) Shevchenko & Yakubov (1989); (9) Crampton & Fisher (1974); (10) Crawford & Barnes (1970); (11) Yang (1990); (12) MacConnell (1968); (13) Levreault (1985); (14) Levreault (1988); (15) Ungerechts & Thaddeus (1989); (16) Hogg (1959); (17) de Zeeuw et al. (1999).

\* The  $^{13}\text{CO}$  clouds in the region of IC 1396 are included in Dobashi et al. (1994), not in Yonekura et al. (1997).

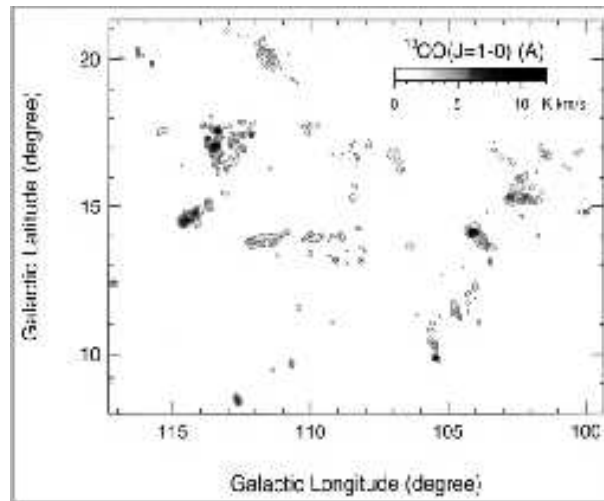


Figure 4. Distribution of  $^{13}\text{CO}$  clouds in the Cepheus Flare (adopted from Yonekura et al. 1997)

and divided them into 8 complexes. They examined the morphology of clouds, and established several empirical relationships between various properties of the clouds.

Olano et al. (2006) studied the space distribution and kinematics of the interstellar matter in Cepheus and Cassiopeia, using the Leiden–Dwingeloo HI data and the Columbia Survey CO data. They found that the broad and often double-peaked spectral line profiles suggest that the Cepheus Flare forms part of a big expanding shell that encloses an old supernova remnant. Assuming a distance of 300 pc for the center of the shell, located at  $(l, b) \approx (120^\circ, +17^\circ)$ , they derived a radius of approximately 50 pc, expansion velocity of  $4 \text{ km s}^{-1}$ , and HI mass of  $1.3 \times 10^4 M_\odot$  for the Cepheus Flare Shell. The supernova bubble proposed by Grenier et al. (1989), the radio continuum structure Loop III (Berkhuijsen 1973), and the Cepheus Flare Shell are various observable aspects of the supernova explosion(s) that shaped the structure of the interstellar medium and triggered star formation in the Cepheus Flare during the past few million years.

## 2.2. Distance to the Cepheus Flare Clouds

Spectroscopic and photometric studies of stars illuminating reflection nebulae in the Cepheus Flare (Racine 1968) indicated, long before the discovery of the molecular cloud complex, that interstellar dust can be found at several distances along the line of sight in this region. The presence of clouds at different velocities also suggests that there are clouds at various distances (Grenier et al. 1989).

At the low Galactic latitude boundary of the Cepheus Flare we find the associations Cep OB2 and Cep OB3 at a distance of  $\sim 800$  pc. Therefore Grenier et al. (1989) propose that the negative velocity component of the Cepheus flare clouds ( $v_{\text{LSR}} \sim -10 \text{ km s}^{-1}$ ) is an extension of these local arm features, while the more positive ( $v_{\text{LSR}} \sim 0 \text{ km s}^{-1}$ ) velocity component corresponds to a nearby cloud complex at a distance of 300 pc.

Table 2 suggests a more complicated pattern of cloud distances. Both the close and the distant components are composed of several complexes, probably located at different distances. Other distance determinations found in the literature support this suggestion. Below we list some results and problems related to the distance of Cepheus Flare clouds.

Distances of individual clouds can reliably be derived by studying the effects of the clouds on the light of associated stars. Racine (1968), in a spectroscopic and photometric study of stars in reflection nebulae, obtained a distance of  $400 \pm 80$  pc for the Cepheus R2 association above the latitude  $+10^\circ$ . Both velocity components are represented among the clouds being illuminated by the stars of Cep R2.

A prominent object of the distant component, in addition to the possible outer parts of Cep OB2 and Cep OB3, is NGC 7129. Though Kun, Balázs & Tóth (1987) and Ábrahám, Balázs & Kun (2000) proposed that NGC 7129 may be associated with the Cepheus Bubble, and thus with Cep OB2, other observations suggest that NGC 7129 may be farther than Cep OB2. Racine (1968) investigated three member stars, and derived  $m - M \approx 12.2$  for BD+65°1637, and 10.0 for both BD+65°1638 and LkH $\alpha$  234, and labeled each value as uncertain. Shevchenko & Yakubov (1989), based on an  $A_V$  vs. distance diagram, derived 1250 pc for NGC 7129. Yonekura et al. (1997) found a group of clouds at  $l \sim 107^\circ - 111^\circ, b \sim +13^\circ$  at similar velocity, and regarded them as an extension of the NGC 7129 clouds to the northeast (group 13 in Table 2). This result suggests that a considerable part of the Cepheus Flare clouds is located at

Table 3. Distance measured for the clouds within the Cepheus Flare region together with their probable lower and upper limits and the method of determination.

Cloud	l ( $^{\circ}$ )	b ( $^{\circ}$ )	d( $\Delta$ d) (pc)	Method	Ref.
L1147/L1158	102.0	15.0	325 $\pm$ 13	$A_V$ vs. distance	4
L1167/L1174	104.0	15.0	440 $\pm$ 100	spectroscopy & photometry of HD 200775	1
L1167/L1174	104.0	15.0	288 $\pm$ 25	$A_V$ vs. distance	4
L1167/L1174	104.0	15.0	430 $^{+160}_{-90}$	<i>Hipparcos</i> parallax of HD 200775	10
L1177	105.14	13.12	300 $\pm$ 30	Wolf diagram	6
L1199	106.50	12.21	500 $\pm$ 100	Wolf diagram	6
L1199	106.50	12.21	800	spectroscopy & photometry of HD 206135	2
TDS400	107.01	16.78	300 $^{+50}_{-10}$	Wolf diagram	6
CB 234	108.10	13.15	300 $^{+50}_{-10}$	Wolf diagram	6
TDS406	108.50	18.15	300 $^{+50}_{-20}$	Wolf diagram	6
L1217	110.34	11.41	400 $^{+50}_{-20}$	Wolf diagram	6
L1219	110.60	11.96	400 $^{+50}_{-20}$	Wolf diagram	6
L1219	110.60	11.96	400	spectroscopy & photometry of BD+69 1231	2, 8
TDS420	111.57	14.25	300 $^{+50}_{-10}$	Wolf diagram	6
L1228	111.63	20.14	200 $^{+100}_{-20}$	Wolf diagram	6
L1228	111.63	20.14	180 $^{+30}_{-10}$	spectroscopy & photometry of BD+76 825	
TDS421	111.71	13.80	250 $^{+30}_{-10}$	Wolf diagram	6
L1235	112.22	13.86	200	$A_V$ vs. distance	3
L1235	112.22	13.86	300 $^{+50}_{-10}$	Wolf diagram	6
L1235	112.22	13.86	400 $\pm$ 80	spectroscopy & photometry of HD 210806	2, 8
L1235	112.22	13.86	300 $^{+80}_{-40}$	<i>Hipparcos</i> parallax of HD 210806	7
L1241	113.03	17.51	300 $^{+50}_{-10}$	Wolf diagram	6
L1242	113.08	13.14	300 $^{+30}_{-10}$	Wolf diagram	6
L1243	113.10	15.64	300 $^{+50}_{-10}$	Wolf diagram	6
L1247	113.60	15.20	300 $^{+50}_{-10}$	Wolf diagram	6
L1251	114.45	14.68	300 $\pm$ 50	$A_V$ vs. distance	5
L1251	114.45	14.68	300 $^{+50}_{-10}$	Wolf diagram	6
L1251	114.45	14.68	337 $\pm$ 50	star count analysis	9
MBM163–165	116.00	20.25	200 $^{+100}_{-20}$	Wolf diagram	6
L1259–1262	117.00	12.40	180 $^{+40}_{-20}$	Wolf diagram	6

References: (1) Viotti (1969); (2) Racine (1968); (3) Snell (1981); (4) Straizys et al. (1992); (5) Kun & Prusti (1993); (6) Kun (1998); (7) ESA (1997); (8) Kun et al. (2000); (9) Balázs et al. (2004); (10) van den Ancker et al. (1997)

about 1 kpc. The situation is, however, far from clear. Simonson & van Someren Greve (1976) found a large HI cloud coinciding both in position and velocity with the molecular clouds of Yonekura et al.'s group 13. They associated this cloud not with NGC 7129, but with the reflection nebulae of Cep R2 (Racine 1968) at a distance of some 400 pc. The Wolf diagrams constructed by Kun (1998) show two layers of extinction towards  $b \sim +11^{\circ} - +13^{\circ}$ , at 300 pc and  $\sim 450$  pc, respectively, thus it is tempting to identify the two velocity components with these two layers.

Another direct distance determination within the area of the Cepheus Flare is that of Viotti (1969), who derived 440 $\pm$ 100 pc for the reflection nebula NGC 7023, based on high resolution spectroscopy and UBV photometry of its illuminating star, HD 200775. In spite of the large uncertainty of this value, this is the most frequently cited distance of

NGC 7023. Alecian et al. (2008) pointed out that HD 200775 is a spectroscopic binary with two nearly identical components, thus its observed luminosity has to be partitioned on both components, which suggests a distance of about 350 pc. The distance from the *Hipparcos* parallax of HD 200775,  $430_{-90}^{+160}$  pc (van den Ancker et al. 1997) has to be treated with some caution, since part of the measured displacement of the star resulted from its orbital motion. The projected separation of the components, estimated by Alecian et al. (2008),  $16 \pm 9$  mas, commensurates with the measured parallax, and the orbital period of 1412 days suggests that *Hipparcos* might have measured the position of the star at any point of the orbit.

Straizys et al. (1992) determined the visual extinction  $A_V$  vs. distance using photometric measurements of 79 stars in the Vilnius photometric system for the L1147/1158 and NGC 7023 (L 1167/1174) regions. They obtained a distance  $288 \pm 25$  pc for NGC 7023, and the same method resulted in  $325 \pm 13$  pc for the L1147/L1158 group.

Snell (1981) studied the interstellar reddening towards L 1235 and pointed out the presence of an absorbing layer at a distance of 200 pc. This value is frequently assumed to be the distance of several other clouds in the region as well (e.g. Benson & Myers 1989).

Kun & Prusti (1993) found a distance of  $300 \pm 50$  pc for L 1251 by examining the interstellar reddening as a function of distance moduli of field stars. Kun (1998) determined distances of dark clouds over the whole area of the Cepheus Flare using Wolf diagrams. The Wolf diagrams indicated that the interstellar matter in the Cepheus Flare is concentrated at three characteristic distances: 200, 300 and 450 pc. The three components, though partly overlapping, can be separated along the Galactic latitude. The three absorbing layers can be identified with Yonekura et al.'s (1997) groups 6, 4, and 1, respectively. The overlap of the layers makes the distance determination of some dark clouds ambiguous. For instance, both the 300 pc and 200 pc layers can be recognized towards L 1228. However, L 1228 differs in radial velocity from the other clouds of the 300 pc component. Moreover, the star BD+76°825 (*spectral type: F2 V, B=11.21, V=10.62*) is projected within a compact group of pre-main sequence stars of L 1228 and illuminates a faint reflection nebula (Padgett et al. 2004). Thus the photometric distance of this star, 180 pc, is a good estimate of the distance of L 1228. The Cepheus Flare shell, proposed by Olano et al. (2006), may explain the existence of dark clouds at both 200 and 300 pc (see Fig. 5). Table 3 summarizes the results of distance determinations in the Cepheus Flare region. The group of clouds whose distance remains controversial is associated with the negative velocity component at  $l \sim 107^\circ - 111^\circ, b \sim +13^\circ$ .

### 2.3. Star Formation in the Cepheus Flare

Star formation takes place in dense cores of molecular clouds. Dense cores within dark clouds are usually designated with letters appended to the name of the cloud, e.g. L 1082 A, L 1251 E. Several dense cores and IRAS sources of the Cepheus Flare clouds have been included in large molecular surveys aimed at studying their various properties and the associated young stellar objects. Below we list some major survey papers including key data for Cepheus Flare clouds, cores, and IRAS sources.

Myers et al. (1983) – CO observations (L1152, L1155 H, L1155 D, L1082 C, L1082 A, L1082 B, L1174, L1172 D, L1172 B, L1262 A);

Clemens & Barvainis (1988) – positions, radial velocities, and IRAS associations of small, optically selected molecular clouds (CB 222, CB 224, CB 229 (L1171), CB 230, CB 232, CB 244);

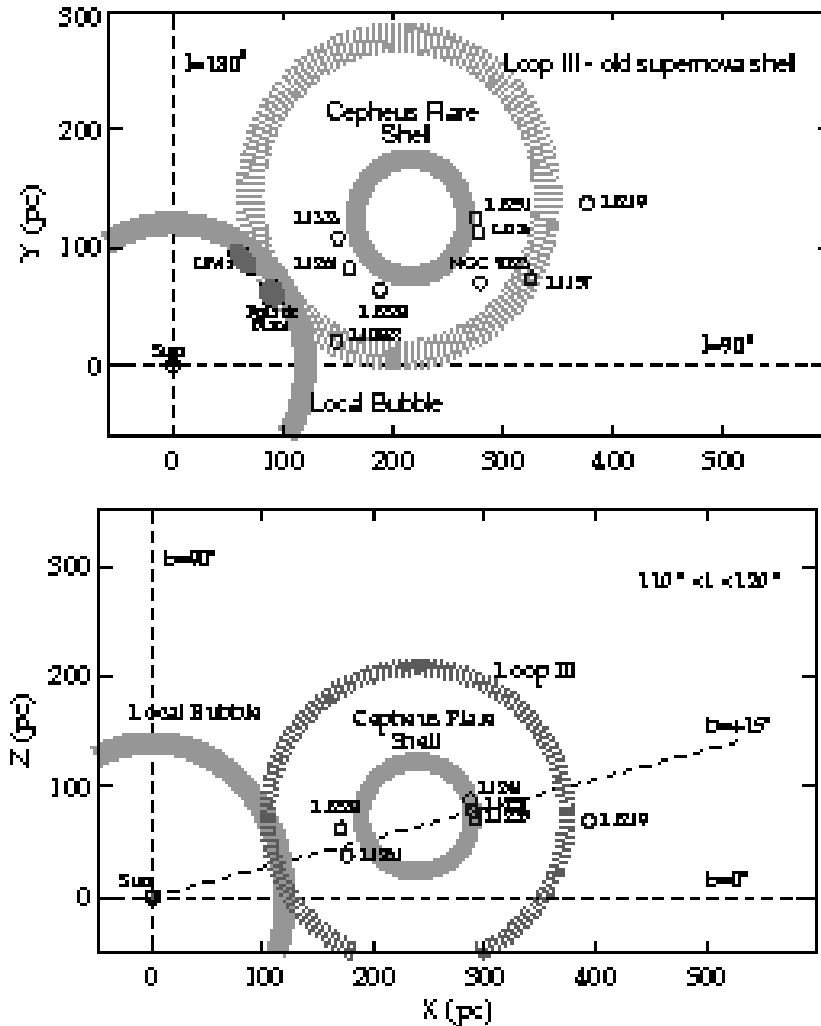


Figure 5. Upper panel: Distribution of the most prominent molecular clouds of the Cepheus Flare and nearby interstellar shells, projected on the Galactic plane, and viewed from the direction of the North Galactic pole. Lower panel: the same objects projected onto a plane perpendicular to the Galactic equator.

Benson & Myers (1989) –  $\text{NH}_3$  observations (L1152, L1155 B, L1155 C, L1155 D, L1155 G, L1158, L1082 C, L1082 A, L1174, L1174 B, L1172 D, L1172 A, L1172 B, L1228 C, L1228 B, L1235, L1251 A, L1262 A);  
 Goodman et al. (1993) – velocity gradients (L1152, L1082 A, L1082 B, L1082 C, L1174, L1172 A, L1251 A, L1251 E, L1262 A);  
 Benson et al. (1998) –  $\text{N}_2\text{H}^+$ ,  $\text{C}_3\text{H}_2$ , and CCS observations (L1155, L1152, L1152 (IR), L1082 A, L1082 C, L1174, L1172 A, L1228, L1228 D, L1221, L1251 A, L1251 E, L1262);  
 Myers et al. (1988) – search for outflows (L1152, L1082 A, L1174, L1172 D, L1262);  
 Fukui (1989) – search for outflows (PV Cep, L1228, L1172, NGC 7129, LkH $\alpha$  234, L1221, L1251 A, L1251 B, L1262);  
 Furuya et al. (2003) – search for  $\text{H}_2\text{O}$  masers (L1082, L1082 A, L1082 B, L1228, L1174,

L1172 D, L1221, L1251 A, L1251 B, L1262);  
Mardones et al. (1997) – search for protostellar infall (IRAS 20353+6742, IRAS 20386+6751, IRAS 21017+6742, IRAS 22343+7501, IRAS 22376+7455, IRAS 23238+7401).

Table 4. Molecular outflows and sources in the Cepheus Flare.

Cloud	RA(2000)	Dec(2000)	Source	References
L 1157	20 39 06	+68 02 13	IRAS 20386+6751	5,17
L 1157	20 45 54	+67 57 39	PV Cep	5,10,12
L 1082	20 47 56.6	+60 04 14	IRAS 20468+5953	22
L 1082	20 51 30.1	+60 18 39	GF9–2	22,23
L 1082	20 53 13.6	+60 14 40	IRAS 20520+6003	22
L 1228 A	20 57 13	+77 35 47	IRAS 20582+7724	5,7,9
L 1228 B	20 57 06	+77 36 56	HH 200 IRS	9
L 1174 A	21 00 22	+68 12 52	L 1174 A	21
L 1172	21 02 24	+67 54 27	IRAS 21017+6742	2, 5,13,
L 1174	21 03 02	+68 06 57	RNO 131A	1,3,20
L 1177	21 17 40	+68 17 32	IRAS 21169+6804	19, 21
L 1183	21 42 57	+66 04 47	RNO 138	1,3,24
L 1183	21 43 01	+66 03 37	NGC 7129 FIRS 2	4,5,8,10
L 1183	21 43 02	+66 06 29	LkH $\alpha$ 234	4,5,8,10
L 1183	21 43 00	+66 11 28	V350 Cep	24
L 1219	22 14 08	+70 15 05	IRAS 22129+7000	14,25
L 1221	22 28 03	+69 01 13	IRAS 22266+6845	6,11,18
TDS 417	22 35 06	+69 10 53	IRAS 22336+6855	6
L 1251 A	22 35 24	+75 17 06	IRAS 22343+7501	5,15
L 1251 B	22 38 47	+75 11 29	IRAS 22376+7455	5,15,16
L 1262	23 25 46	+74 17 33	IRAS 23238+7401	5,17,20

References. 1: Armstrong (1989); 2: Beichman, Myers & Emerson (1986); 3: Cohen (1980); 4: Edwards & Snell (1983); 5: Fukui (1989); 6: Haikala & Dietrich (1989); 7: Haikala & Laureijs (1989); 8: Harvey, Wilking & Joy (1984); 9: Bally et al. (1995); 10: Lada (1985); 11: Lee et al. (2002); 12: Levreault (1984); 13: Myers et al. (1988); 14: Nikolić & Kun (2004); 15: Sato & Fukui (1989); 16: Sato et al. (1994); 17: Terebey et al. (1989); 18: Umemoto et al. (1991); 19: Wang et al. (1995); 20: Wu et al. (1992); 21: Yun & Clemens (1992); 22: Wiesemeyer et al. (1999); 23: Furuya et al. (2006); 24: Liseau & Sandell (1983); 25: Goicoechea et al. (2008).

The Cepheus Flare cloud cores can be found among the targets of infrared, submillimeter and millimeter continuum surveys of embedded low mass young stellar objects as well:

Connelley et al. (2007) – a K-band atlas of reflection nebulae (IRAS 20353+6742, IRAS 20453+6746, IRAS 21017+6742, IRAS 22266+6845, IRAS 22376+7455);

Young et al. (2006) – submillimeter (450 and 850  $\mu$ m) survey of cores included in the Spitzer c2d project (L 1152, CB 224, L 1157, L 1082 C, L 1082 A, L 1228, L 1177 (CB 230), L 1221, L 1251 C, L 1251 E, L 1155 C);

Rodríguez & Reipurth (1998) – VLA observations of HH exciting sources (L 1152, L 1157, L 1221).

We find these objects in statistical studies of dense cores and young stellar objects:

Fuller & Myers (1992) – line width–size relations (L 1152, L 1262);

Myers et al. (1991) – shapes of cores (L 1152, L 1251, L 1262);

Wu et al. (2004) – properties of outflows (L 1152, L 1155, L 1082, L 1174, L 1172,

L 1228, L 1177, L 1221, L 1251, L 1262);

Wu et al. (2007) – submm (350  $\mu\text{m}$ ) survey of cores included in the Spitzer c2d project (L 1152, L 1157, L 1148, L 1177, L 1228, RNO 129, L 1221, L 1251).

The molecular outflows discovered in the Cepheus Flare and their driving sources are listed in Table 4, and the Herbig–Haro objects and driving sources can be found in Table 5.

Figure 3 shows the surface distribution of pre-main sequence stars and candidates in the Cepheus Flare. Apparently star formation occurs in small aggregates, especially along the boundaries of the complex. The central part of the cloud complex contains clouds of low density and is avoided by known signposts of star formation.

The samples of T Tauri stars, displayed in Fig. 3, result from several surveys for  $\text{H}\alpha$  emission stars conducted in the region of Cepheus Flare. Only 10 pre-main sequence objects are catalogued in the Herbig–Bell Catalog (Herbig & Bell 1988, hereinafter HBC). Ogura & Sato (1990) reported on 69 detected and 49 suspected  $\text{H}\alpha$  emission stars in a wide environment of L 1228. Kun (1998) reported 142  $\text{H}\alpha$  emission stars, distributed over the whole area of the Cepheus Flare, identified on objective prism photographic Schmidt plates and 128 IRAS sources as possible YSOs. Spectroscopic follow up observations of both samples are underway (Kun et al., in preparation). We show in Fig. 3 and list in Table 7 those stars from these two surveys whose pre-main sequence nature has already been confirmed. The known Herbig Ae/Be stars are also listed in Table 7.

Tachihara et al.’s (2005) spectroscopic observations toward the ROSAT X-ray sources resulted in detecting 16 Li-rich stars, representing weak line T Tauri stars. The main properties of these WTTSs are listed in Table 6.

The distribution of the WTTSs in the Cepheus Flare differs from that of other YSOs. In the CO void found by Grenier et al. (1989), a group of WTTSs is separated from the  $^{13}\text{CO}$  cloud by  $\gtrsim 10$  pc. The cloud-to-WTTS separations are significantly larger in Cepheus than in other nearby SFRs such as Chamaeleon. Because of their grouping, Tachihara et al. propose the in-situ formation model for them. From the total mass of the group of TTSs, a  $\sim 800 M_{\odot}$  molecular cloud might have formed them, while only  $\sim 200 M_{\odot}$  molecular gas remained in their vicinity. An external disturbance might have dissipated the molecular cloud within several  $10^5$  yr. As the distances to the WTTSs are unknown, Tachihara et al. suggest two possible scenarios for the history of the formation of the WTTS sample isolated from the cloud complex: (1) The WTTSs in the CO void were formed at 300 pc and affected by the supernova shock discussed by Grenier et al. (1989); or (2) They are at 200 pc and an unknown supernova explosion has the responsibility for the parent cloud dissipation. Radial velocity measurements might help to find the relationship between the stars and the cloud complex. Taking into account the picture of the Cepheus Flare Shell, the same supernova might have triggered star formation at both 200 and 300 pc.

#### 2.4. Notes on Individual Objects

*L 1147/L 1158* The cloud group often referred to as the *L 1147/L 1158 complex* consists of the clouds Lynds 1147, 1148, 1152, 1155, 1157, and 1158. L 1157 harbors a Class 0 object, L 1157-mm, with  $L_{\text{bol}} \sim 11 L_{\odot}$ . It coincides with IRAS 20386+6751 and drives a spectacular outflow. The L 1157 outflow has been studied in detail through many molecular lines, such as CO (Umamoto et al. 1992; Gueth, Guilloteau & Bachiller 1996; Bachiller & Pérez Gutiérrez 1997; Hirano & Taniguchi 2001), SiO (Mikami et al.

Table 5. Herbig–Haro objects and their sources in the Cepheus Flare.

Name	RA(2000)	Dec(2000)	Source	Cloud	D(pc)	Reference
HH 376B	20 35 06.1	+67 48 47	IRAS 20359+6745	L1152	440	11,13
HH 376A	20 36 02.4	+67 54 28	IRAS 20359+6745	L1152	440	11,13
HH 376	20 36 55.3	+67 59 28	IRAS 20359+6745	L1152	440	15,19
HH 375	20 39 06.2	+68 02 15	IRAS 20386+6751	L1157	440	2,18,19
HH 315C	20 45 06.9	+68 04 50	PV Cep	L1158	500	2,8,13
HH 315	20 45 34.0	+68 03 25	PV Cep	L1158	500	2,8,13
HH 315B	20 45 34.0	+68 03 25	PV Cep	L1158	500	2,8,13
HH 315A	20 45 38.4	+68 00 55	PV Cep	L1158	500	2,8,13
HH 215	20 45 53.8	+67 57 39	PV Cep	L1158	500	10,12,13
HH 415	20 46 04.6	+68 00 28		L1158	500	8,11,16
HH 315D	20 46 06.4	+67 54 13	PV Cep	L1158	500	2,8,13
HH 315E	20 46 28.1	+67 52 20	PV Cep	L1158	500	2,8,13
HH 315F	20 47 09.9	+67 50 05	PV Cep	L1158	500	2,8,13
HHL 65	20 53 06.0	+67 10 00			300	7
HH 199R3	20 54 49.1	+77 32 16	IRAS 20582+7724	L1228	200	4
HH 199R2	20 54 56.2	+77 32 21	IRAS 20582+7724	L1228	200	4
HH 200B6	20 55 09.4	+77 31 20	HH 200 IRS	L1228	200	4
HH 199R1	20 55 12.2	+77 33 11	IRAS 20582+7724	L1228	200	4
HH 200B5	20 55 22.5	+77 32 17	HH 200 IRS	L1228	200	4
HH 200B4	20 55 33.9	+77 33 07	HH 200 IRS	L1228	200	4
HH 200B4a	20 56 11.0	+77 34 18	HH 200 IRS	L1228	200	4
HH 200B3	20 56 22.2	+77 35 01	HH 200 IRS	L1228	200	4
HH 200B2	20 56 35.9	+77 35 34	HH 200 IRS	L1228	200	4
HH 200B1	20 56 51.2	+77 36 21	HH 200 IRS	L1228	200	4
HH 199B1	20 57 27.2	+77 35 38	IRAS 20582+7724	L1228	200	4
HH 199B2	20 57 31.0	+77 35 44	IRAS 20582+7724	L1228	200	4
HH 199B3	20 57 34.1	+77 35 53	IRAS 20582+7724	L1228	200	4
HH 199B4	20 58 21.7	+77 37 42	IRAS 20582+7724	L1228	200	4
HH 199B5	20 59 08.0	+77 39 25	IRAS 20582+7724	L1228	200	4
HH 198	20 59 09.7	+78 22 48	IRAS 21004+7811	L1228	200	4,14,16,17
HH 200R1	20 59 48.2	+77 43 50	HH 200 IRS	L1228	200	4
HH 199B6	21 00 27.4	+77 40 54	IRAS 20582+7724	L1228	200	4
HHL 67	21 05 00.0	+66 47 00			300	7
HH 450	22 14 24.1	+70 14 26	IRAS 22129+7000	L1219	400	5
HH 450X	22 14 50.1	+70 13 47		L1219	400	5
HH 363	22 27 46.7	+69 00 38	IRAS 22266+6845	L1221	200	1,9
HH 149	22 35 24.2	+75 17 06	IRAS 22343+7501	L1251	300	3,13
HH 373	22 37 00.0	+75 15 16		L1251	300	16
HH 374	22 37 39.1	+75 07 31		L1251	300	16
HH 374A	22 37 39.2	+75 07 31		L1251	300	1
HH 374B	22 37 50.0	+75 08 13		L1251	300	1
HH 364	22 38 19.2	+75 13 07		L1251	300	16
HH 189C	22 38 39.4	+75 09 49		L1251	300	6
HH 189	22 38 39.9	+75 10 41	IRAS 22376+7455?	L1251	300	6
HH 189B	22 38 40.0	+75 10 40	KP 44?	L1251	300	6
HH 189E	22 38 40.3	+75 13 52		L1251	300	1
HH 189A	22 38 40.4	+75 10 53		L1251	300	6
HH 189D	22 38 44.2	+75 13 28		L1251	300	1
HH 358	23 24 39.0	+74 12 35		L1262	180	1,16
HH 359	23 26 29.0	+74 22 28		L1262	180	1,16

References. 1: Alten et al. (1997); 2: Arce & Goodman (2002); 3: Balázs et al. (1992); 4: Bally et al. (1995); 5: Bally & Reipurth (2001); 6: Eiroa et al. (1994); 7: Gyulbudaghian et al. (1987); 8: Gómez et al. (1997); 9: Lee et al. (2002); 10: Moreno-Corral et al. (1995); 11: Movsessian et al. (2004); 12: Neckel et al. (1987); 13: Reipurth, Bally, & Devine (1997); 14: Movsessian & Magakian (2004); 15: Rodríguez & Reipurth (1998); 16: Wu et al. (1992); 17: Brugel & Fesen (1990); 18: Devine, Reipurth & Bally (1997); 19: Davis & Eislöffel (1995).



1992; Zhang et al. 1995; Gueth, Guilloteau & Bachiller 1998; Zhang, Ho & Wright 2000; Bachiller et al. 2001), H<sub>2</sub> (Hodapp 1994; Davis & Eisloffel 1995), NH<sub>3</sub> (Bachiller et al. 2001; Tafalla & Bachiller 1995; Umemoto et al. 1999), and CH<sub>3</sub>OH (Bachiller et al. 1995, 2001; Avery & Chiao 1996). Many other lines have been detected (Bachiller & Pérez Gutiérrez 1997; Bachiller et al. 2001; Beltrán et al. 2004; Benedettini et al. 2007; Arce et al. 2008), making L 1157 the prototype of chemically active outflows. Gas phase shock chemistry models have been used by Amin (2001) to study the production of the observed species in the L 1157 outflow. Arce & Sargent (2006) studied the outflow–envelope interaction on a 10<sup>4</sup> AU scale using high angular resolution multiline observations. Velusamy et al. (2002) detected spatially resolved methanol emission at 1 mm from L 1157. Their results indicate the presence of a warm gas layer in the infall–disk interface, consistent with an accretion shock. Regarding the protostar itself, dust continuum observations have been carried out at 2.7 mm (Gueth et al. 1996, 1997; Beltrán et al. 2004), 1.3 mm (Shirley et al. 2000; Chini et al. 2001; Gueth, Bachiller & Tafalla 2003; Beltrán et al. 2004), 850  $\mu$ m (Shirley et al. 2000; Chini et al. 2001; Young et al. 2006), 450  $\mu$ m (Chini et al. 2001), as well as 60, 100, 160, and 200  $\mu$ m (Froebrich et al. 2003). Using the VLA, Rodríguez & Reipurth (1998) detected the protostar as a radio continuum source at 3.6 cm. Froebrich et al. (2003) obtained a far-infrared spectrum of the L 1157 protostar using the LWS on board ISO. Deep Spitzer *IRAC* images of L 1157 reveal many details of the outflow and the circumstellar environment of the protostar. Looney et al. (2007) report on the detection of a flattened structure seen in absorption at 8  $\mu$ m against the background emission. The structure is perpendicular to the outflow and is extended to a diameter of 2 arcmin. This structure is the first clear detection of a flattened circumstellar envelope or pseudo-disk around a Class 0 protostar.

Table 6. Weak-line T Tauri stars in the Cepheus Flare (Tachihara et al. 2005)

ID	GSC	RA(2000)	Dec(2000)	Sp. Type	<i>V</i>	<i>V</i> − <i>I</i> <sub>C</sub>	<i>M</i> <sup>1</sup> ( <i>M</i> <sub>⊙</sub> )	Age(My <sub>r</sub> ) <sup>1</sup>
4c1	0450001478	00 38 05.4	+79 03 21	K1	10.43	0.92	1.6	2
4c2		00 38 05.4	+79 03 21	K7	13.86	1.77	0.8	15
5c1	0450001549	00 39 06.1	+79 19 10	K6	12.18	1.52	0.6	1
5c2		00 39 06.1	+79 19 10	M2 <sup>2</sup>	14.12	2.10	0.4	1
19	0458901101	20 20 29.3	+78 07 22	G8	10.39	0.82	1.6	6
20	0445900083	20 25 15.4	+73 36 33	K0	10.62	0.84	1.6	4
28	0458601090	21 11 29.4	+76 14 29	G8	11.66	0.81	1.0	25
34	0460801986	22 11 11.0	+79 18 00	K7	13.09	1.55	0.7	3
36c1	0427200174	22 27 05.3	+65 21 31	K4	12.92	1.13	0.9	20
36c2		22 27 05.3	+65 21 31	M4 <sup>2</sup>	15.55	2.50	0.2	0.2
37c1	0448000917	22 33 44.9	+70 33 18	K3	11.63	1.65	1.0	0.4
38	0460400743	22 39 58.1	+77 49 40	K2	11.88	1.03	1.2	8
40	0460502733	23 00 44.4	+77 28 38	K0	10.98	0.88	1.4	6
41	0460500268	23 05 36.1	+78 22 39	K6	13.19	1.59	0.8	7
43c1	0448900036	23 09 43.4	+73 57 15	K7	13.21	1.86	0.3	4
43c2		23 09 43.4	+73 57 15	M3 <sup>2</sup>	15.55	2.50	0.7	3
44	0460500170	23 16 18.1	+78 41 56	K4	11.77	1.24	1.0	2
45	0447900348	23 43 41.9	+68 46 27	K2	12.64	1.00	0.9	25
46	0461001318	23 51 10.0	+78 58 05	K1	11.34	0.93	1.3	6

<sup>1</sup>Derived from the evolutionary tracks by D’Antona & Mazzitelli (1994).

<sup>2</sup>Derived only from the *V* − *I*<sub>C</sub> color.

The K’ image of the outflow source, presented by Hodapp (1994), is dominated by nebulosity of bipolar morphology, indicative of an in-plane bipolar outflow. Knots of nebulosity extend to the north and south of the outflow position. Both the northern and the southern lobes contain bow shock fronts.

X-ray observations of L 1157, performed by the ASCA satellite, have been published by Furusho et al. (2000).

The molecular cloud L 1155 was mapped by Harjunpää & Mattila (1991) in the lines of  $C^{18}O$ ,  $HCO^+$ , and  $NH_3$ . The observations revealed that L 1155 consists of two separate clumps, L1155 C1 and L1155 C2. The optically visible pre-main sequence star associated with L 1152 is HBC 695 (RNO 124), studied in detail by Movsessian et al. (2004).

Recently Kauffmann et al. (2005), using the data base of the Spitzer Space Telescope Legacy Program *From Molecular Cores to Planet Forming Disks* (c2d, Evans et al. 2003) found a candidate sub-stellar ( $M \ll 0.1M_{\odot}$ ) mass protostellar object in L 1148. The object L 1148–IRS coincides with IRAS F20404+6712.

*PV Cep* The highly variable pre-main sequence star PV Cep lies near the northeastern edge of the dark cloud complex L 1147/L 1158. It is a bright IRAS source, and has been detected in radio continuum (Anglada et al. 1992). It illuminates a reflection nebula, known as GM–29 (Gyulbudaghian & Magakian 1977) and RNO 125 (Cohen 1980). A dramatic brightening of the star (an EXor-like outburst) was observed in the period 1976–1978, and at the same time the shape of the associated nebula changed drastically (Cohen, Kuhl & Harlan 1977).

The stellar parameters of PV Cep are somewhat uncertain. Most of its optical spectrograms available show no photospheric absorption features. Cohen et al. (1977), based on measurements of narrow-band continuum indices, estimated a spectral type about A5. Cohen et al. (1981) found the same spectral type based on the strength of the  $H\delta$  absorption line, apparent in two blue spectra. They note, however, that the hydrogen features probably represent merely a shell spectrum. Magakian & Movsessian (2001) estimated a spectral type of G8–K0, based on a spectrum taken in July 1978, when the star was some 2 magnitudes fainter than during the outburst. No other estimate of spectral type can be found in the literature (see Hernández et al. 2004, for a review). The spectral type of F, quoted by Staude (1986) and Neckel et al. (1987) is also based on the spectral information presented by Cohen et al. (1981).

Cohen et al. (1981) found a distance of about 500 pc for PV Cep. Their estimate was based on three independent arguments. (1) PV Cep is probably related to NGC 7023. The spectroscopic and photometric data of its illuminating star, HD 200775, suggest a distance of 520 pc. (2) The spectroscopic and photometric data of the nebulous star RNO 124, located in the same cloud complex as PV Cep, suggest the same distance. (3) A similar distance can be obtained from the light travel time from the star to a nebular spike which brightened about a year after the outburst of the star. On the contrary, Straizys et al. (1992) obtained a distance of 325 pc for the L 1147/L 1158 dark cloud complex (see Table 3).

The environment of the star shows a bipolar and rapidly changing optical morphology (Cohen et al. 1981; Neckel & Staude 1984; Staude 1986; Neckel et al. 1987; Levreault & Opal 1987; Scarrott et al. 1991a,b), as well as a bipolar CO outflow parallel to the symmetry axis of the reflection nebula (Levreault 1984). Neckel et al. (1987) detected several HH-knots, known as HH 215, emanating from PV Cep. Reipurth, Bally, & Devine (1997) and Gómez, Kenyon & Whitney (1997) discovered a giant ( $\sim 2.3$  pc long) Herbig-Haro flow, HH 315, consisting of 23 knots. HH 215 is also part of this giant flow. Reipurth, Bally, & Devine (1997) detected a further small knot, HH 415, located north-east of PV Cep, but this may be a dwarf galaxy with  $H\alpha$  redshifted into the [SII] passband (Bally, priv. comm.). Near-infrared spectroscopy of PV Cep is presented

by Hamann & Persson (1994) and Greene & Lada (1996), and optical spectroscopy by Corcoran & Ray (1997).

Far-infrared data obtained by ISOPHOT (Ábrahám et al. 2000) indicate the presence of an extended dust component on arcminute scale around PV Cep. The existence of a dust core close to PV Cep is also supported by the  $^{13}\text{CO}$  (J=1–0) mapping of the region by Fuente et al. (1998b), who found a molecular core with a size of some  $60''$ .



Figure 6. Optical image of a field of  $36' \times 24'$  of L 1082, obtained by Giovanni Benintende (<http://www.astrogb.com/>).

*L 1082* is a remarkable filamentary cloud (see Fig. 6), first catalogued by E. E. Barnard (1927) as Barnard 150. It appears as GF 9 in the catalog of globular filaments by Schneider & Elmegreen (1979). Several dense cores, namely L 1082 A,B,C (Myers et al. 1983), and LM99 349, 350, 351 ( $\equiv$  L 1082 C), 352 (Lee & Myers 1999), as well as four IRAS sources, IRAS 20468+5953, 20503+6006, 20520+6003, and 20526+5958 are found along the filament. A finding chart for the objects in L 1082 is given in Figure 7.

No distance determination is available in the literature for L 1082. Several authors assume that L 1082 is close to NGC 7023 not only on the sky, but also in space, and thus accept 440 pc as its distance (e.g. Ciardi et al. 1998). We note that the angular separation of  $10^\circ$  between NGC 7023 and L 1082 corresponds to 70 pc at the distance of NGC 7023. If both objects belong to the same complex, a similar difference can be expected between their distances. Wiesemeyer et al. (1997), based on statistical arguments, assume a distance of  $100 \pm 50$  pc. Furuya et al. (2003) refer to 150 pc, and Furuya et al. (2006) derive the physical parameters of GF 9–2 using 200 pc. Kun (2007) speculates that L 1082 may lie at the interaction region of the Local Bubble and Loop III (Cepheus Flare Shell). In this case its likely distance is about 150 pc.

Ciardi et al. (1998) performed near-infrared observations of a core and a filament region within GF 9 (GF 9-Core and GF 9-Fila, see Fig. 7). They found that neither the core nor the filament contains a Class I or Class II YSO. The extinction maps of the two  $7' \times 7'$  fields observed reveal masses 26 and 22  $M_{\odot}$  in the core and the filament, respectively (at a distance of 440 pc). The core contains a centrally condensed extinction maximum that appears to be associated with IRAS 20503+6006, whereas GF 9-Fila does not show centrally peaked dust distribution.

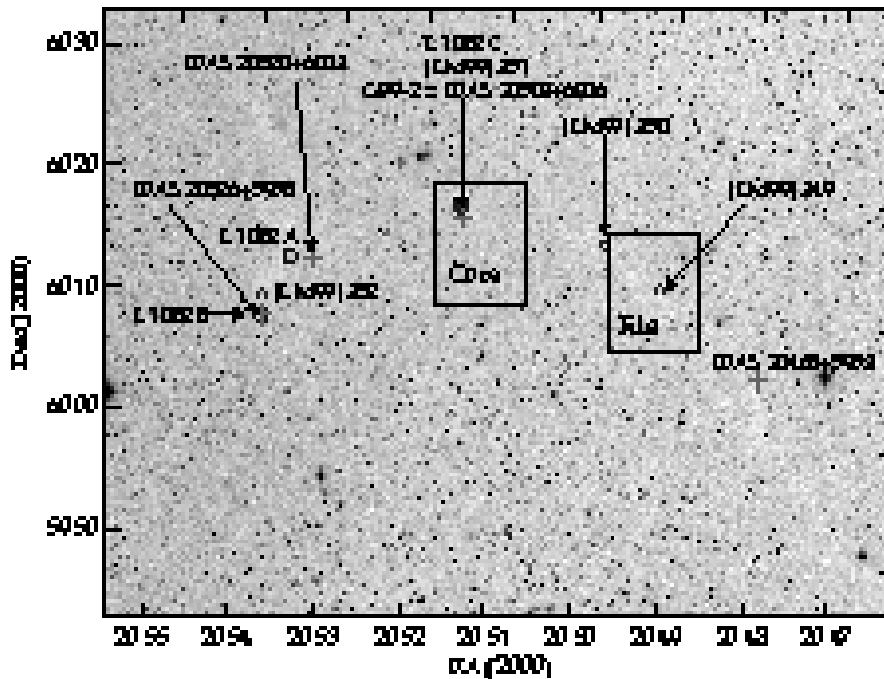


Figure 7. Finding chart for the structure of L 1082, based on Poidevin & Bastien's (2006) Fig. 1 and Wiesemeyer et al.'s (1998) Fig. 1. Crosses indicate the positions of the IRAS and ISOCAM point sources, open circles mark the dense cores L 1082 A, B, and C (Benson & Myers 1989), diamonds show the dense cores catalogued by Lee & Myers (1999). Two rectangles show the regions GF 9 Core and GF 9 Fila, studied in detail by Ciardi et al. (1998; 2000). The size of the underlying DSS red image is  $70' \times 50'$ .

Wiesemeyer et al. (1998) presented mid-infrared ISOCAM observations of L 1082. They identified 9 sources along the filament, and designated them as GF 9-1, 2, 3a, 3b, 4, 5, 6, 16, and 7. The designations probably follow Mezger (1994) who labeled dense cores along the filament by the same numbers. GF 9-2 coincides in position with IRAS 20503+6006, GF 9-3b with IRAS 20520+6003, GF 9-16 with IRAS 20468+5953, and GF 9-4 lies at  $12''$  west of IRAS 20526+5958. They find that these latter two sources are Class 0 protostars, both associated with CO outflows, whereas GF 9-6 and GF 9-7 are most likely reddened background stars. They speculate that the other ISOCAM sources, not associated with outflows, may be transitional objects between prestellar (Class -1) and Class 0 evolutionary stages. Wiesemeyer et al. (1999)

presented far-infrared ISOPHOT and millimeter continuum measurements for GF 9–2, GF 9–3a/3b, and GF 9–4.

Ciardi et al. (2000) performed CO,  $^{13}\text{CO}$ , and CS observations of the GF 9–Core and GF 9–Fila regions, determined excitation temperatures, densities and masses. The CS observations reveal that both regions contain centrally condensed, high-density gas cores. The temperatures and masses of the two regions and of the cores contained within the regions are similar, but the densities in GF 9–Core are twice those of GF 9–Fila.

De Gregorio Monsalvo et al. (2006) detected CCS emission from GF 9–2. The structure of the magnetic field associated with GF 9 was studied by Jones (2003) and Poidevin & Bastien (2006).

Furuya et al. (2003) detected  $\text{H}_2\text{O}$  maser emission from GF 9–2. Furuya et al. (2006) studied in detail the spatial and velocity structure of GF 9–2, using several molecular transitions obtained by single-dish and interferometric radio observations and  $350\ \mu\text{m}$  continuum data. The observations revealed a dense core with a diameter of  $\sim 0.08\ \text{pc}$  and mass of  $\sim 3\ M_{\odot}$ . Within the core a protostellar envelope with a size of  $\sim 4500\ \text{AU}$  and mass of  $\sim 0.6\ M_{\odot}$  could be identified. The radial column density profile of the core can be well fitted by a power-law form of  $\rho(r) \propto r^{-2}$  for the  $0.003 < r/\text{pc} < 0.08$  region. The power-law index of  $-2$  agrees with the expectation for an outer part of the gravitationally collapsing core. They found no jet-like outflow, but a compact, low-velocity outflow may have formed at the center. They discovered a potential protobinary system with a projected separation of  $\sim 1200\ \text{AU}$ , embedded in a circumbinary disk-like structure with  $\sim 2000\ \text{AU}$  radius at the core center. The binary consists of a very young protostar and a pre-protostellar condensation. The studies led to the conclusion that GF 9–2 is very likely at an extremely early stage of low-mass star formation before arriving at its most active outflow phase.

Stecklum, Meusinger & Froebrich (2007) discovered 14 Herbig–Haro objects in the GF 9 region which apparently belong to at least three large HH-flows. Five HH-objects and GF 9–2 are linearly aligned, suggesting that they constitute an HH-flow driven by IRAS 20503+6006. Its overall length amounts to  $43.5\ \text{arcmin}$ , which corresponds to  $2.3\ \text{pc}$  for an assumed distance of  $200\ \text{pc}$ . The presence of a well-developed, parsec-scale outflow from GF 9–2 indicates a more advanced evolutionary stage of this source than previously believed.

Furuya et al. (2008) mapped GF 9 in the  $\text{NH}_3$  (1,1) and (2,2) inversion lines, using the Nobeyama 45-m telescope, with an angular resolution of  $73''$ . The large-scale map reveal that the filament contains at least 7 dense cores, as well as 3 candidates, located at regular intervals of  $\sim 0.9\ \text{pc}$  (at an assumed distance of  $200\ \text{pc}$ ). The cores have kinetic temperatures of  $\lesssim 10\ \text{K}$  and LTE-masses of  $1.8 - 8.2\ M_{\odot}$ , making them typical sites of low-mass star formation, probably formed via the gravitational fragmentation of the natal filamentary cloud.

*NGC 7023* is a reflection nebula, illuminated by the young massive star HD 200775 and a group of fainter stars. It was discovered by William Herschel in 1794. HD 200775 (also known as V380 Cep and HBC 726) is a Herbig Be star that has been extensively studied (e.g. Herbig 1960; Altamore et al. 1980; Pogodin et al. 2004; Alecian et al. 2008). The surrounding reflection nebula has been observed in detail (e.g. Slipher 1918; Witt & Cottrell 1980; Witt et al. 1982; Rogers et al. 1995; Laureijs et al. 1996; Fuente et al. 2000; Werner et al. 2004; Berné et al. 2008). Figure 8 shows an optical image of the reflection nebula.



Figure 8. Optical image of NGC 7023, illuminated by the Herbig Be star HD 200775. The size of the field is about  $30' \times 20'$ . Courtesy of Richard Gilbert of the Star Shadows Remote Observatory.

Weston (1953) found that, centered on the reflection nebula, there is a small cluster consisting of stars which are variable and show  $H\alpha$  line in emission. Some two dozens of variable stars of the region were studied by Rosino & Romano (1962). Nevertheless, the HBC lists only four of these stars (HBC 726, 304, 306, 307, see Table 7) as confirmed T Tauri type stars. Recently Goodman & Arce (2004) speculated that the young Herbig Ae star PV Cep, located more than 10 pc to the west of the cluster, might have been ejected from NGC 7023 at least 100,000 years ago. HD 200775 is located at the northern edge of an elongated molecular cloud, corresponding to the dark clouds L 1167, 1168, 1170, 1171, 1172, 1173 and 1174, referred to as the *L 1167/L 1174 complex*. The cloud complex has been mapped in CO by Elmegreen & Elmegreen (1978). They found that the size of the cloud is  $0.5^\circ \times 1.0^\circ$ , or  $3.9 \text{ pc} \times 7.7 \text{ pc}$ , and the mass of the molecular hydrogen is some  $600 M_\odot$ .

Table 7.: Pre-main sequence stars in the Cepheus Flare – (A) Classical T Tauri stars

Names	IRAS	2MASS J/ RA,Dec(J2000)	2MASS magnitudes			IRAS fluxes			
			J	H	K	F(12)	F(25)	F(60)	F(100)
HBC 695n, RNO 124, K98 6	20359+6745	20361986+6756316	11.364	9.739	8.781	0.44	1.05	1.81	
GSC 04472-00143	20535+7439	20530638+7450348	10.149	9.405	8.861	0.42	0.63	0.68	
HH 200 IRS, L 1228 VLA 4		20570670+7736561*							
FT Cep, K98 26	20587+6802	20592284+6814437	10.588	9.342	8.532	0.55	0.92	0.89	
K98 30, OSHA 42	F20598+7728	20584668+7740256	11.513	10.365	9.699	0.09	0.16		
RNO 129 S1, OSHA 44, K98 32	21004+7811	20591409+7823040	9.437	7.530	6.319	6.23	11.12	36.30	76.60:
RNO 129 S2, OSHA 44, K98 32	21004+7811	20591256+7823078	10.993:	12.060	9.174				
RNO 129 A		20590373+7823088	12.565	11.280	10.726				
HBC 304, FU Cep, LkH $\alpha$ 427	21009+6758	21014672+6808454	11.792	10.798	10.159				
K98 35, PRN S5	F21016+7651	21005285+7703149	11.290	10.288	9.773	0.12	0.15	0.34	
	F21022+7729	21011339+7741091	12.676	11.202	10.327	0.08	0.13	0.17	
NGC 7023 RS 2		21012706+6810381	12.323	11.150	10.417				
NGC 7023 RS 2		21012637+6810385	11.107	10.084	9.571				
PW Cep, LkH $\alpha$ 425, NGC 7023 RS 3		21013590+6808219	12.336	11.564	11.052				
NGC 7023 RS 5		21014250+6812572	11.911	10.892	10.421				
LkH $\alpha$ 428, NGC 7023 RS 8		21022829+6803285	11.141	10.457	9.723				
HZ Cep, NGC 7023 RS S3		21014358+6809361	11.218	10.415	10.156				
HBC 306, FV Cep, LkH $\alpha$ 275, K98 38	F21017+6813	21022039+6825240	11.513	10.529	9.880	0.12	0.14		
PRN S1(b)		21012508+7706540	17.212:	14.640	13.156				
PRN S1(a)		21012638+7707029	16.460:	14.622	13.244				
OSHA 48, PRN S6		21012919+7702373	9.919	9.093	8.563				
OSHA 49, K98 40, PRN S7	F21023+7650	21013097+7701536	11.669	10.910	10.614	0.17	0.23	0.72	
OSHA 50, K98 41, PRN S8		21013267+7701176	11.993	11.060	10.419	0.08	0.08	0.09	
PRN S4		21013505+7703567	13.217	12.018	11.084				
PRN S2		21013945+7706166	15.399	14.007	12.973				
PRN S3		21014960+7705479	12.449	11.272	10.802				
OSHA 53, K98 43, PRN S9	F21028+7645	21020488+7657184	11.108	10.352	10.027	0.09	0.20	0.24	
FW Cep, NGC 7023 RS 9		21023299+6807290	11.559	10.713	10.411				
NGC 7023 RS 10	21023+6754	21025943+6806322	13.871	13.083	12.357	0.27	0.39		
K98 46	F21037+7614	21030242+7626538	11.585	10.843	10.471	0.13	0.18		
HBC 307, EH Cep, LkH $\alpha$ 276, K98 42	21027+6747	21032435+6759066	9.538	8.767	8.196	0.59	0.71		

\*No 2MASS counterpart.

Table 7.: Pre-main sequence stars in the Cepheus Flare – (A) Classical T Tauri stars (cont.)

Names	IRAS	2MASS J/ RA/Dec(J2000)	2MASS magnitudes			IRAS fluxes			
			J	H	K	F(12)	F(25)	F(60)	F(100)
OSHA 59, K98 49	F21066+7710	21055189+7722189	10.689	9.755	9.086	0.17	0.24	0.18	
K98 53		21153595+6940477	11.585	10.843	10.471	0.13	0.18		
K98 58	F21202+6835	21205785+6848183	14.318	13.035	11.866		0.20		5.49:
RNO 135, K98 61	21326+7608	21323108+7621567	11.101	10.072	9.688			1.46	5.01
K98 66		21355434+7201330	11.323	10.724	10.463				
K98 71	F21394+6621	21402754+6635214	11.344	10.540	10.046	0.34	0.64	2.56	
HBC 731, SVS 6		21425961+660433.8	12.886	11.624	10.948				
HBC 732, V350 Cep, MMN 13		21430000+6611279	12.714	11.691	11.008				
NGC 7129 S V1		21401174+6630198	13.161	12.173	11.591				
NGC 7129 S V2		21402277+6636312	13.882	12.671	11.890				
NGC 7129 S V3		21403852+6635017	13.108	11.888	11.267				
V391 Cep, K98 72	F21404+6608	21413315+6622204	11.680	10.555	9.750	0.36	0.40		
NGC 7129 MMN 1		21422308+6606044	15.059	14.050	13.394				
NGC 7129 HL85 14, MMN2 2		21423880+6606358	14.796	13.479	12.514				
NGC 7129 MMN 3		21424194+6609244	15.179	14.340	13.987				
NGC 7129 MMN 5		21425142+6605562	15.199	14.128	13.573				
NGC 7129 MEG 1		21425177+6607000	16.679	15.546	14.675				
NGC 7129 MMN 6		21425262+6606573	13.821	12.650	11.803				
NGC 7129 MMN 7		21425314+6607148	14.338	13.193	12.679				
NGC 7129 MMN 8		21425346+6609197	16.990	15.497	14.578				
NGC 7129 MMN 9		21425350+6608054	13.214	12.365	12.124				
NGC 7129 MMN 10		21425481+6606128	14.192	13.254	12.907				
NGC 7129 MEG 2		21425476+6606354	14.183	13.179	12.564				
NGC 7129 MMN 11		21425626+6606022	12.423	11.657	11.406				
RNO 138, V392 Cep		21425771+6604235	14.567:	14.478	13.658				
NGC 7129 MMN 12		21425810+6607394	14.299	13.532	13.030				
NGC 7129 MEG 3		21425878+6606369	13.487	12.561	12.337				
NGC 7129 MMN 14		21430024+6606475	14.161	12.778	12.085				
NGC 7129 MMN 15		21430246+6607040	14.004	13.109	12.256				
GGD 33A		21430320+6611150	16.619	15.461	14.337				
NGC 7129 MMN 17		21431162+6609115	12.605	11.800	11.487				

\*No 2MASS counterpart.



Table 7.: Pre-main sequence stars in the Cepheus Flare – (A) Classical T Tauri stars (cont.)

Names	IRAS	2MASS J/ RA/Dec(J2000)	2MASS magnitudes			IRAS fluxes			F(100)
			J	H	K	F(12)	F(25)	F(60)	
NGC 7129 MMN 18		2143124+661238*							
NGC 7129 MMN 19		21431683+6605487	14.184	13.300	13.123				
NGC 7129 MMN 20		21433183+6608507	13.935	12.894	12.295				
NGC 7129 MMN 21		21433271+6610113	14.986	13.792	13.547				
NGC 7129 MMN 22		21434345+6607308	13.655	12.609	12.146				
K98 73		21443229+7008130	11.777	10.939	10.535		0.14	0.25	
K98 95		22131219+7332585	10.987	10.048	9.498	0.3	0.26	0.32	0.28
GSC 04467-00835	22129+6949	2214068+7005043	9.620	9.072	8.753	0.254	0.567	0.484	0.50:
K98 108		22190203+7319252	10.666	9.947	9.561	0.15	0.26	0.3	
K98 109		22190169+7346072	11.677	10.738	10.234	0.06	0.12	0.16	0.4
K98 110		22190343+7349596	12.848	12.264	12.162	0.15	0.19	0.12	0.16
K98 119	22256+7102	22265660+7118011	10.967	9.646	8.525	1.74	2.28	2.48	4.17
KP 1, XMMU J223412.2+751809	22331+7502	22341189+7518101	10.095	8.808	7.827				
KP 39, XMMU J223516.6+751848		22351668+7518471	11.808	10.589	9.858				
KP 2, XMMU J223605.8+751831	22350+7502	2236059+7518325	11.957	10.894	10.253				
KP #10	22355+7505	2236345+7521352	11.984	10.628	10.026	0.11	0.24	0.23	
KP 43, XMMU J223727.7+751525		22372780+7515256	11.289	10.202	9.854				
KP 3, XMMU J223750.1+750408		22374953+7504065	11.785	10.974	10.680				
ETM Star 3, XMMU J223818.8+751154		22381872+7511538	11.248	9.815	8.912				
KP 44, ETM Star 1, XMMU J223842.5+751146		22384249+7511455	12.166	11.313	11.028				
KP 45, XMMU J22397.3+751029		22392717+7510284	11.748	10.851	10.377				
KP 46, XMMU J223942.9+750644	22385+7457	22394030+7513216	10.920	9.481	8.698				
GSC 04601-03483	F22424+7450	22433926+7506302	10.958	10.379	10.216	0.080	0.240	0.522	
K98 128		22490470+7513145	12.011	11.208	10.814				
TYC 4601-1543-1	22480+7533	22491626+7549438	9.938	9.256	8.727	0.61	0.90	0.81	
HBC 741, AS 507, K98 140	23189+7357	23205208+7414071	8.308	7.754	7.480				

\*No 2MASS counterpart.

Table 7. Pre-main sequence stars the Cepheus Flare – (B) Herbig Ae/Be stars

Names	IRAS	2MASS J RA/Dec(J2000)	2MASS magnitudes			IRAS fluxes			
			J	H	K	F(12)	F(25)	F(60)	F(100)
HBC 696n, PV Cep, K98 9	20453+6746	20455394+6757386	12.453	9.497	7.291	12.82	32.93	48.85	57.92
HBC 726, HD 200775, MWC 361	21009+6758	21013691+6809477	6.111	5.465	4.651	26.700	76.800	638.000	1100.000
HD 203024	21153+6842	21160299+6854521	8.377	8.209	8.120	3.680	10.800	4.260	
GSC 04461-01336, BD+68° 1118	21169+6842	21173917+6855098	9.269	8.741	8.105	1.570	3.480	4.130	2.59
HBC 730, V361 Cep, AS 475, BD +65° 1637		21425018+6606352	8.973	8.729	8.474				
HBC 309, LkH $\alpha$ 234, V373 Cep	21418+6552	21430682+6606542	9.528	8.201	7.081	14.78	78.96	687.70	1215.00
HBC 734, BH Cep, K98 83	22006+6930	22014287+6944364	9.686	8.993	8.310	0.524	1.200	1.390	
HBC 735, BO Cep, K98 100	F22156+6948	22165406+7003450	10.319	9.849	9.581	0.285	1.428		
HBC 736, SV Cep, K98 113	22205+7325	22213319+7340270	9.350	8.560	7.744	4.22	5.22	2.66	1.76
GSC 04608-02063	22219+7908	22220233+7923279	11.509	10.920	10.266				

*References to star names:* NGC 7023 RS – variable stars from Rosino & Romano (1962); OSHA – H $\alpha$  emission stars from Ogura & Sato (1990); KP – H $\alpha$  emission star from Kun & Prusti (1993), Table 2; KP# – IRAS point source from Kun & Prusti (1993), Table 3; ETM – Eiroa et al. (1994); K98 – H $\alpha$  emission stars from Kun (1998); NGC 7129 MEG – Miranda et al. (1993); NGC 7129 MMN – Magakian et al. (2004); PRN – Padgett et al. (2004); NGC 7129 S – Semkov (2003); XMMU – Simon (2006)

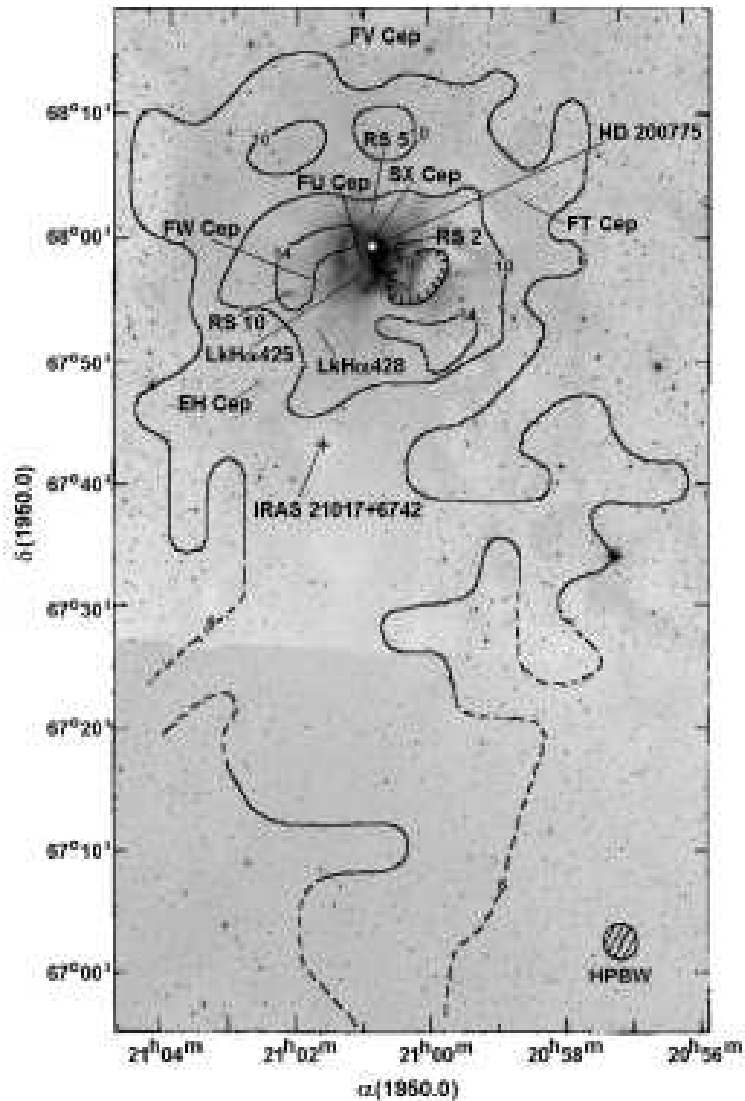


Figure 9.  $^{13}\text{CO}$  contours of the molecular cloud associated with NGC 7023, overplotted on the DSS red image (Elmegreen & Elmegreen 1978). Positions of HD 200775 and lower mass pre-main sequence stars, as well as the protostar IRAS 21017+6742 are indicated.

Watt et al. (1986) found a bipolar outflow associated with HD 200775. The region of the outflow has been mapped in  $^{13}\text{CO}(1-0)$  by Fuente et al. (1998). These observations show that the star is located within a biconical cavity, which has probably been excavated by a bipolar outflow. However, Fuente et al. found no evidence for current high-velocity gas within the lobes of the cavity.

Myers et al. (1988) detected another molecular outflow centered on the IRAS source IRAS 21017+6742. Hodapp's (1994)  $K'$  image of the L 1172 outflow shows four stars associated with localized nebulosity. None of them are close to the nominal outflow position. Visser, Richer & Chandler (2002) detected three submillimeter sources at the

position of IRAS 21017+6742: L 1172 SMM 1–SMM 3. They found that L 1172 SMM 1, located at RA(2000)= $21^{\text{h}}02^{\text{m}}21.5^{\text{s}}$ , Dec(2000)= $+67^{\circ}54'14''$  is a protostar and the driving source of the outflow, whereas SMM 2 and SMM 3 are starless dust clumps. Figure 9 shows the  $^{13}\text{CO}$  contour map of the L 1167/L 1174 complex, adopted from Elmegreen & Elmegreen (1978). Known pre-main sequence stars of the region are also indicated.

*L 1177* (CB 230) contains a molecular outflow driven by the IRAS source 21169+6804 (Yun & Clemens 1994). Near infrared observations by Yun (1996) revealed this source to be a binary protostar with a projected separation of  $12''$ , and embedded in a common infrared nebula. The stars can be found near the center of a dense core whose size is about  $360''$  (0.5 pc at 300 pc). Further CO and infrared studies can be found in Clemens, Yun & Heyer (1991). Submillimeter polarization measurements by Wolf, Launhardt & Henning (2003) reveal a magnetic field strength of  $218 \mu\text{G}$  for the envelope of CB 230. Wolf et al. found that the outflow is oriented almost perpendicular to the symmetry axis of the globule core, whereas the magnetic field is parallel to the same axis. They discuss the possibility that the orientation of the magnetic field relative to the outflow directions reflects the evolutionary stage of the globule. Two A-type emission line stars, HD 203024 and BD + $68^{\circ}1118$  can be found to the north of the globule, at the edge of the diffuse outer part of the cloud. Their formation history may be connected to each other (Kun 1998). Miroshnichenko et al. (1997) and Kun, Vinkó & Szabados (2000) classify these objects as candidate Herbig Ae/Be stars, whereas Mora et al. (2001) state that they are main sequence stars.

*L 1228* is a small cloud stretching some  $3^{\circ}$  along a north-south direction. Its most probable distance is 180 pc (see Sect. 2.2.). *L 1228* differs kinematically from the rest of the Cepheus Flare molecular clouds, suggesting that the cloud is located on the near side of the Cepheus Flare shell. Numerous  $\text{H}\alpha$  emission stars have been found around this cloud (Ogura & Sato 1990; Kun 1998), as well as several molecular outflows (Haikala & Laureijs 1989) and Herbig–Haro objects (Bally et al. 1995).

The elongated cloud consists of three centers of star formation.

(1) The northernmost part is a small, nebulous group of stars, *RNO 129*, associated with IRAS 21004+7811. Bally et al. (1995) found Herbig–Haro emission from *RNO 129*. A detailed study of *RNO 129* can be found in Movsessian & Magakian (2004). Arce & Sargent (2006) included *RNO 129* in their study of the evolution of outflow-envelope interactions in low-mass protostars.

(2) The *L 1228 core* or *L 1228 A* contains the Class I source IRAS 20582+7724. A  $^{13}\text{CO}$  map of the cloud is presented in Miesch & Bally (1994). A dense core, mapped in ammonia by Anglada, Sepúlveda & Gómez (1997), contains at least two sources driving molecular outflows as well as two Herbig–Haro flows, HH 199 and HH 200, revealed by the  $\text{H}\alpha$  image of *L 1228 A*, obtained by Bally et al. (1995) and shown in Fig. 10. HH 199 emerges from IRAS 20582+7724, associated with an east–west oriented infrared reflection nebula (Hodapp 1994; Reipurth et al. 2000). Whereas the molecular outflow and the HH 199 flow have a position angle of about  $60^{\circ}$ , Hodapp (1994) and Bally et al. (1995) found a well-collimated  $\text{H}_2$  emission flow at a position angle of about  $100^{\circ}$ . Either IRAS 20582+7724 is a possibly wide binary where each component is launching a separate flow, or one of the components of a very close binary is precessing rapidly, giving rise to the two very different flow angles. HH 200 is driven by an embedded T Tauri star about 1.5 arcmin further to the northwest (Bally et al. 1995). A low-resolution 3.6 cm survey of the *L 1228* cloud by Rodríguez & Reipurth

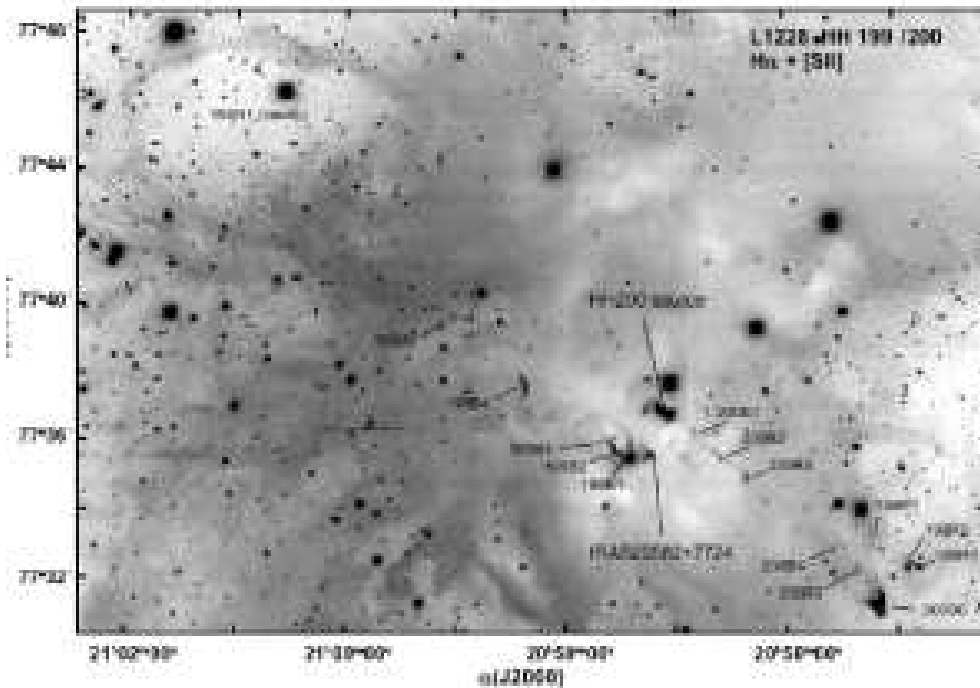


Figure 10.  $H\alpha + [SII]$  image of L 1228 A, based on KPNO 4 m images obtained with the Mosaic 1 prime focus CCD camera through narrow-band  $H\alpha$  and  $[SII]$  filters (80A passband). HH objects discussed in Bally et al. (1995) are marked. (Courtesy of John Bally).

(1996) revealed two sources. L 1228 VLA 1 is associated with the IRAS source, and the other, VLA 2, has no known counterpart but is located in the direction of the high extinction part of the L 1228 core. Reipurth et al. (2004) detected two further 3.6 cm sources, VLA 3 and VLA 4. VLA 4 is supposed to be the driving source of the HH 200 flow. The environment of IRAS 20582+7724 was studied in detail by Tafalla & Myers (1997), Arce & Sargent (2004), and Arce & Sargent (2006).

The  $K'$  image of L 1228 A, presented by Hodapp (1994), shows a star associated with a parabola-shaped nebula, located near the molecular outflow position. Two other stars further north at offsets  $(-21'', 72'')$  and  $(12'', 75'')$  are also associated with some less extended nebulae. The relatively bright stars in this region clearly stand out against the faint background stars, so that Hodapp classified this region as a cluster.

(3) *L 1228 South* contains a small aggregate of low-mass pre-main sequence stars. Padgett et al. (2004) identified 9 infrared sources in the images taken with IRAC on board the *Spitzer Space Telescope* (see Table 7).

*L 1219 (B 175)* is a small cometary shaped cloud at the southernmost edge of the Cepheus Flare cloud complex. The cloud is illuminated by the B9.5V type star BD +69° 1231, associated with the reflection nebula Ced 201 (see Cesarsky et al. 2000, and references therein). Two cold IRAS sources, 22129+7000 and 22127+7014, are projected

within the dark cloud. By an imaging and spectroscopic study Bally & Reipurth (2001) discovered a Herbig-Haro object, HH 450, emerging from IRAS 22129+7000. Furthermore, they found several parsec-scale filaments of emission that trace the rim of a new supernova remnant, G 110.3+11.3, which appears to be approaching the globule (see Figure 11). At 400 pc, G 110.3+11.3 is one of the closest known supernova remnants. The supernova remnant and the HH flow appear to be heading toward a frontal collision in about 1000 yr. Nikolić & Kun (2004) discovered a CO outflow from IRAS 22129+7000. Goicoechea et al. (2008) present Spitzer IRAC and MIPS data, 1.2-mm dust continuum map, as well as observations of several molecular lines for IRAS 22129+7000. They detected a collimated molecular outflow in the CO  $J = 3 - 2$  line, whereas the profile of the HCO<sup>+</sup>  $J = 1 - 0$  line suggested inward motion. Based on the SED they classified the object as either a transition Class 0/I source or a multiple protostellar system. They discuss the role of the photodissociation region associated with Ced 201 in triggering the star formation in L 1219.

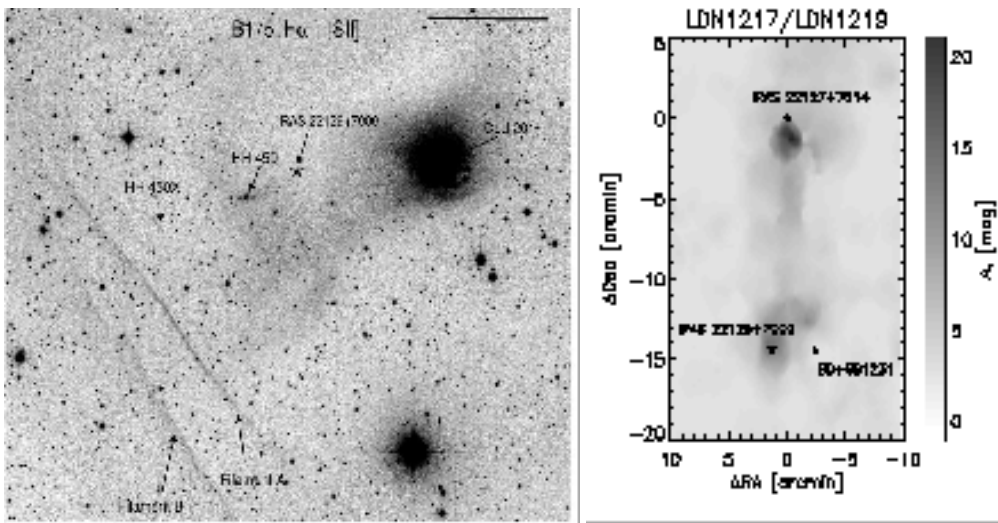


Figure 11. Left: An image of B 175 (L 1219) from Bally & Reipurth (2001). Right: the map of visual extinction, obtained from the 2MASS data using the NICER algorithm of Lombardi & Alves (2001), shows the northern core of the cloud centered on IRAS 22127+7014.

Three known pre-main sequence stars can be found to the south of L 1219: the Herbig Ae stars BH Cep and BO Cep (HBC 734 and 735, respectively) and a T Tauri star, associated with IRAS 22129+6949. The head of the cometary globule with IRAS 22129+7000 is pointing toward south. The embedded source IRAS 22127+7014, located to the north of IRAS 22129+7000, may be the youngest object associated with this cloud. The left panel of Fig. 11 shows the head of the globule B 175 and the supernova filaments, adopted from Bally & Reipurth (2001), and the right panel shows the extinction map of the whole cloud, revealing another core to the north.

*L 1221* is a small, isolated cometary dark cloud to the south of the main body of the Cepheus Flare cloud complex. No distance determination has been published for this cloud. A frequently assumed distance is 200 pc (e.g. Fukui 1989; Umemoto et al.

1991). Inside the cloud, Umemoto et al. (1991) found an unusual U-shaped CO outflow associated with a low-luminosity ( $2.7L_{\odot}$ ) Class I source, IRAS 22266+6845. More recent CO observations at high resolution showed that the U-shaped outflow may actually consist of two bipolar outflows, an east-west outflow associated with the IRAS source and a north-south outflow about  $25''$  to the east of the IRAS source, interacting with each other (Lee et al. 2002). To the south of the IRAS source, a fairly bright compact object, HH 363, is detected in  $H\alpha$  and [S II] (Alten et al. 1997). There are three infrared sources within the error ellipse of the IRAS source: a close binary consisting of an east source and a west source around the IRAS source position and another source  $45''$  to the southeast. The east source is identified as the IRAS source. Furuya et al. (2003) detected  $H_2O$  maser emission associated with IRAS 22266+6845. Lee & Ho (2005) mapped IRAS 22266+6845 in 3.3 mm continuum, CO,  $HCO^+$ , and  $N_2H^+$ . Continuum emission is seen around the east source and the southeast source at 3.3 mm, probably tracing the dust around them. Assuming a temperature of 40 K, the masses of the dust plus gas are estimated to be 0.02 and 0.01  $M_{\odot}$  around the east source and southeast source, respectively. No continuum emission is seen toward the west source. The east-west outflow is likely powered by the east source, which shows a southeast extension along the outflow axis in the  $K'$  image (Connelley et al. 2007). Wu et al. (2007) detected two submillimeter sources in the cloud, L 1221 SMM 1 and L 1221 SMM 2, apparently coinciding with the binary and the southeast source, respectively.

*L 1251* is a cloud elongated east-west at the eastern boundary of the Cepheus Flare molecular complex. Its cometary shape suggests interaction with the supernova bubble described by Grenier et al. (1989). Recent star formation is indicated by two molecular outflows, driven by IRAS 22343+7501 and IRAS 22376+7455, respectively (Sato & Fukui 1989).

The distance of L 1251 was determined by three different methods (see Table 3). The cloud has been mapped in several molecular lines, such as  $^{13}CO$ ,  $C^{18}O$ ,  $H^{13}CO^+$ , SiO (Sato et al. 1994),  $NH_3$  (Benson & Myers 1989; Tóth & Walmsley 1996), HNC, HCN,  $HCO^+$ , CS (Nikolić, Johansson, & Harju 2003). Kun & Prusti (1993) studied the YSO population and reported on 12  $H\alpha$  emission stars and IRAS point sources as YSO candidates. Balázs et al. (1992) discovered an optical jet, HH 149, originating from IRAS 22343+7501. Rosvick & Davidge (1995) found that this IRAS source is associated with a cluster of five near-infrared sources spread over a  $10' \times 10'$  area (sources A–E). Meehan et al. (1998) found two thermal radio continuum sources, VLA A and VLA B, coinciding with the near infrared sources D and A, respectively. Beltrán et al. (2001) found 9 radio continuum sources around IRAS 22343+7501, two of them, VLA 6 and VLA 7 separated by  $7''$ , are located within the error ellipse of the IRAS source and identical with Meehan et al.'s VLA A and VLA B, respectively. Beltrán et al. found a third source, VLA 5 to be a probable YSO, based on the positive spectral index. Nikolić et al. (2003) concluded that both VLA 6 and VLA 7 are protostars driving their own outflow.

The high resolution VLA observations by Reipurth et al. (2004) revealed four radio continuum sources in the region around IRAS 22343+7501, three of which were known from previous studies. The high resolution VLA A map has revealed a new source, VLA 10, close to VLA 6, with which it was blended in the earlier low-resolution data of Meehan et al. (1998). The designations VLA 10 and 11 is a continuation of the numbering scheme of Beltrán et al. (2001). Meehan et al. (1998) suggest that VLA 6

corresponds to the very red and embedded source IRS D, while VLA 7 is the brighter source IRS A.

Eiroa et al. (1994) discovered a chain of Herbig–Haro objects, HH 189A,B,C near IRAS 22376+7455 (L 1251 B). The Spitzer Space Telescope observed L 1251 B as part of the Legacy Program *From Molecular Cores to Planet Forming Disks* (Evans et al. 2003) at wavelengths from 3.6 to 70  $\mu\text{m}$ . The observations revealed a small cluster of protostars, consisting of 5 Class 0/I and 14 Class II objects (Lee et al. 2006). Three Class 0/I objects are projected on IRAS 22376+7455, the most luminous is located 5'' north of the IRAS position. Thus the molecular outflow observed from IRAS 22376+7455 (Sato & Fukui 1989) is probably a combined effect of more outflows. Lee et al. (2007) studied the complex motions in the region, based on both single-dish and interferometric molecular line observations. The data have shown very complex kinematics including infall, rotation, and outflow motions. The well-known outflow, associated with L 1251 B, was resolved into a few narrow and compact components. They detected infall signatures in the shape of HCO<sup>+</sup>, CS, and HCN lines to the east of L 1251 B, where no infrared object has been detected, and an extended emission has been found at 850  $\mu\text{m}$ . This result shows that, in addition to the Class 0–Class II objects, the young cluster contains a pre-protostellar core as well. Results of spectroscopic follow-up observations of the optically visible candidate YSOs reported by Kun & Prusti (1993) are given in Eredics & Kun (2003). Simon (2006) detected 41 X-ray sources in the image obtained with the XMM-Newton telescope. The list of X-ray sources contains both outflow sources and 8 optically visible T Tauri stars.

The structure of the cloud and the properties of its dust grains were studied, based on optical extinction maps, by Kandori et al. (2003) and Balázcs et al. (2004).

Young et al. (2006) and Wu et al. (2007) observed submm sources associated with the dense cores L 1251 A, B, and C.

*L 1261/L 1262 (CB 244)* are small clouds to the east of the main body of the Cepheus Flare cloud complex, at a probable distance of 180 pc from the Sun (Kun 1998). Two young, low luminosity objects, the G2 type classical T Tauri star HBC 741 (AS 507) and the cold IRAS source IRAS 23238+7401 are projected on the cloud. A CO outflow centered on IRAS 23238+7401 was found by Parker et al. (1988). Wolf et al.'s (2003) submillimeter polarization measurements resulted in a magnetic field strength of 257  $\mu\text{G}$  for the envelope of CB 244.

## 2.5. NGC 7129

Though NGC 7129 lies in the Cepheus Flare, it is more distant than the clouds discussed above. NGC 7129 (Ced 196) is a reflection nebula in the region of a young cluster, containing three B-type stars, namely BD +65°1637, BD +65°1638, and LkH $\alpha$  234, as well as several low-mass pre-main sequence stars (e.g. Herbig 1960; Strom, Vrba & Strom 1976; Cohen & Schwartz 1983; Magakian, Movsessian & Nikogossian 2004, see Table 7). Whereas BD +65°1638 is regarded a young main sequence star (but see Matthews et al. 2003), BD +65°1637 and LkH $\alpha$  234 are pre-main sequence stars (Herbig 1960; Hernández et al. 2004). An optical image of NGC 7129, displaying several spectacular signposts of the interactions between the young stars and their environments, is shown in Fig. 12. A finding chart for the most prominent objects, related to star formation, is displayed in Fig. 13.





Figure 12. An optical image of NGC 7129, displaying the young cluster, embedded in a reflection nebula, as well as several HH objects. The size of the area is about  $15' \times 18'$ . Photograph by Robert Gendler.

*LkH $\alpha$  234 and its environments* It has been suggested that LkH $\alpha$  234 is the youngest among the three B-type stars (Hillenbrand et al. 1992). This star and its environment have been studied extensively at optical, infrared, radio, centimeter to submillimeter wavelengths. Photometric and spectroscopic variability of LkH $\alpha$  234 have been studied by Shevchenko et al. (1991) and Chakraborty & Mahadevan (2004), respectively.

Wilking et al. (1986) presented high-resolution continuum and molecular-line observations of the circumstellar environment of LkH $\alpha$  234. Sandell & Olofsson (1981) and Tofani et al. (1995) detected three H<sub>2</sub>O maser sources from the environment of LkH $\alpha$  234. Ray et al. (1990) identified an optical jet originating from this region. Mitchell & Matthews (1994) detected a molecular jet associated with LkH $\alpha$  234, and Schultz et al. (1995) observed shocked molecular hydrogen in the LkH $\alpha$  234 region. VLA observations by Trinidad et al. (2004) of water masers and radio continuum emission at 1.3 and 3.6 cm show that the LkH $\alpha$  234 region contains a cluster of YSOs. In a field of  $\sim 5''$  they detected five radio continuum sources (VLA 1, VLA 2, VLA 3A, VLA 3B, and LkH $\alpha$  234) and 21 water maser spots. These water masers are mainly distributed in three clusters associated with VLA 1, VLA 2, and VLA 3B. The VLA observations suggest that there are at least four independent, nearly parallel outflows in the LkH $\alpha$  234 region. Probably all sources observed in this region ( $\sim 5''$  in diameter) form a cluster of YSOs, which were born inside the same core in the NGC 7129 molecular cloud. This fact could explain that the major axes of the outflows have nearly the same orientation. Marvel (2005) performed VLBI observations of maser sources around LkH $\alpha$  234, and detected maser emission associated with LkH $\alpha$  234–VLA 2 and LkH $\alpha$  234–VLA 3b. No maser source associated with LkH $\alpha$  234 itself has been detected.

Tommasi et al. (1999) obtained far-infrared spectra of the LkH $\alpha$  234 region, using the Long Wavelength Spectrograph of ISO. The observed spectra are consistent with a photodissociation region, associated with not LkH $\alpha$  234, but with BD +65° 1637. Morris et al. (2004) have obtained mid-IR spectroscopy of regions around LkH $\alpha$  234, with the Spitzer Space Telescope Infrared Spectrograph (IRS). They detected warm material at 16  $\mu$ m around BD +65° 1638 which clearly shows that this region is not free of gas and dust. Wang & Looney (2007) identified a group of low-mass young stars around LkH $\alpha$  234 using the *Spitzer* data base.

*Interstellar matter associated with NGC 7129* Molecular line observations of the region (Bechis et al. 1978; Font, Mitchell & Sandell 2001; Miskolczi et al. 2001; Ridge et al. 2003) revealed a kidney-shaped molecular cloud of about 11 pc in extent to the east and south of the cluster. BD +65° 1637 and most of the fainter cluster members are found in a cavity of the cloud, bordered by a prominent molecular ridge, while LkH $\alpha$  234, located to the east of the main cluster, is associated with a peak of <sup>13</sup>CO emission. The optical jet detected by Ray et al. (1990) is pointing southwest into the cavity. Torrelles et al. (1983) and Güsten & Marcaide (1986) presented ammonia observations of NGC 7129.

Matthews et al. (2003) observed the region in the 21 cm line of HI with an angular resolution of 1'. The observations revealed a ring of HI emission about 30' in extent. The HI ring appears to be part of the surface of a molecular cloud and is centered on a relatively dense concentration of HI with unusually wide line profiles and positionally coincident with BD +65° 1638. An infrared point source, IRAS 21418+6552, coincides within the positional errors with the HI knot.

A continuum source coincident with BD +65° 1638 has also been detected at 1420 MHz, which shows a significant extension to the northeast overlapping the position of LkH $\alpha$  234. Comparing the radio continuum data with other radio observations of BD +65° 1638, Matthews et al. (2003) found that BD +65° 1638 has a flat centimeter-wave spectrum, consistent with an optically thin H II region around the star. The authors conclude that the physical association of the star with the HI knot indicates that



luminosity of  $430 L_{\odot}$ , a dust temperature of 35 K, and a mass of  $6 M_{\odot}$ . The low dust temperature and the low  $L_{\text{bol}}/L_{1.3 \text{ mm}}$  ratio of this source suggest that it is an intermediate mass counterpart of Class 0 sources. Fuente, Neri & Caselli (2005a) detected a hot molecular core associated with FIRS 2, and Fuente et al. (2005b) carried out a molecular survey of FIRS 2 and LkH $\alpha$  234 with the aim of studying the chemical evolution of the envelopes of intermediate-mass young stellar objects. Fuente (2008) present high angular resolution imaging of the hot core of NGC 7129 FIRS 2, using the Plateau de Bure Interferometer. This is the first chemical study of an intermediate-mass hot core and provides important hints to understand the dependence of the hot core chemistry on the stellar luminosity.

Two molecular outflows were found in NGC 7129 by Edwards & Snell (1983). They seem to be associated with LkH $\alpha$  234 and FIRS 2. Weintraub et al. (1994), via near infrared polarimetry, identified a deeply embedded source, NGC 7129 PS 1, located about  $3''$  northwest of LkH $\alpha$  234. This source was not identified in the direct near-infrared images of LkH $\alpha$  234, which revealed 5 sources (IRS 1–IRS 5, IRS 1  $\equiv$  LkH $\alpha$  234) in a  $20'' \times 20''$  field centered on LkH $\alpha$  234. Weintraub et al. (1996) detected NGC 7129 PS 1 at  $3.8 \mu\text{m}$ , and proposed that it was the actual outflow source instead of LkH $\alpha$  234.

Cabrit et al. (1997) present high-resolution imaging of the region around LkH $\alpha$  234 in the  $10 \mu\text{m}$  and  $17 \mu\text{m}$  atmospheric windows and in the H $_2$   $v=1-0$  S(1) line and adjacent continuum. The cold mid-infrared companion, detected at  $2.7''$  to the north-west of the optical star, corresponds to NGC 7129 PS 1. The companion illuminates an arc-shaped reflection nebula with very red colors, and is associated with a radio continuum source, H $_2$ O masers, and a bright extended H $_2$  emission knot, indicating that it is deeply embedded and has strong outflow activity. Cabrit et al. (1997) refer to this star as IRS 6, extending Weintraub et al.'s notation.

Fuente et al. (2001) obtained single-dish and interferometric continuum images at 2.6 mm and 1.3 mm of both FIRS 2 and LkH $\alpha$  234. They identified two millimeter sources associated with FIRS 2: FIRS 2–MM1, apparently associated with the CO outflow, and a weaker source, FIRS 2–MM2, which does not present any sign of stellar activity. The interferometric 1.3 mm continuum image of FIRS 1 reveals that LkH $\alpha$  234 is a member of a cluster of embedded objects. Two millimeter clumps are associated with this far-infrared source. The stronger is spatially coincident with IRS 6. A new millimeter clump, FIRS 1–MM1, is detected at an offset ( $-3.23''$ ,  $3.0''$ ) from LkH $\alpha$  234. The extremely young object FIRS 1–MM1 (it has not been detected in the near- and mid-infrared) is the likely driving source of the H $_2$  jet. There is no evidence for the existence of a bipolar outflow associated with LkH $\alpha$  234. In addition to FIRS 1 and FIRS 2, six other compact millimeter clumps are detected in the region, NGC 7129 MM1 to MM5 (see Fig. 13), and the sixth coincides with the bipolar nebula RNO 138.

Submillimeter continuum observations by Font et al. (2001) revealed three compact sources: LkH $\alpha$  234 SMM 1, LkH $\alpha$  234 SMM 2 and FIRS 2. SMM 1 coincides with IRS 6, which, according to the submillimeter observations, may be a deeply embedded Herbig Be star, whereas SMM 2 is a newly discovered source (see Figure 14). Table 8 shows the coordinates, wavelengths of detection, measured fluxes and sizes of the deeply embedded young stellar objects in NGC 7129, observed in submillimeter, millimeter, and centimeter continuum.

*Low-mass pre-main sequence members of NGC 7129* were identified as H $\alpha$  emission objects by Hartigan & Lada (1985), Miranda et al. (1993), and Magakian et al.

Table 8. Embedded YSOs in NGC 7129.

Name	RA(2000)	Dec(2000)	$\lambda$ (mm)	Flux(mJy)	Ref.
NGC 7129 FIRS1 IRS6	21 43 06.4	66 06 55.6	2.6	91	1
NGC 7129 FIRS1 IRS6	21 43 06.5	66 06 55.2	1.3	313	1
NGC 7129 FIRS1 MM 1	21 43 06.3	66 06 57.4	1.3	180	1
LkH $\alpha$ 234	21 43 06.8	66 06 54.4	1.3	< 20	1
NGC 7129 FIRS2 MM 1	21 43 01.7	66 03 23.6	2.6	72	1
	21 43 01.7	66 03 23.6	1.3	381	1
NGC 7129 FIRS2 MM 2	21 43 01.6	66 03 26.1	2.6	22	1
	21 43 01.7	66 03 24.7	1.3	137	1
NGC 7129 FIRS2 IR	21 43 01.8	66 03 27.4	2.6	<15	1
	21 43 01.8	66 03 27.4	1.3	<19	1
NGC 7129 FIRS 1	21 43 06.5	66 06 52.3	1.3	690	1
	21 43 06.5	66 06 52.3	1.3	4283	1
NGC 7129 FIRS 2	21 43 01.4	66 03 22.3	1.3	597	1
	21 43 01.4	66 03 22.3	1.3	2613	1
NGC 7129 MM 1	21 42 57.9	66 05 21.4	1.3	96	1
NGC 7129 MM 2	21 42 58.7	66 05 34.5	1.3	89	1
NGC 7129 MM 3	21 42 38.1	66 06 50.2	1.3	62	1
NGC 7129 MM 4	21 43 23.7	66 08 29.0	1.3	60	1
NGC 7129 MM 5	21 43 26.3	66 03 24.7	1.3	29	1
RNO 138	21 42 57.6	66 04 26	1.3	22	1
LkH $\alpha$ 234 SMM 1	21 43 06.76	66 06 56.0	0.85	3120	2
LkH $\alpha$ 234 SMM 1	21 43 06.76	66 06 56.0	0.45	20700	2
LkH $\alpha$ 234 SMM 2	21 43 03.20	66 07 13.1	0.85	730	2
LkH $\alpha$ 234 SMM 2	21 43 03.20	66 07 13.1	0.45	6200	2
NGC 7129 FIRS 2	21 43 01.51	66 03 24.2	0.85	3350	2
NGC 7129 FIRS 2	21 43 01.51	66 03 24.2	0.45	18100	2
NGC 7129 VLA 1	21 43 06.093	66 06 58.13	36.0		3
NGC 7129 VLA 1			13.0		3
NGC 7129 VLA 2	21 43 06.321	66 06 55.95	36.0	0.1	3
NGC 7129 VLA 2			13.0	<0.33	3
NGC 7129 VLA 3A	21 43 06.479	66 06 55.02	36.0	0.67	3
NGC 7129 VLA 3A			13.0	1.96	3
NGC 7129 VLA 3B	21 43 06.462	66 06 55.22	36.0	0.61	3
NGC 7129 VLA 3B			13.0	1.19	3

References: 1: Fuente et al. (2001); 2: Font et al. (2001); 3: Trinidad et al. (2004)

(2004), as variable stars (Semkov 2003) and near-infrared sources (Strom et al. 1976; Cohen & Schwartz 1983). Muzerolle et al. (2004) presented observations of NGC 7129 taken with the *Multiband Imaging Photometer for Spitzer* (MIPS). A significant population of sources, likely pre-main sequence members of the young stellar cluster, have been revealed outside the central photoionization region. Combining *Infrared Array Camera* (IRAC) and ground-based near-infrared images, Gutermuth et al. (2004) obtained colors and spectral energy distributions for some 60 objects. Most of the pre-main sequence candidates are associated with the densest part of the molecular cloud, indicating active star formation over a broad (some 3 pc) area outside the central cluster.

A remarkable object is the small bipolar nebula RNO 138, located at the southern edge of NGC 7129. Several authors (Cohen & Schwartz 1983; Draper et al. 1984) suggest that the T Tauri star SVS 6, located 15'' NE of RNO 138, is the illuminating source. However, Miranda et al. (1994) report that a star within the nebulosity, RNO 138 S, appeared as an optically visible object in 1993. It brightened by  $\sim 1.2$  mag

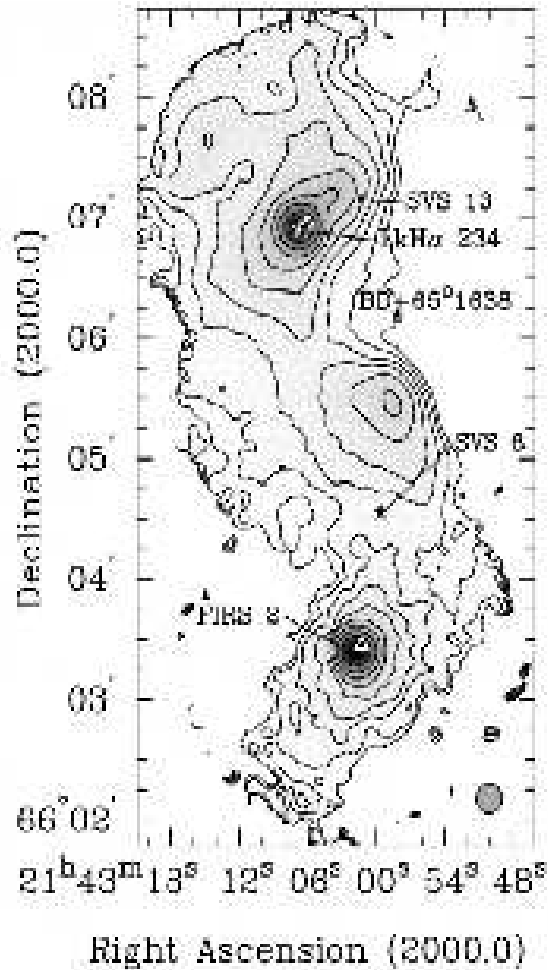


Figure 14. Dust continuum emission of NGC 7129, observed at  $850\ \mu\text{m}$  by Font et al. (2001). Near-infrared sources are marked by star symbols, and H<sub>2</sub>O maser sources by triangles.

between 1988 and 1993. The Li I absorption characteristic of young low-mass stars and P Cygni profile of the H $\alpha$  line were recognized in the optical spectrum of RNO 138 S. Miranda et al. (1994) suggest that RNO 138 S, probably a FUor, is the illuminating source of RNO 138. Another interesting star is V350 Cep (denoted as IRS 1 by Cohen & Schwartz 1983), which brightened about 4 mag in the 1970's (Semkov 2004), and has been staying at the high level since then. Liseau & Sandell (1983) detected CO outflows associated with both RNO 138 and V350 Cep. Herbig (2008) has shown that V350 Cep does not belong to the class of the EXor-type eruptive young stars. The list of low-mass pre-main sequence stars in NGC 7129, based on a literature search, is given in Table 7.

*Herbig-Haro objects* In the optical, a large number of HH-objects in and near NGC 7129 have been reported (Gyulbudaghian, Glushkov & Denisyuk 1978; Hartigan & Lada

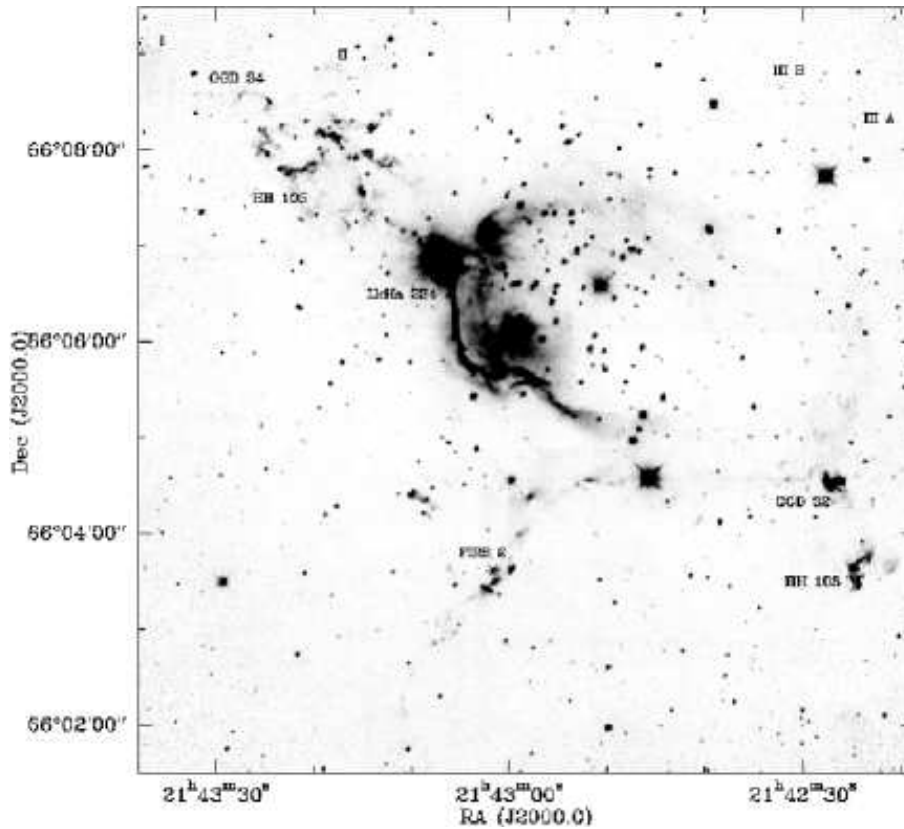


Figure 15. Mosaic of the NGC 7129 region in the 1-0 S(1) line of  $H_2$  + cont. at  $2.12 \mu\text{m}$ , adopted from Eislöffel (2000). Emission from several molecular outflows, as well as from a probable photodissociation region to the east and south of the stellar cluster can be seen. Some  $H_2$  outflows and  $H_2$  counterparts of optical Herbig–Harro objects are labeled.

1985; Eiroa, Gómez de Castro & Miranda 1992; Gómez de Castro, Miranda & Eiroa 1993; Miranda, Eiroa, & Birkle 1994; Gómez de Castro & Robles 1999, see Table 9). Molecular hydrogen emission in the near-infrared has been detected from several of the optical Herbig–Harro objects (Wilking et al. 1990). An infrared search for the exciting sources of the optical HH objects was presented by Cohen & Schwartz (1983). Spectroscopic observations of HH objects are presented by Cohen & Fuller (1985). Fuente et al. (2001) suggest that NGC 7129 MM4 is the illuminating star of the nebular object GGD 34. Eislöffel (2000) used deep imaging in the near-infrared 1-0 S(1) line of  $H_2$  at  $2.12 \mu\text{m}$  to search for parsec-scale outflows in NGC 7129 (Fig. 15). They identified numerous outflows (see Table 9), but likely driving sources could be identified for only three of them. For most of the other emission-line knots and molecular flows no evident sources could be identified. The Spitzer observations revealed several distinct outflow arcs, traced by  $4.5 \mu\text{m}$  bright knots, associated with FIRS 2 (Muzerolle et al. 2004). The multipolar nature of this outflow system, in general agreement with the outflow analysis of Fuente et al. (2001), supports the claim by Miskolczi et al. (2001) that FIRS 2 is a multiple protostellar system.

Table 9. Herbig–Haro objects in NGC 7129.

name	RA(2000)	Dec(2000)	Source	Reference
HH 822	21 41 42.1	+66 01 45	LkH $\alpha$ 234	5
HH 103A	21 42 23.8	+66 03 47	LkH $\alpha$ 234	5,13
HH 103B	21 42 24.7	+66 03 40	LkH $\alpha$ 234	1,13
HH 232, GGD 32	21 42 26.9	+66 04 27		6,8
HH 242	21 42 38.7	+66 06 36		6,10,12
HH 825	21 42 39.2	+66 10 56	IRAS 21416+6556	5
HH 238	21 42 40.3	+66 05 41	LkH $\alpha$ 234	6,10
HH 237	21 42 42.3	+66 05 23	LkH $\alpha$ 234	6,10
HH 239	21 42 44.1	+66 06 37	LkH $\alpha$ 234	6,10
HH 824	21 42 56.9	+66 09 10	IRAS 21416+6556	4,10
HH 236	21 42 59.2	+66 07 39	LkH $\alpha$ 234	6,10
HH 233, GGD 33	21 43 00.0	+66 12 00	GGD 33a	1,3,13
HH 167	21 43 06.7	+66 06 54	LkH $\alpha$ 234	4
HH 105B	21 43 19.8	+66 07 53	LkH $\alpha$ 234	1,6,9
HH 105A	21 43 22.1	+66 07 47	LkH $\alpha$ 234	1,6,9
HH 823	21 43 27.9	+66 11 46		4
HH 234	21 43 29.7	+66 08 38		6
GGD 34	21 43 30.4	+66 03 43	NGC 7129 MM 4	1,2,7,11
HH 235, GGD 35	21 43 42.0	+66 09 00		6,8,13
HH 821	21 43 43.4	+66 08 47	LkH $\alpha$ 234	5
HH 820	21 43 47.9	+66 09 50	LkH $\alpha$ 234	5
HH 818	21 43 57.7	+66 10 26	LkH $\alpha$ 234	5
HH 819	21 44 01.0	+66 09 52	LkH $\alpha$ 234	5
HH 817	21 44 13.3	+66 10 55	LkH $\alpha$ 234	5
HH 816	21 44 26.4	+66 10 58	LkH $\alpha$ 234	5
HH 815	21 44 29.9	+66 13 42	LkH $\alpha$ 234	5

References: 1 – Eiroa, Gómez de Castro & Miranda (1992); 2 – Gómez de Castro & Robles (1999); 3 – Miranda, Eiroa, & Birkle (1994); 4 – Moreno-Corral, Chavarría-K., & de Lara (1995); 5 – McGroarty et al. (2004); 6 – Wu et al. (2002); 7 – Gómez de Castro et al. (1993); 8 – Cohen & Schwartz (1983); 9 – Hartigan & Lada (1985); 10 – Miranda et al. (1993); 11 – Fuente et al. (2001); 12 – Avila et al. (2001); 13 – Cohen & Fuller (1985).

### 3. Star Formation in the Association Cep OB2

The association Cep OB2 was discovered by Ambartsumian (1949). Simonson (1968) identified 75 bright members, including the runaway O6 Iab star  $\lambda$  Cep (HIP 109556). The clusters NGC 7160 and Trumpler 37 (Tr 37), with its associated H II region IC 1396 (Fig. 16), have similar distances as Cep OB2, about 800 pc. Simonson & van Someren Greve (1976) suggested the division of Cep OB2 into two subgroups. The younger subgroup, Cep OB2b is Tr 37, one of the youngest known open clusters, with an age of 3.7 Myr (e.g., Marschall, Karshner & Comins 1990). Garrison & Kormendy (1976) suggested that the bright star  $\mu$  Cep (HIP 107259, M2 Ia) is a member of Tr 37. The main source of excitation of IC 1396 is the O6 star HD 206267 (HIP 106886), a Trapezium-like system (Harvin 2004). IC 1396 and neighboring areas contain a large number of H $\alpha$  emission objects (e.g. Kun 1986; Kun & Pásztor 1990; Balázs et al. 1996), classical T Tauri stars (Sicilia-Aguilar et al. 2004, 2005) and several globules containing embedded young stellar objects (e.g., Duvert et al. 1990; Schwartz, Wilking & Gyulbudaghian 1991). The other subgroup, Cep OB2a, contains a large number of evolved massive stars that are



spread over a large area, between  $100^\circ \leq l \leq 106^\circ$  and  $+2^\circ \leq b \leq +8^\circ$ . The age of this subgroup is about 7-8 Myr, and contains NGC 7160. This subgroup is surrounded by a  $9^\circ$  diameter infrared emission ring, the Cepheus Bubble (see Fig. 2), which possibly resulted from a supernova explosion (Kun et al. 1987). This supernova might have triggered star formation in the ring, as suggested by the presence of several H II regions, and a number of infrared sources that have the characteristics of embedded young stellar objects (Balázs & Kun 1989).



Figure 16. Optical image of the HII region IC 1396. Color composite by Davide De Martin.

De Zeeuw et al. (1999) determined the distance of Cep OB2, based on Hipparcos results on 76 members (one O, 56 B, 10 A, five F, one G, two K, and one M type stars). They obtained a mean distance of  $615 \pm 35$  pc.

Daflon et al. (1999) studied the chemical abundances of OB stars in Cep OB2. Their results indicate that this association is slightly metal-poor. The highest mass association members have been involved in several studies of the interstellar matter in the region of the association. Clayton & Fitzpatrick (1987) detected anomalous dust in the region of Tr 37, by studying the far-ultraviolet extinction curves of 17 early-type stars. In order to measure the value of  $R_V = A_V/E_{B-V}$ , Roth (1988) combined near-infrared photometry of OB stars with existing optical and ultraviolet data of the same sample. The results suggest anomalous grain size distribution with respect to an average Galactic extinction curve. Morbidelli et al. (1997) performed *VRIJHK* photometry of 14 bright cluster members. They obtained the normal Galactic value of  $R_V = 3.1$ .

In order to establish the velocity structure and column density of the interstellar matter in the region of Cep OB2, Pan et al. (2004; 2005) studied several interstellar absorption lines in high resolution spectra of early-type association members. Their results are consistent with the large-scale structure suggested by radio molecular maps, and suggest significant variations in the column density on small ( $\sim 10000$  AU) scales.

Cep OB2 was mapped in the 21 cm line of HI by Simonson & van Someren Greve (1976). They detected an HI concentration of  $2 \times 10^4 M_\odot$  surrounding the HII region and bright-rimmed dark clouds associated with Cep OB2b, and found no significant amount of neutral hydrogen associated with Cep OB2a. Wendker & Baars (1980) constructed a three-dimensional model of the ionized region based on a 2695 MHz radio continuum map. The first molecular study of IC 1396 was performed by Loren, Peters & Vanden Bout (1975). Heske & Wendker (1985) surveyed the dark clouds of IC 1396 in the 6 cm absorption line of the  $H_2CO$ . Large-scale  $^{12}CO$  and  $^{13}CO$  mapping of the dark clouds in IC 1396 are presented by Patel et al. (1995) and Weikard et al. (1996). Both IC 1396 and NGC 7160 have been included in the CO survey of regions around 34 open clusters performed by Leisawitz, Bash, & Thaddeus (1989).

The low and intermediate mass members of Cep OB2 belong to different populations, born in various subgroups during the lifetime of the association. Significant low mass populations, born together with and thus nearly coeval with the high luminosity members, are expected in both Cep OB2b and Cep OB2a. Younger subgroups are being born in the clouds bordering the HII region IC 1396, due to triggering effects by the luminous stars of Cep OB2b.

### 3.1. Pre-main Sequence Stars in the Open Cluster Tr 37

Marschall & van Altena (1987) derived kinematic membership probabilities for stars of Tr 37, and identified 427 probable members. Marschall et al. (1990) performed  $UBV(RI)_C$  photometry of 120 members, most of them brighter than  $V \approx 13.5$ . Their HR diagram indicated a number of probable pre-main sequence members.

During a search for intermediate mass pre-main sequence members of Tr 37, Contreras et al. (2002) found three emission-line stars (MVA 426, MVA 437, and Kun 314S). They suggest that the low frequency of emission-line activity in the sample of B–A type stars indicates that inner disks around intermediate-mass stars evolve faster than those of low-mass stars.

Sicilia-Aguilar et al. (2004), based on spectroscopic and photometric observations of candidate objects, presented the first identifications of low-mass (spectral types K–

M) pre-main sequence members of Tr 37 and NGC 7160. They expanded the studies in a second paper (Sicilia-Aguilar et al. 2005). In all, they identified and studied 130 members of Tr 37, and  $\sim 30$  for NGC 7160. They confirmed previous age estimates of 4 Myr for Tr 37 and 10 Myr for NGC 7160, and found active accretion in  $\sim 40\%$  of the stars in Tr 37, with average accretion rates of  $10^{-8} M_{\odot} \text{yr}^{-1}$ , derived from their U-band excesses. These results expand the existing samples of accreting stars. Only 1 accreting star was detected in the older cluster NGC 7160, suggesting that disk accretion ends before the age of 10 Myr.

In order to follow the evolution of protoplanetary accretion disks through the ages  $\sim 3$ –10 Myr, Sicilia-Aguilar et al. (2006a) utilized the wavelength range 3.6–24  $\mu\text{m}$ , offered by the *IRAC* and *MIPS* instruments of the *Spitzer Space Telescope*. They found detectable disk emission in the *IRAC* bands from 48% of the low mass stars of Tr 37. Some 10% of these disks have been detected only at wavelengths  $> 4.5 \mu\text{m}$ , indicating optically thin inner disks. Comparison of the SEDs of Tr 37 members with those of the younger Taurus region indicates that the decrease of infrared excess is larger at 6–8  $\mu\text{m}$  than at 24  $\mu\text{m}$ , suggesting that disk evolution is faster at smaller radii.

Sicilia-Aguilar et al. (2004, 2005) also investigated the spatial asymmetries in Tr 37 and the possible presence of younger populations triggered by Tr 37 itself. They found a spatial east-west asymmetry in the cluster that cannot yet be fully explained. The low-mass Tr 37 members are concentrated on the western side of the O6 star HD 206267. In contrast, the B-A stars (Contreras et al. 2002) are more uniformly distributed, with a small excess to the east. Both the high and intermediate-mass stars and the low-mass stars show a clear “edge” to the east of HD 206267. The youngest stars are found preferentially on the western side of HD 206267. The presence of dense globules in this region suggests that the expansion of the HII region into an inhomogeneous environment triggered this later epoch of star formation. Larger amounts of interstellar material on the western side may also have helped to shield disk systems from the photoevaporating effects of the central O6 star.

Sicilia-Aguilar et al. (2006b) obtained high-resolution spectra of a large number of stars in the region of Tr 37. They derived accretion rates from the  $H\alpha$  emission line, and found lower average accretion rate in Tr 37 than in the younger Taurus. They used radial velocities as membership criterion, and thus confirmed the membership of 144 stars and found 26 new members. They also calculated rotational velocities, and found no significant difference between the rotation of accreting and non-accreting stars. In order to study the dust evolution in protoplanetary disks, Sicilia-Aguilar et al. (2007) studied the 10  $\mu\text{m}$  silicate feature in the Spitzer IRS spectra of several members of Tr 37. GM Cep, a solar-type member of Tr 37 exhibiting EXor-like outbursts, was studied in detail by Sicilia-Aguilar et al. (2008).

Tr 37 was searched for X-ray sources as possible WTTs by Schulz, Berghöfer & Zinnecker (1997). Soft X-ray observations with the ROSAT PSPC revealed X-ray emission from an area of 30' radius around the center of globule IC 1396A, which was resolved into 85 discrete sources of which 13 sources were identified as foreground objects. Most of the detected X-ray sources, except HD 206267, are very weak, which causes the measured luminosity function to be cut off at  $\log L_x < 30.3 \text{ erg s}^{-1}$ . X-ray sources are located not only in Tr 37 but are also scattered around the molecular globules IC 1396A and B (see Sect. 3.2.). Their X-ray spectra appear hard with luminosities between  $\log L \sim 30$  and 31. LkH $\alpha$  349, a  $10^5$  yr old pre-main sequence star at the very center of globule A,

appears very luminous with  $L_x = 5.1 \times 10^{30} \text{ erg s}^{-1}$ . The source density within  $5'$  of the center of emission is 270 sources per square degree.

Getman et al. (2007) detected 117 X-ray sources in a field centered on the globule IC 1396N (see Sect. 3.2.), of which 50-60 are likely members of Trumpler 37.

Table 10. A. Bright rimmed globules and dark clouds associated with IC 1396.

Names	RA(J2000) [h m]	D(J2000) [ $^{\circ}$ ' ]	IRAS Source	Ref.
FSE 12	21 25	57 53		
FSE 13	21 25	58 37		
FSE 1, IC 1396 W	21 26	57 58	21246+5743	4,14,16,17
FSE 14, LDN 1086	21 28	57 31		
BRC 32	21 32 24	57 24 08	21308+5710	
BRC 33, Pottasch IC 1396C	21 33 12	57 29 33	21316+5716	
BRC 34, GRS 3, Pottasch IC 1396D	21 33 32	58 03 29	21320+5750	
GRS 1	21 32 25	57 48 44		
FSE 2, GRS 2	21 33 54	57 49 44	21312+5736	
FSE 15	21 33	59 30		
FSE 16, LDN 1102	21 33	58 09		
FSE 3, LDN 1093, LDN 1098, GRS 4, Pottasch IC 1396B	21 34 11	57 31 06	21324+5716	29
Weikard Rim I	21 34 35	58 19.5		
FSE 4, Pottasch IC 1396A, GRS 6, BRC 36	21 36 12	57 27 34	21346+5714	5,6,7,14,19, 29,32,33
GRS 5, BRC 35	21 36 05	58 32 17	21345+5818	
FSE 5, LDN 1099, LDN 1105, GRS 6	21 36 54	57 30	21352+5715	
FSE 6, LDN 1116	21 37	58 37	21354+5823	
FSE 17, LDN 1088, GRS 9	21 38 56	56 07 36		
GRS 7	21 37 56	57 47 57		
Weikard Rim J	21 38 56	56 21.3		
FSE 7, GRS 12, BRC 37, Pottasch IC 1396H	21 40 25	56 35 52	21388+5622	8,9,10,11,14,20, 25,28,31,33,34
WB89 108	21 40 38	56 48	21390+5634	
GRS 13	21 40 30	57 46 28		
GRS 14	21 40 41	58 15 52		
FSE 19, IC 1396 N(orth), LDN 1121, GRS 14, WB89 110, BRC 38, Pottasch IC 1396E	21 40 43	58 20 09	21391+5802	1,2,3,13,14,15, 18,25,30,32
FSE 8, GRS 20, LDN 1130, Pottasch IC 1396F	21 44 00	58 17 00	21428+5802	29
GRS 26	21 44 51	57 08 00		
GRS 23	21 45 05	56 59 22	21443+5646	
GRS 24	21 45 09	56 47 52		
LDN 1132	21 45 45	58 29.3		
GRS 25, WB89 122	21 45 58	57 13 54	21436+5657	
GRS 27	21 46 03	57 08 41		
GRS 28	21 46 27	57 18 07		
FSE 9, IC 1396 E(ast), WB89 123, LDN 1118, GRS 29, BRC 39, Pottasch IC 1396 G	21 46 38	57 25 55	21445+5712	14,21,25,33
BRC 40	21 46 14	57 08 59	21446+5655	
BRC 41	21 46 29	57 18 41	21448+5704	
BRC 42	21 46 37	57 12 25	21450+5658	
FSE 21, LDN 1129	21 46 27	57 46 37		
FSE 22	21 49	56 43		

References to globule names and column 5 can be found under Table 10 B.

Table 10. B. Other clouds in the IC 1396 region whose relation to Cep OB2 is uncertain.

Names	RA(J2000) [h m]	D(J2000) [ $^{\circ}$ ' ]	IRAS source	Ref.
FSE 18, LDN 1131	21 40	59 34		
FSE 20, LDN 1131	21 41	59 36		
FSE 10, LDN 1139	21 55 36	58 35	21539+5821	14
FSE 23, LDN 1153	22 01	58 54		
FSE 11, LDN 1165, LDN 1164	22 07 00	59 02	22051+5848	
GRS 32, LDN 1165	22 07 00	59 00	22051+5848	12,14,15,22,23, 24,25,26,27,28
FSE 24, LBN 102.84+02.07	22 08	58 23		
FSE 25, LBN 102.84+02.07	22 08	58 31		

*References to globule names:* Pottasch–Pottasch (1956); GRS–Gyulbudaghian (1985); WB89–Wouterloot & Brand (1989); BRC–Sugitani et al. (1991); Weikard–Weikard et al. (1996); FSE–Froebrich et al. (2005).

*References to column 5.* 1. Beltrán et al. (2002); 2. Nisini et al. (2001); 3. Codella et al. (2001); 4. Froebrich & Scholz (2003); 5. Nakano et al. (1989); 6. Hessman et al. (1995); 7. Reach et al. (2004); 8. Duvert et al. (1990); 9. Sugitani et al. (1991); 10. de Vries et al. (2002); 11. Ogura et al. (2002); 12. Reipurth & Bally (2001); 13. Reipurth et al. (2003); 14. Schwartz et al. (1991); 15. Reipurth, Bally, & Devine (1997); 16. Froebrich et al. (2003); 17. Zhou et al. (2006); 18. Getman et al. (2007); 19. Sicilia-Aguilar et al. (2006a); 20. Sugitani et al. (1997); 21. Serabyn et al. (1993); 22. Reipurth & Aspin (1997); 23. Tapia et al. (1997); 24. Parker et al. (1991); 25. Connelley et al. (2007); 26. Visser et al. (2002); 27. Slysh et al. (1997); 28. Bronfman et al. (1996); 29. Moriarty-Schieven et al. (1996); 30. Neri et al. (2007); 31. Ogura et al. (2007); 32. Valdetaro et al. (2005); 33. Valdetaro et al. (2008); 34. Ikeda et al. (2008).

### 3.2. Star Formation in Globules of IC 1396

The HII region IC 1396 is powered by the O6.5 V star HD 206267. It appears that the expansion of this HII region has resulted in sweeping up a molecular ring of radius 12 pc (Patel et al. 1998). Patel et al. derive an expansion age of the molecular ring of about 3 Myr.

The ring-like HII region, shown in Fig. 16, is some  $3^{\circ}$  in diameter and is surrounded by a number of bright-rimmed globules which are probable sites of triggered star formation due to compression by ionization/shock fronts and radiation pressure. Many bright rimmed clouds harbor IRAS point sources of low dust temperature. They also frequently contain small clusters of near-IR stars. The most prominent globules are located in the western and northern portions of the H II region.

The globules of IC 1396 received different designations during various studies. Pottasch (1956) labeled the most prominent bright rimmed globules with letters from A to H, in the order of their increasing distance from the exciting star. Weikard et al. (1996) supplemented this list by rims I and J. IC 1396A corresponds to the famous Elephant Trunk Nebula. Gyulbudaghian (1985) identified 32 globules in the region of Cep OB2, and designated them as *GRS* (globules of radial systems) 1–32. Four radial systems of globules have been identified near IC 1396. One system, consisting of 16 globules, is centered on IC 1396. Another system of 12 globules, slightly south of IC 1396, appears to be associated with BD +54 $^{\circ}$ 2612, whereas two further radial sys-

tems have been identified to the east and south-east of the main system of globules surrounding HD 206267. The system associated with HD 206267 is dominated by bright-rimmed globules with diffuse tails generated by the radiation field of HD 206267. The other systems appear as opaque globules without rims. The systems partially overlap spatially. Gyulbudaghian, Rodríguez & Cantó (1986) have surveyed the GRS globules for CO emission. They found that the radial systems separate in radial velocity. The mean LSR velocity of the HD 206267 system is  $-2.8 \pm 2.4 \text{ km s}^{-1}$ , whereas the same for the BD+54°2612 system is  $+6.5 \pm 1.0 \text{ km s}^{-1}$ . Two of the globules, GRS 12 and GRS 14, are associated with H<sub>2</sub>O masers (Gyulbudaghian, Rodríguez & Curiel 1990).

Schwartz et al. (1991) used the IRAS data base to locate young stellar object candidates associated with the globules of IC 1396. They found that only six globule-related sources have point-like structure and luminosities considerably in excess of that which can be caused by external heating. Most of the IRAS point sources associated with the globules are probably externally heated small-scale dust structures not related to star formation. Eleven globules of IC 1396 can be found in the catalog of bright rimmed clouds by Sugitani, Fukui & Ogura (1991) (BRC 32–42). Froebrich et al. (2005) presented a large-scale study of the IC 1396 region using new deep NIR and optical images, complemented by 2MASS data. They identified 25 globules (FSE 1–25) using extinction maps and the list of Schwartz et al. (1991). Four of them were previously uncatalogued in the SIMBAD database. In all but four cases the masses (or at least lower limits) of the globules could be determined, and the size could be measured properly for all but seven objects. For ten globules in IC 1396 they determined (J–H, H–K) color-color diagrams and identified the young stellar population. Five globules contain a rich population of reddened objects, most of them probably young stellar objects. The five globules with many red objects include the targets with the highest extinction values,

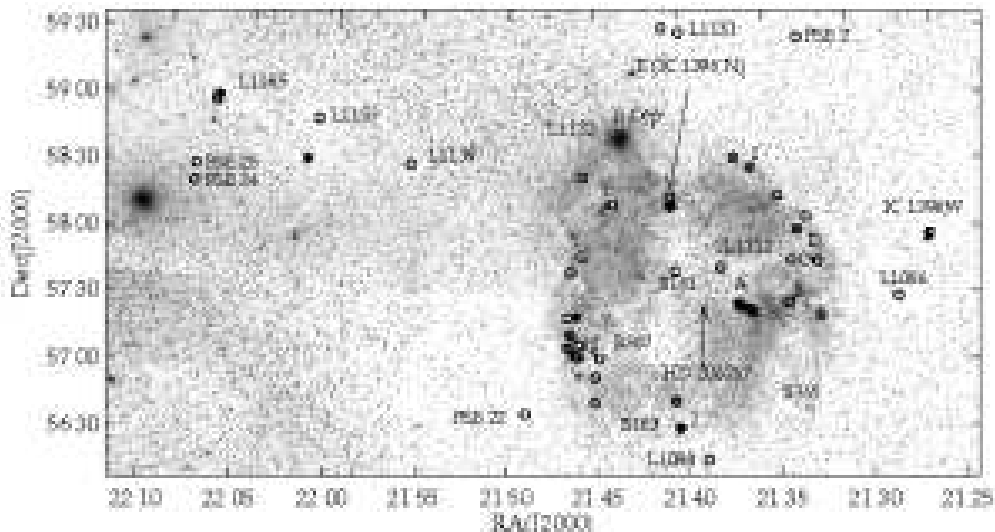


Figure 17. Distribution of the globules listed in Table 10 and other dark clouds projected near IC 1396, overplotted on a DSS red image of the region (open circles). Star symbols show the embedded protostars, and pluses mark the IRAS sources of uncertain nature (Schwartz et al. 1991).

suggesting a correlation of the strength of the star formation activity with the mass of the globule.

Moriarty-Schieven et al. (1996) have made the first arcminute resolution images of atomic hydrogen toward IC 1396, and have found remarkable “tail”-like structures associated with the globules IC 1396A, B and F, extending up to 6.5 pc radially away from the central ionizing star. These HI “tails” may be material which has been ablated from the globule through ionization and/or photodissociation and then accelerated away from the globule by the stellar wind, but which has since drifted into the “shadow” of the globules.

Star formation in small globules is often thought to be strongly influenced by the radiation pressure of a nearby bright star. Froebrich et al. therefore investigated how the globule properties in IC 1396 depend on the distance from the O star HD 206267. The masses of the globules have clearly shown positive correlation with the distance from this star, suggesting that evaporation due to photo-ionization affects the mass distribution of the globules around HD 206267. Their data are consistent with a scenario in which the radiation pressure from the O-type star regulates the star forming activity in the globules, in the sense that the radiation pressure compresses the gas and thus leads to enhanced star formation.

The names and coordinates of the known globules of IC 1396, as well as their associated IRAS sources are listed in Table 10, and the distribution of the same objects with respect to the HII zone is shown in Fig. 17. Some of the globules in IC 1396 were already investigated in detail and/or are known to harbor outflow sources. We give references for the works on individual globules in the last column of the table.

Ogura et al. (2002) performed  $H\alpha$  grism spectroscopy and narrow band imaging observations of the BRCs listed by Sugitani et al. (1991) in order to search for candidate pre-main sequence stars and Herbig-Haro objects. They have detected a large number of  $H\alpha$  emission stars down to a limiting magnitude of about  $R = 20$ . Their results for IC 1396 are reproduced in Table 11, and the finding charts for the  $H\alpha$  emission stars are shown in Fig. 18. Submillimeter observations of bright rimmed globules are presented by Morgan et al. (2008).

The primary indicators of star formation in the globules are the embedded IRAS point sources, molecular outflows and Herbig–Haro objects. Table 12 lists the Herbig–Haro objects found for the IC 1396 region.

### 3.3. Notes on Individual Globules

*IC 1396 W* lies about  $1^{\circ}75$  W–NW of HD 206267. In the center of the small (about  $6'$ ) dark cloud, the IRAS source 21246+5743 can be found. This source is not detected at  $12 \mu\text{m}$ . The very red IRAS colors and the extended appearance in the  $100 \mu\text{m}$  IRAS image suggest a young, deeply embedded source. Observations of this object with the photometer ISOPHOT confirmed that IRAS 21246+5743 is a Class 0 source that will reach about one solar mass on the main sequence (Froebrich & Scholz 2003). The ISOPHOT maps at  $160$  and  $200 \mu\text{m}$  show two further cold objects ( $2.5$  arcmin SW and NE, respectively) in the vicinity of the central source. This might be an indication of other newly forming stars or cold dust in the IC 1396 W globule.

Froebrich & Scholz (2003) have observed the IC 1396 W globule in J, H,  $K'$ , and a narrow band filter centered on the  $2.122 \mu\text{m}$  1-0 S(1) line of molecular hydrogen. They detected three molecular outflows in the field. The flow axes are parallel within  $3^{\circ}$  in projection. Magnetic fields cannot consistently explain this phenomenon. A

Table 11.  $H\alpha$  emission stars associated with bright rimmed clouds in IC 1396, identified by Ogura et al. (2002), and revised by Ikeda et al. (2008)

N	RA(J2000.0)	Dec(J2000.0)	EW	N	RA(J2000.0)	Dec(J2000.0)	EW
BRC 33				BRC 38			
1	21 34 19.8	57 30 01	53.4	4	21 40 31.7	58 17 55	...
2	21 34 20.8	57 30 47	3.3	5	21 40 36.7	58 13 46	4.0
3	21 34 49.2:	57 31 25:	66.2	6	21 40 37.0	58 14 38	63.3
BRC 34				7	21 40 37.2	58 15 03	29.8
1	21 33 29.4	58 02 50	43.0	8	21 40 40.5	58 13 43	...
2	21 33 55.8	58 01 18	...	9	21 40 41.3	58 15 11	26.1
BRC 37				10	21 40 41.7	58 14 25	14.8
1	21 40 25.3	56 36 43	...	11	21 40 45.0	58 15 03	75.7
2	21 40 26.1	56 36 31	18.4	12	21 40 48.1	58 15 38	19.0
3	21 40 26.8	56 36 23	40.9	13	21 40 48.9	58 15 00	...
4	21 40 27.2	56 36 30	...	14	21 40 49.0	58 15 12	...
5	21 40 27.4	56 36 21	...	15	21 40 49.2	58 17 09	22.2
6	21 40 28.2	56 36 05	...	16	21 41 02.0	58 15 25	...
7	21 40 28.8	56 36 09	78.8	BRC 39			
8	21 40 32.4	56 38 39	14.4	1	21 45 50.3	57 26 49	...
BRC 38				2	21 46 01.6	57 29 38	3.1
1	21 40 26.2	58 14 24	22.2	3	21 46 07.1	57 26 31	13.0
2	21 40 27.4	58 14 21	59.3	4	21 46 26.0	57 28 28	...
3	21 40 28.1	58 15 14	20.7	5N	21:45:54.08	57:28:18.5	9.3

parallel initial angular momentum of these objects, caused by the fragmentation of small clouds/globules, might be the reason for the alignment. NIR photometry, IRAS and ISOPHOT observations (Froeblich et al. 2003) led to the discovery of the driving sources of the outflows. The brightest outflow is driven by the Class 0 source IRAS 21246+5743. Two flows are driven by more evolved Class I/II objects. The JHK photometry of the globule also revealed a population of young stars, situated mainly in a dense embedded subcluster, about 2.5 arcmin south-west of IRAS 21246+5743. This cluster coincides with a clump of dense gas. The other young stars are almost uniformly distributed in the observed field.

Zhou et al. (2006) mapped IC 1396 W in the CO(1-0) line, and found that its CO molecular cloud may consist of three physically distinct components with different velocities. They detected neither molecular outflows nor the dense cores associated with candidate driving sources. One possible reason is that CO(1-0) and its isotopes cannot trace high density gas, and another is that the beam of the observation was too large to observe them. The CO cloud may be part of the natal molecular cloud of IC 1396 W, in the process of disrupting and blowing away. The CO cloud seems to be in the foreground of the  $H_2$  outflows.

*IC 1396A, Elephant Trunk nebula* contains an intermediate mass ( $M \sim 3 M_{\odot}$ , Sp. type: F9 – Hernández et al. 2004) pre-main sequence star, LkH $\alpha$  349 (Herbig & Rao 1972; Hessman et al. 1995) and a K7 type T Tauri star LkH $\alpha$  349c (Cohen & Kuhi 1979; Herbig & Bell 1988). No other YSOs were known before the *Spitzer Space Telescope*. Radio continuum maps of IC 1396A at 6 cm and 11 cm were obtained



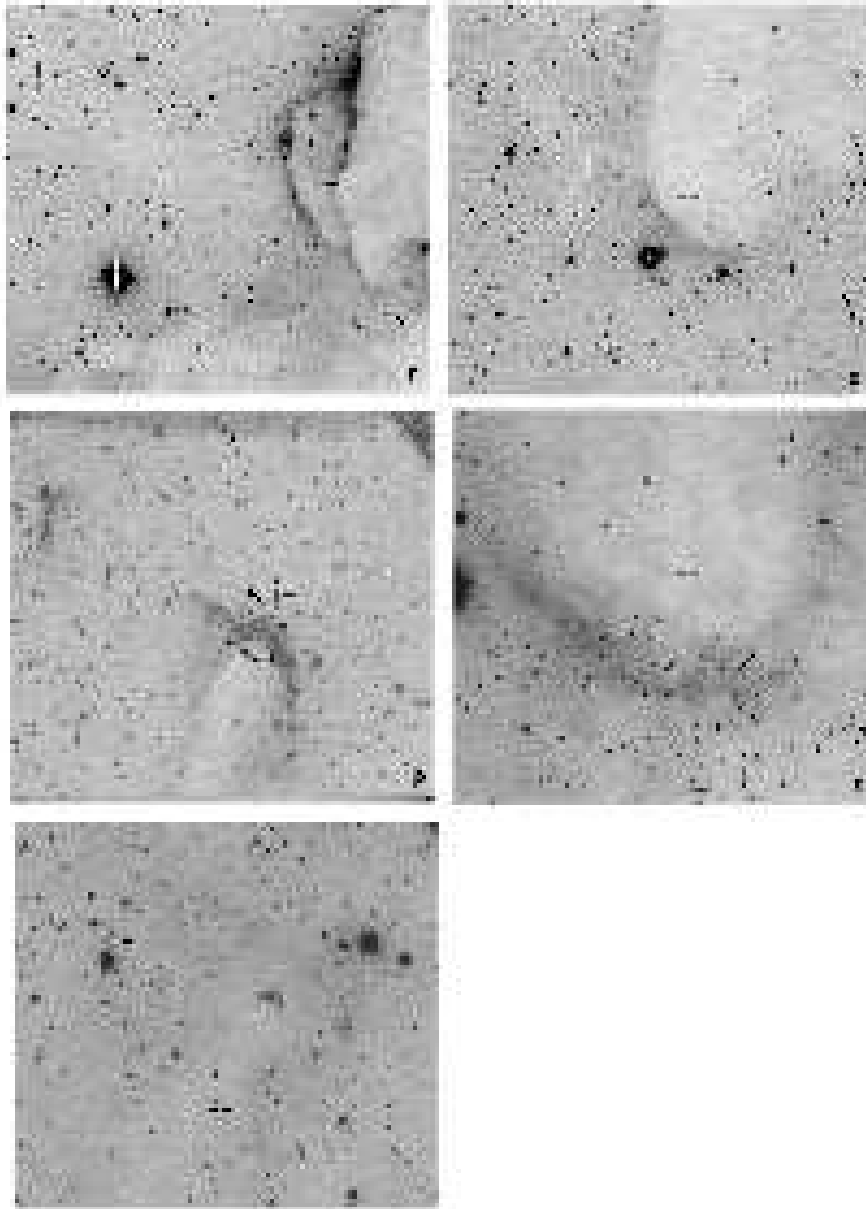


Figure 18.  $H\alpha$  emission stars in bright rimmed globules of IC 1396, found by Ogura et al. (2002). Top: BRC 33, BRC 34; middle: BRC 37, BRC 38(≡ IC 1396N); bottom: BRC 39. The position of the IRAS source associated with the globule is drawn by a pair of thick tick marks.

by Baars & Wendker (1976). The maps suggested the presence of an HII region within the globule.

Table 12. Herbig–Haro objects in IC 1396

name	RA(J2000)	Dec(J2000)	source	Ref.
HH 864 A	21 26 01.4	57 56 09	IRAS 21246+5743	1
	21 26 02.0	57 56 09	IRAS 21246+5743	1
HH 864 B	21 26 07.9	57 56 03	IRAS 21246+5743	1
HH 864 C	21 26 21.3	57 57 40	IRAS 21246+5743	1
	21 26 18.6	57 57 12	IRAS 21246+5743	1
HH 588SW2D	21 40 10.5	56 33 46	IRAS 21388+5622	2
HH 588SW2C	21 40 12.2	56 34 08	IRAS 21388+5622	2
HH 588SW2A	21 40 16.7	56 33 55	IRAS 21388+5622	2
HH 588SW2B	21 40 18.4	56 34 16	IRAS 21388+5622	2
HH 777	21 40 21.6	58 15 49	IRAS 21391+5802	3
HH 778	21 40 22.8	58 19 19		3
HH 588SW1A	21 40 24.6	56 35 07	IRAS 21388+5622	2
HH 588SW1B	21 40 26.6	56 34 40	IRAS 21388+5622	2
HH 588SW1C	21 40 27.5	56 34 55	IRAS 21388+5622	2
HH 588	21 40 29.1	56 35 55	IRAS 21388+5622	2
HH 588NE1B	21 40 32.1	56 36 25	IRAS 21388+5622	2
HH 588NE1C	21 40 32.1	56 36 30	IRAS 21388+5622	2
HH 588NE1A	21 40 33.5	56 36 16	IRAS 21388+5622	2
HH 588NE1D	21 40 33.5	56 36 32	IRAS 21388+5622	2
HH 588NE1E	21 40 34.6	56 36 33	IRAS 21388+5622	2
HH 589C	21 40 35.0	58 14 37	IRAS 21391+5802	2
HH 590	21 40 35.1	58 17 52		2
HH 591	21 40 35.8	58 18 21		2
HH 592	21 40 36.8	58 17 02		2
HH 589A	21 40 37.5	58 14 45	IRAS 21391+5802	2
HH 589B	21 40 37.7	58 14 25	IRAS 21391+5802	2
HH 593	21 40 45.2	58 16 09		2
HH 588NE2E	21 40 45.6	56 37 15	IRAS 21388+5622	2
HH 588NE2D	21 40 47.8	56 37 02	IRAS 21388+5622	2
HH 779	21 40 47.9	58 13 35		3
HH 588NE2C	21 40 49.0	56 37 07	IRAS 21388+5622	2
HH 588NE2B	21 40 49.3	56 37 09	IRAS 21388+5622	2
HH 588NE2A	21 40 49.7	56 37 27	IRAS 21388+5622	2
HH 780	21 40 53.1	58 14 16		3
HH 594	21 40 53.8	58 17 02		2
HH 595	21 41 00.2	58 16 52		2
HH 588NE3	21 41 00.0	56 37 19	IRAS 21388+5622	1
	21 41 01.0	56 37 25	IRAS 21388+5622	1
HH 865A	21 44 28.5	57 32 01	IRAS 21445+5712	1
	21 44 29.3	57 32 24	IRAS 21445+5712	1
HH 865B	21 45 10.5	57 29 51	IRAS 21445+5712	1
GGD 36	21 58 30.0	58 56 00		4
HH 354	22 07 42.5	59 11 53	IRAS 22051+5848	1,5

References. 1 – Froebrich et al. (2005); 2 – Ogura et al. (2002); 3 – Reipurth et al. (2003); 4 – Gyulbudaghian et al. (1987); 5 – Reipurth, Bally, & Devine (1997).

*Spitzer Space Telescope* images at 3.6, 4.5, 5.8, 8, and 24  $\mu\text{m}$  (Reach et al. 2004) revealed this optically dark globule to be infrared-bright and to contain a set of previously unknown protostars. The mid-infrared colors of the sources detected at 24  $\mu\text{m}$  indicate several very young (Class I or 0) protostars and a dozen Class II stars. Three of the new sources (IC 1396A  $\gamma$ , 1396A  $\delta$ , and 1396A  $\epsilon$ ) emit over 90% of their bolometric luminosities at wavelengths longer than 3  $\mu\text{m}$ , and they are located within 0.02 pc of the ionization front at the edge of the globule. Many of the sources have spectra that are

still rising at  $24\ \mu\text{m}$ . The two previously known young stars LkH $\alpha$  349 and 349*c* are both detected, with component *c* harboring a massive disk and LkH $\alpha$  349 itself being bare. About 5% of the mass of the globule is presently in the form of protostars in the  $10^5$ – $10^6$  yr age range.

The globule mass was estimated to be  $220\ M_{\odot}$  from a high-resolution CO map (Patel et al. 1995), much smaller than the virial mass, estimated as  $300$ – $800\ M_{\odot}$  (Patel et al. 1995; Weikard et al. 1996).

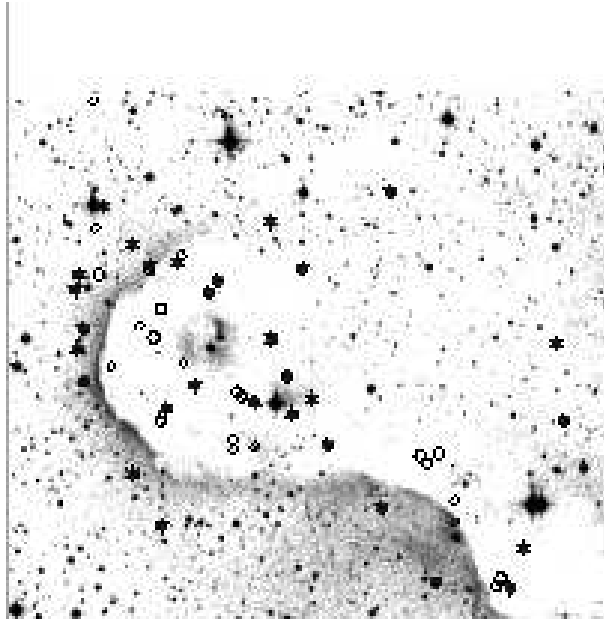


Figure 19. YSOs in IC 1396A, discovered by Spitzer Space Telescope (Sicilia-Aguilar et al. 2006a), overplotted on the DSS red image of the globule. Circles mark Class I, and star symbols Class II sources. Diamonds mark uncertain members.

Sicilia-Aguilar et al. (2006a), based on *IRAC* and *MIPS* photometry, identified 57 YSOs born in the Elephant Trunk. Most of them have no optical counterparts. Based on the color indices and the shape of the SEDs, Sicilia-Aguilar et al. identified 11 Class I and 32 Class II objects. Their average age is about 1 Myr. The surface distribution of these objects is displayed in Fig. 19, adopted from Sicilia-Aguilar et al. (2006a).

Valdettaro et al. (2005, 2008) detected H<sub>2</sub>O maser emission from the direction of IRAS 21345+5714, associated with IC 1396A. Probably each protostar observed by *Spitzer* contribute to the fluxes of the IRAS source.

**BRC 37, IC 1396H** High resolution  $^{12}\text{CO}$ ,  $^{13}\text{CO}$  and CS observations of this globule have been performed by Duvert et al. (1990). They detected a bipolar outflow and identified the possible optical counterpart of the driving source IRAS 21388+5622. Sugitani et al. (1997) reported on interferometric  $^{13}\text{CO}$  observations of BRC 37. They found evidence of interaction with the UV radiation from the exciting star of IC 1396. Bronfman et al. (1996) included IRAS 21388+5622 in their CS(2–1) survey of IRAS point sources with color characteristic of ultracompact H II regions. In order to study the age distribution of stars Ogura et al. (2007) undertook  $BVI_cJHK_s$  photometry of

stars in and around some bright rimmed globules including BRC 37. Their results indicate that star formation proceeds from the exciting star outward of the HII region. Ikeda et al. (2008) carried out near-IR/optical observations of BRC 37 in order to study the sequential star formation in the globule. Several results published by Ogura et al. (2002) are revised in the paper. Valdetarro et al. (2008) detected H<sub>2</sub>O maser emission from IRAS 21388+5622.

*IC 1396N* Serabyn et al. (1993) estimated the density and temperature structure of this globule (they use the designation IC 1396E), and found evidence of the possibility that recent internal star formation was triggered by the ionization front in its southern surface. On the basis of NH<sub>3</sub> data, gas temperatures in the globule are found to increase outward from the center, from a minimum of 17 K in its tail to a maximum of 26 K on the surface most directly facing the stars ionizing IC 1396. Sugitani et al. (2000) performed 2 mm continuum observations of IC 1396N (BRC 38). Codella et al. (2001) reported mm-wave multiline and continuum observations of IC 1396N. Single-dish high resolution observations in CO and CS lines reveal the cometary structure of the globule with unprecedented detail. The globule head contains a dense core of 0.2 pc, whereas the tail, pointing away from the exciting star, has a total length of 0.8 pc. Two high velocity bipolar outflows have been identified in the CO maps: the first one is located around the position of the strong infrared source IRAS 21391+5802 in the head of the globule, and the second one is located in the northern region. The outflows emerge from high density clumps which exhibit strong line emission of CS, HCO<sup>+</sup>, and DCO<sup>+</sup>. The sources driving the outflows have been identified by mm-wave continuum observations (e.g. Beltrán et al. 2002). The globule head harbors two YSOs separated by about 10<sup>4</sup> AU. SiO line observations of the central outflow unveil a highly collimated structure with four clumps of sizes pc, which are located along the outflow axis and suggest episodic events in the mass loss process from the central star.

Nisini et al. (2001) presented near infrared images of IC 1396N in the H<sub>2</sub> 2.12 μm narrow band filter as well as in broad band J, H, and K filters. They detected several chains of collimated H<sub>2</sub> knots inside the globule, having different luminosities but similar orientations in the sky. Most of the knots are associated with peaks of high velocity CO emission, indicating that they trace shocked regions along collimated stellar jets. From the morphology and orientation of the H<sub>2</sub> knots, they identify at least three different jets: one of them is driven by the young protostar associated with IRAS 21391+5802, while only one of the two other driving sources could be identified by means of near infrared photometry. The NIR photometry revealed the existence of a cluster of young embedded sources located in a south-north line which follows the distribution of the high density gas and testifies to a highly efficient star formation activity through all the globule. Valdetarro et al. (2005) and Furuya et al. (2003) detected H<sub>2</sub>O maser emission from IC 1396N.

Saraceno et al. (1996) present a far-infrared spectrum of IRAS 21391+5802, together with submillimeter and millimeter photometry. A rich spectrum of CO, OH, and H<sub>2</sub>O lines are detected in the ISO-LWS spectrum, indicative of a warm, dense region around the source. They also obtained an accurate measure of the bolometric luminosity and an estimate of the total envelope mass.

Reipurth et al. (2003) identified a major Herbig-Haro flow, HH 777, that is bursting out of the IC 1396N cometary cloud core. Near- and mid-infrared images reveal a very red object embedded in the center of the core, located on the symmetry axis of the large HH 777 flow, suggesting that this is likely the driving source. The projected

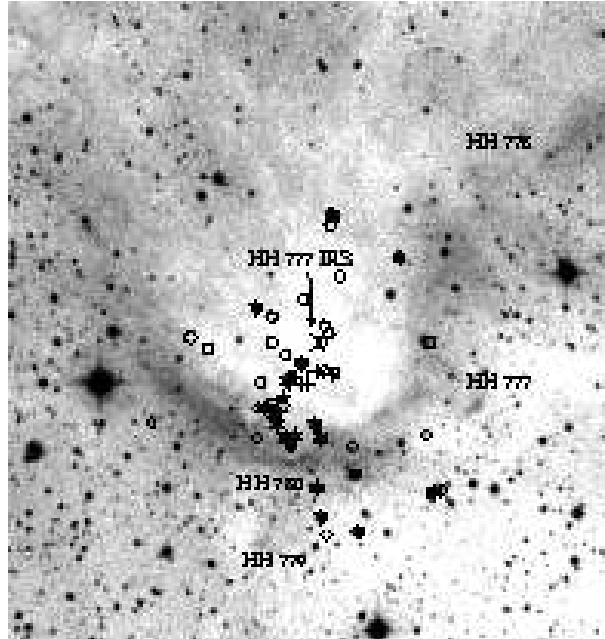


Figure 20. Members of the young cluster born in IC 1396N, overplotted on the DSS red image of the globule. Star symbols show the X-ray sources associated with Class II objects, pluses mark those corresponding to Class I objects (Getman et al. 2007), diamonds show the  $H\alpha$  emission stars detected by Ogura et al. (2002), and open circles indicate the near-infrared sources found by Nisini et al. (2001). Positions of the HH objects, discovered by Reipurth et al. (2003), are indicated and a large thick cross shows the position of HH 777 IRS.

separation of the working surface from the source is 0.6 pc. Additionally, 0.4 pc to the east of the source and on the flow axis, there is a faint, previously known HH object (HH 594) that may be part of the counterflow (Ogura et al. 2002). It thus appears that we are seeing a blowout of a parsec-scale flow into the surrounding H II region.

IC 1396N has been observed with the ACIS detector on board the Chandra X-Ray Observatory (Getman et al. 2007). 25 of the 117 detected X-ray sources are associated with young stars formed within the globule. Infrared photometry (2MASS and Spitzer) shows that the X-ray population is very young: 3 older Class III stars, 16 classical T Tauri stars, and 6 protostars including a Class 0/I system. The total T Tauri population in the globule, including the undetected population, amount to  $\sim 30$  stars, which implies a star formation efficiency of 1%-4%. Four of the X-ray-selected members coincide with near-infrared sources reported by Nisini et al. (2001), and 9 of them correspond to  $H\alpha$  emission stars detected by Ogura et al. (2002). An elongated spatial distribution of sources with an age gradient oriented toward the exciting star is discovered in the X-ray population. The geometric and age distribution is consistent with the radiation-driven implosion model for triggered star formation in cometary globules by H II region shocks. The large number of X-ray-luminous protostars in the globule suggests either an unusually high ratio of Class I/0 to Class II/III stars or a nonstandard initial mass function favoring higher mass stars by the triggering process. The Chandra source associated with the luminous Class 0/I protostar IRAS 21391+5802 is one of the

Table 13. Young stellar objects in IC 1396N detected by Chandra, and their infrared counterparts (Getman et al. 2007)

No.	Source	NIR(2MASS)					MIR			Class	Other Id.*
	CXOU J	J (mag)	H (mag)	K <sub>s</sub> (mag)	[3.6] (mag)	[4.5] (mag)	[5.8] (mag)				
41	214027.31+581421.1	14.30	13.30	12.88	11.62	11.09	10.74	II	OSP 2		
49	214031.58+581755.2	14.03	12.89	12.39	11.51	11.16	10.23	II	OSP 4		
53	214036.57+581345.8	13.51	12.58	12.24	12.13	11.94	12.01	III	OSP 5		
55	214036.90+581437.9	11.90	10.89	10.23	9.38	9.10	8.76	II	OSP 6		
60	214039.62+581609.3				11.29	9.42	8.31	I <sup>a</sup>	NMV 2		
61	214039.87+581834.8	>18.29	15.30	13.36	11.63	10.95	10.21	II	NMV 3		
62	214041.12+581359.0	12.96	12.08	11.77	11.61	11.72	11.49	III			
63	214041.16+581511.2	12.97	11.61	10.68	9.15	8.61	8.05	II	OSP 9		
65	214041.56+581425.5	13.65	12.62	12.17	11.40	11.20	10.68	II	OSP 10		
66	214041.81+581612.3				11.30	8.90	7.50	0/I <sup>b</sup>			
67	214041.91+581523.1	15.68	14.30	13.65	12.69	12.49	>9.82	II			
68	214042.89+581601.0				10.60	8.78	7.60	I <sup>c</sup>			
70	214043.47+581559.7				12.89	11.95	>9.85	I/II			
71	214043.64+581618.9	>17.89	>16.09	13.51	9.97	8.72	8.00	I	NMV 10		
72	214044.34+581513.3	16.05	14.59	13.60	12.42	11.64	10.60	II			
73	214044.84+581605.1	>15.85	14.28	12.89	11.73	11.15	10.68	II	NMV 11		
74	214044.85+581503.4	14.62	13.35	12.66	12.29	11.40	10.96	II	OSP 11		
76	214045.18+581559.8				11.95	10.82	10.03	I			
77	214045.51+581511.4	14.65	13.71	13.11	12.54	12.21	11.82	II			
78	214045.53+581602.9	15.68	13.73	12.85	12.23	11.84	>10.37	II			
80	214045.79+581549.0				12.59	11.19	10.04	I			
81	214046.49+581523.2	12.81	11.95	11.65	11.37	11.33	11.39	III			
82	214046.89+581533.3	15.30	13.55	12.63	11.97	11.80	11.15	II			
85	214048.03+581537.9	13.89	12.95	12.67	12.08	11.91	10.77	II	OSP 12		
87	214049.09+581709.3	14.14	12.86	12.13	10.77	10.19	9.69	II	OSP 15		

\*OSP: Ogura et al. (2002); NMV: Nisini et al. (2001)

<sup>a</sup> X-ray source 60 is offset by 3.2'' to the north of the radio continuum source VLA 1 and by 5.0'' to the northwest of the millimeter source BIMA 1 of Beltrán et al. (2002).

<sup>b</sup> X-ray source 66 is within 0.5'' of the radio continuum source VLA 2 and millimeter source BIMA 2 of Beltrán et al. (2002). This is also millimeter source A of Codella et al. (2001).

<sup>c</sup> X-ray source 68 is within 1.0'' of the radio continuum source VLA 3 and millimeter source BIMA 3 of Beltrán et al. (2002).

youngest stars ever detected in the X-ray band. Table 13 shows the list of young stars identified by their X-ray emission, together with their NIR (2MASS) and MIR (Spitzer IRAC) magnitudes. Positions of the young stars born in this globule and some of the associated HH objects are displayed in Fig. 20.

Neri et al. (2007) investigated the mm-morphology of IC 1396N at a scale of  $\sim 250$  AU. They have mapped the thermal dust emission at 3.3 and 1.3 mm, and the emission from the  $J=13_k \rightarrow 12_k$  hyperfine transitions of methyl cyanide ( $\text{CH}_3\text{CN}$ ) in the most extended configurations of the IRAM Plateau de Bure interferometer. The observation revealed the existence of a sub-cluster of hot cores in IC 1396 N, consisting of at least three cores, and distributed in a direction perpendicular to the emanating outflow. The cores are embedded in a common envelope of extended and diffuse

dust emission. The CH<sub>3</sub>CN emission peaks towards the most massive hot core and is marginally extended in the outflow direction. The protocluster IC 1396N has been included in a high angular resolution imaging survey of the circumstellar material around intermediate mass stars conducted by Fuente (2008), as well as in a study of clustering properties of Class 0 protostars by Fuente et al. (2007).

*IC 1396 East (IC 1396G)* IRAS 21445+5712, associated with this globule, coincides with a faint, red, nebulous star (Schwartz et al. 1991). Ogura et al. (2002) detected H $\alpha$  emission in the spectrum of this star (BRC 39 No. 3). Fukui (1989) detected a molecular outflow associated with IRAS 21445+5712. Connelley et al. (2007) found a small, elongated near-infrared nebula around the star. IRAS 21445+5712 has been included in several surveys for H<sub>2</sub>O maser sources (Felli et al. 1992; Wouterloot et al. 1993; Furuya et al. 2003; Valdetaro et al. 2008). High-resolution VLA observations by Valdetaro et al. (2008) resulted in the first detection of water maser emission associated with IRAS 21445+5712.

*L 1165* This cloud, harboring IRAS 22051+5848, is included in several studies of the globules associated with IC 1396 (e.g. Schwartz et al. 1991; Gyulbudaghian 1985; Froebrich et al. 2005), though it lies at 2.6° east of the H II zone (corresponding to some 30 pc at the distance of IC 1396). IRAS 22051+5848 is associated with a small reflection nebula, catalogued as Gy 2–21 by Gyulbudaghian (1982). Schwartz et al. (1991) note that, according to its CO radial velocity (Gyulbudaghian et al. 1986), this globule may be foreground to IC 1396. Parker, Padman & Scott (1991) observed a bipolar CO outflow originating from IRAS 22051+5848. Tapia et al. (1997) presented near-infrared, *IJHK*, images of the globule. They identified the NIR counterpart of the IRAS source and an extended infrared nebula around it. Reipurth, Bally, & Devine (1997) detected a giant Herbig–Haro flow, HH 354, associated with IRAS 22051+5848. Reipurth & Aspin (1997) obtained a near-infrared spectrum of the source, also known as HH 354 IRS. They concluded that the detected CO absorption and the high luminosity of the star suggest that HH 354 IRS is probably a FUor. Visser et al. (2002) detected a submillimeter source, L 1165 SMM 1, associated with the globule. Slysh et al. (1997) observed an OH maser emission at the position of the IRAS source. L 1165 is included in the CS(2–1) survey of IRAS point sources with colors characteristic of ultracompact H II regions published by Bronfman et al. (1996). The distance of L 1165 is uncertain. Several authors (e.g. Reipurth, Bally, & Devine 1997; Froebrich et al. 2005) associate this cloud with IC 1396, whereas others, e. g. Tapia et al. (1997) assume a kinematic distance of 200 pc, and Visser et al. (2002) use 300 pc, with a reference to Dobashi et al. (1994). This value is based on the assumption that the cloud is part of the Lindblad ring. Gyulbudaghian et al. (1986) associate L 1165 with a radial system of globules centered on the A0 type giant HD 209811. The Hipparcos parallax of this star suggests a distance of about 400 pc.

#### 4. Star Formation along the Cepheus Bubble

The Cepheus Bubble is a giant far infrared ring-like structure around Cep OB2a, described by Kun et al. (1987), and identified as an HI shell by Patel et al. (1998) and Abraham et al. (2000). Several H II regions, such as IC 1396, S 140, S 134, S 129, and G 99.1+07.4 (Kuchar & Clark 1997) are located on the periphery of the ring. The sim-

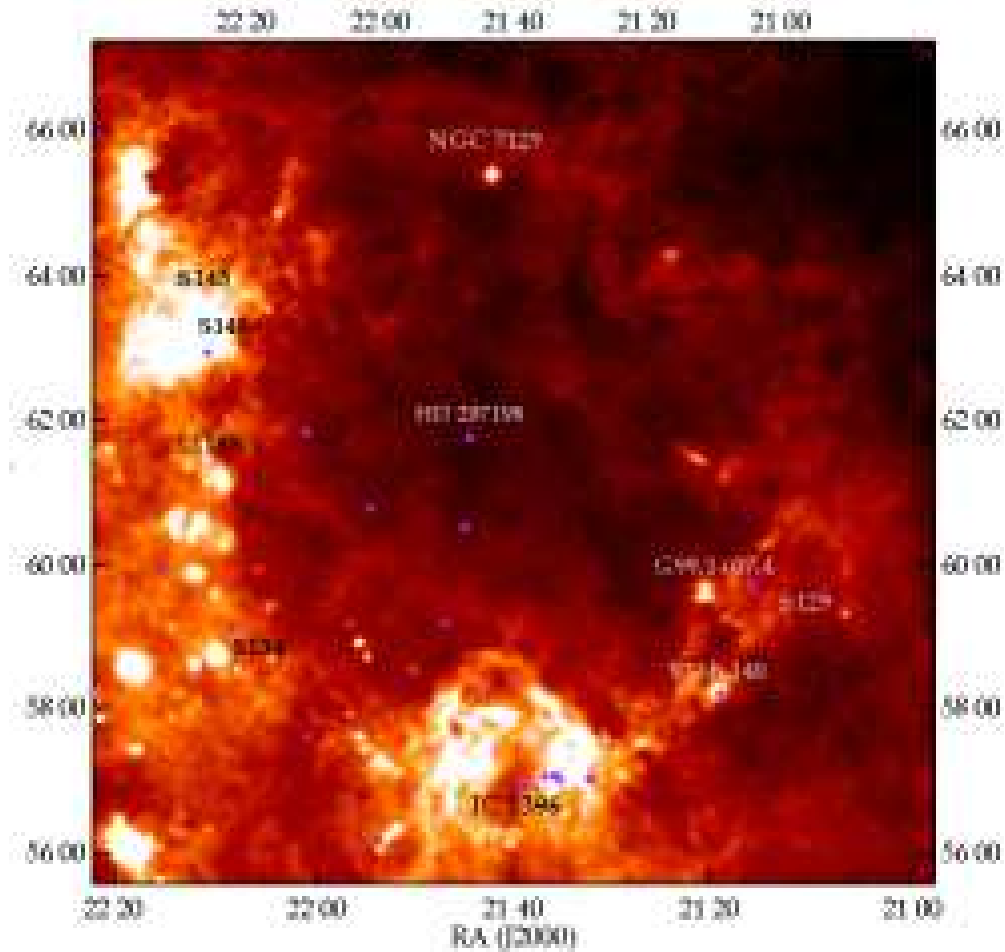


Figure 21. IRAS 100  $\mu\text{m}$  (IRIS) image of the Cepheus Bubble. The HII regions and reflection nebulae, probably associated with the Bubble (Kun et al. 1987), are indicated. Star symbols show the O-type and supergiant members of Cep OB2 (Humphreys 1978).

ilarity of the distances of these HII regions (700–900 pc) and the presence of the infrared ring-like structure apparently connecting them suggest that the infrared ring is a real feature and is physically connected with the HII regions. It was probably created by the stellar winds and supernova explosions of the evolved high-mass members of Cep OB2a. In particular, the O9 Ite type star HD 207198, located near the center of the Bubble, may be a major source of powerful stellar wind (Ábrahám et al. 2000). Figure 21 shows the distribution of the IRAS 100  $\mu\text{m}$  emission over the area of the Bubble. The known HII regions and reflection nebulae, as well as the O-type and supergiant members of Cep OB2 are indicated in the figure. CO observations performed by Patel et al. (1998) over the  $10^\circ \times 10^\circ$  area of the Cepheus Bubble revealed the molecular clouds associated with it. They found a total molecular mass of  $1 \times 10^5 M_\odot$ . Most of the molecular mass is associated with L 1204/S 140 and IC 1396, but there are further molecular clouds whose star forming activity has not yet been studied. Patel et al.



have shown that the shapes and kinematic properties of the IC 1396 globules indicate their interaction with the Bubble. The most comprehensive list of clouds and star forming regions associated with the Cepheus Bubble can be found in Kiss, Moór & Tóth's (2004) Table C.

#### 4.1. Star Formation in S 140

The HII region S 140 is located at the southwestern edge of the L 1204 dark cloud, along the Cepheus Bubble (Ábrahám et al. 2000), at a distance of about 900 pc from the Sun (Crampton & Fisher 1974). The ionization of the clouds is maintained by HD 211880, a B0V star (Blair et al. 1978). It is separated from L 1204 by a nearly edge-on ionization front. The core of the cloud is totally invisible in optical images while even the earliest infrared and radio observations have suggested that there is a dense cluster in the center of the core. Rouan et al. (1977) detected far-infrared emission from a region in L 1204, a few arcmin NE of S 140. They deduced a dust temperature of about 35 K, computed the total IR intensity, and estimated a mass of  $600 M_{\odot}$  for the observed area. Further infrared and submillimeter studies of the infrared source, S 140 IRS (Tokunaga et al. 1978; Dinerstein et al. 1979; Beichman et al. 1979; Little et al. 1980; Hackwell et al. 1982; Thronson et al. 1983) confirmed that the heating source of the cloud is a small cluster of embedded stars.

Several observational studies have been carried out to study the region in different wavelength regimes. These are mostly focused on the photon-dominated region (PDR) at the edge of L 1204, and on the embedded infrared sources located right behind it (e.g. Hayashi et al. 1985; Keene et al. 1985; Lester et al. 1986; Schwartz et al. 1989; Hasegawa et al. 1991; Golyntkin & Konovalenko 1991; Smirnov et al. 1992; Plume et al. 1994; Wilner & Welch 1994; Zhou et al. 1994; Schneider et al. 1995; Minchin et al. 1995a,c; Stoerzer et al. 1995; Park & Minh 1995; Preibisch & Smith 2002; Bally et al. 2002; Poelman & Spaans 2006, 2005). VLA observations of the 6 cm  $H_2CO$  line by Evans et al. (1987) revealed absorption of the cosmic background radiation towards a  $4' \times 3'$  region of the S 140 molecular cloud with structures on scales from  $20''$  to  $4'$ . They attributed these structures to clumps with masses around  $40 M_{\odot}$  and suggested that the clumps represent the first stages of the fragmentation of this portion of the cloud (although they did not rule out the possibility that the absorption maxima are low density holes surrounded by high-density regions). VLA observation of  $NH_3$  by Zhou et al. (1993), however, showed absence of significant  $NH_3$  (1,1) emission at the  $H_2CO$  absorption peaks, indicating that the peaks correspond to low density “holes” rather than high-density clumps. The high density molecular gas was studied by Ungerechts et al. (1986), who mapped the region using  $NH_3$  (1,1) and (2,2), and found that the column density and rotational temperature peak at the position of the embedded infrared source. The kinetic temperature is peaked at 40 K and decreasing smoothly to 20 K within the neighborhood of the infrared source. Zeng et al. (1991) studied the hyperfine structures of HCN (1-0) emission from the high density molecular core.

Several optical, near-, mid- and far-infrared, and radio surveys were carried out looking for young stars in the region (e.g. Rouan et al. 1977; Beichman et al. 1979; Hayashi et al. 1987; Evans et al. 1989; Persi et al. 1995; Ogura et al. 2002; Bally et al. 2002; Preibisch & Smith 2002). Beichman, Becklin & Wynn-Williams (1979) provided the first catalog of young stellar objects, consisting of three infrared sources, IRS 1, 2, 3. Later Evans et al. (1989) added two additional sources (VLA 4 and NW) to the catalog from observations using the VLA at 6 and 2 cm. The positions of the sources can

be found in Table 14. From the spectral indices of IRS 1–3 they concluded that the radio emission from these sources originates from optically thin HII regions ionized by Lyman-continuum photons from single, main sequence stars with spectral type of B1.5-B2. Evans et al. (1989) also carried out near-IR photometry using the NOAO infrared camera at 1.2, 1.65, and 2.2  $\mu\text{m}$ . They detected all known far-IR sources except IRS 2 and found additional 11 sources in the near-IR. At least five of these near-IR sources appear to be discrete sources, suggesting that a deeply embedded young cluster is forming in the region. Another cluster, containing about 100 near-IR sources associated with S 140, was discovered north of the region by a K'-band imaging survey by Hodapp (1994).

Joyce & Simon (1986) carried out a near-infrared polarization study and found an extremely high level of 2.2  $\mu\text{m}$  polarization towards S 140 IRS 1, indicating an outflow directed nearly along our line of sight. This finding was later confirmed by Hayashi et al. (1987) who observed the HII region in  $^{12}\text{CO}$  and  $^{13}\text{CO}$ . Minchin et al. (1993) found that the blue and redshifted lobes of the CO bipolar outflow have position angles of  $160^\circ$  and  $340^\circ$ , respectively. The high-resolution CS map obtained by Hayashi & Murata (1992) reveals a prominent V-shaped ridge or a ring around the S 140 IR cluster encircling the blue and red lobes of the molecular outflow, with no emission detected in the vicinity of the IR sources. The observations suggest that the CS ring is a remnant of a nearly pole-on massive gaseous disk interacting with the high-velocity outflow.

A self-consistent model of the region, consistent with all the molecular, atomic and submm continuum data was provided by Minchin et al. (1995b) (see Fig. 22). According to their model the eastern ridge is the dense, clumpy edge of the blueshifted outflow lobe that is closest to the observer. This outflow has expanded towards the edge of the molecular cloud so its blueshifted lobe is bounded by the HII region. Outside this edge is an externally illuminated PDR. The CI emission emanates from the outer edge of the cloud, with the CS emission tracing the compressed high density gas between the expanding outflow and PDR regions. The  $\text{NH}_3$  and continuum emission emanate from the inner edge of the outflow lobe, shielded from the external UV field.

Optical and near-infrared images of S 140, adopted from Preibisch & Smith (2002) are displayed in Fig. 23. According to the catalog of Porras et al. (2003) the S 140 region contains two young stellar groups. One is S 140 itself, another one is S 140 N identified by Hodapp (1994).

Schwartz (1989) found that the IRS 1 radio source consists of a core source with a jetlike appendage pointing toward an extended radio source suggesting ejection of an interstellar bullet of material from IRS 1.

Harker et al. (1997) observed the protostellar system in S 140 at 2.2, 3.1 and 3.45  $\mu\text{m}$ . They developed a simple model of the region which has been used to derive the physical conditions of the dust and gas. IRS 1 is surrounded by a dense dusty disk viewed almost edge-on. Photons leaking out through the poles of the disk illuminate the inner edge of a surrounding shell of molecular gas as seen at locations NW and VLA4. Their thick disk model can explain both the observed K-[3.45] color and scattered light intensity distributions. The observed K-[3.45] color of the bluest regions implies a cool radiation field with a color temperature of 850-900K. Most likely, these cool temperatures are the result of reprocessing of the protostellar radiation field by dust close to the protostar.

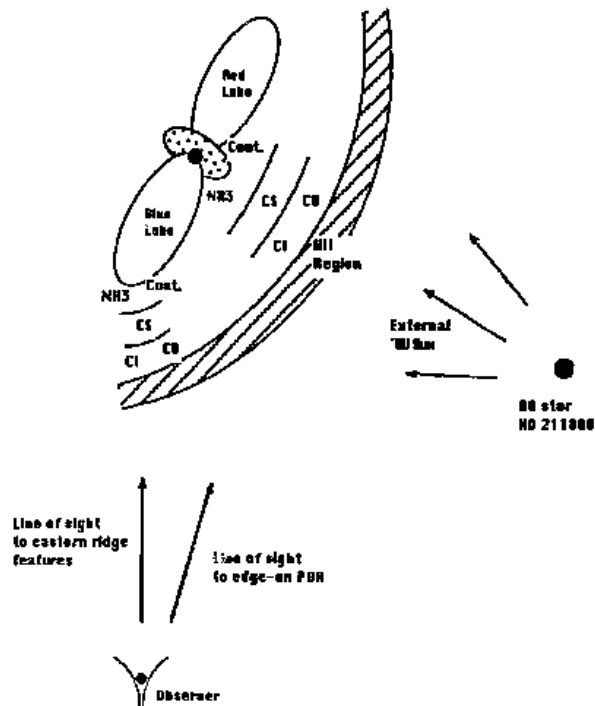


Figure 22. Schematic representation of the S 140/L 1204 region showing the plane that contains the observer, the external illuminating star HD 211880, the HII region/molecular cloud interface and the embedded molecular outflow. Fig 2. of Minchin et al. (1995b).

K band ( $2.0\text{-}2.3\ \mu\text{m}$ ) and  $\text{H}_2$  observations have revealed two bipolar outflows in the region (Preibisch & Smith 2002; Weigelt et al. 2002), one of them with an orientation similar to the CO outflow ( $160/340^\circ$ ) and the other one in the  $20/200^\circ$  direction. Both bipolar outflows seem to be centered on IRS 1.

Ogura et al. (2002) catalogued 8 stars with visible  $\text{H}\alpha$  emission (Table 15, Fig. 24). The emission line stars are mostly concentrated around the tip of the bright rim, similarly to the distribution found for near-IR clusters in the vicinity of an IRAS source.

Table 14. Position of far-infrared sources in S 140

number	RA (J2000)	Dec (J2000)
IRS 1	22 19 18.4	+63 18 55
IRS 2	22 19 18.2	+63 19 05
IRS 3	22 19 19.6	+63 18 50
VLA 4	22 19 17.5	+63 18 41
NW	22 19 18.8	+63 18 57

Table 15. List of H $\alpha$  emission objects in S 140 (Ogura et al. 2002; Ikeda et al. 2008)

number	RA (J2000)	Dec(J2000)	EW(H $\alpha$ )
1	22 18 47.8	+63 18 18	...
2	22 18 48.5	+63 16 40	13.6
3	22 18 49.6	+63 18 56	...
4	22 18 59.0	+63 18 12	94.8
5	22 18 59.4	+63 19 07	...
6	22 19 03.5	+63 18 01	...
7	22 19 09.9	+63 17 21	26.4
8	22 19 16.9	+63 17 22	163.5

Table 16. List of HH objects in S 140

Name	RA (J2000)	Dec (J2000)	Remark from Bally et al. (2002)	Ref.
HH 615	22 19 15.6	+63 17 29	[S II] jet aimed at HH 616A	1
HH 616A	22 19 05.9	+63 16 43	Northern tip	1
HH 616B	22 19 05.9	+63 16 26	Middle tip	1
HH 616C	22 19 05.7	+63 16 19	Southern tip	1
HH 616D	22 19 07.1	+63 16 40	Inner shock	1
HH 616E	22 19 12.8	+63 16 43	[S II] edge, southern rim of HH 616	1
HH 616F	22 19 14.3	+63 16 28	[S II] edge, southeastern rim of HH 616	1
HH 617	22 19 03.0	+63 17 53	Northern bow; tip of northern breakout	1
HH 623	22 19 55.0	+63 19 30	Faint knot east of S 140IR	1
HH 618A	22 19 53.0	+63 19 29	Western part of pair, east of S 140IR	1
HH 618B	22 19 54.9	+63 19 30	Eastern part of pair, east of S 140IR	1
Filament	22 18 52.1	+63 16:08	H $\alpha$ filament at P.A. = 300 $^\circ$	1
HH 251	22 19 34.4	+63 32 57	–	2
HH 252	22 19 37.8	+63 32 38	–	2
HH 253	22 19 45.0	+63 31 45	–	2
HH 254	22 19 49.6	+63 31 14	–	2
HH 619	22 19 16.4	+63 32 49	Two knots in east-west flow	1
HH 620	22 19 27.6	+63 32 50	Cluster of three knots south of nebular star	1
HH 621	22 19 21.5	+63 34 44	Cluster of knots: HH 251-254 counterflow	1
HH 622	22 19 50.6	+63 35 18	Pair of knots at P.A. = 220 $^\circ$ from nebular star	1
HH 609	22 21 28.8	+63 30 02	Southwestern [S II] knot in chain of two	1
HH 610	22 21 33.3	+63 37 34	Tiny knot west of reflection nebula	1
HH 611	22 21 39.5	+63 36 53	Compact groups of [S II] knots	1
HH 612	22 21 54.5	+63 34 39	Compact diffuse [S II] knot	1
HH 613	22 21 58.5	+63 33 23	Faint [S II] group	1
HH 614	22 22 01.2	+63 27 56	Diffuse [S II] complex	1

References: (1) Bally et al. (2002); (2) Eiroa et al. (1993).

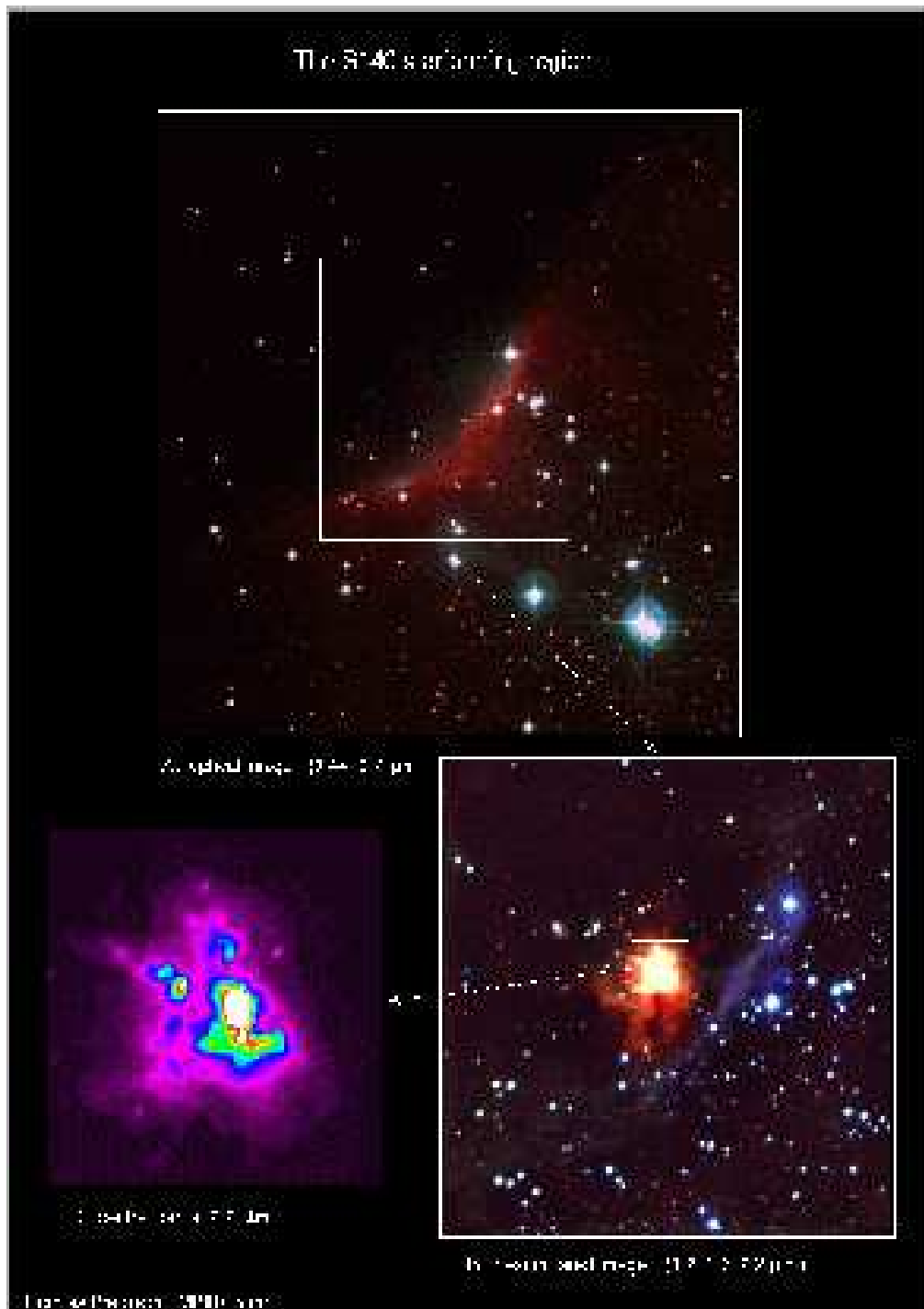


Figure 23. Optical and NIR images of S 140 (Preibisch & Smith 2002).

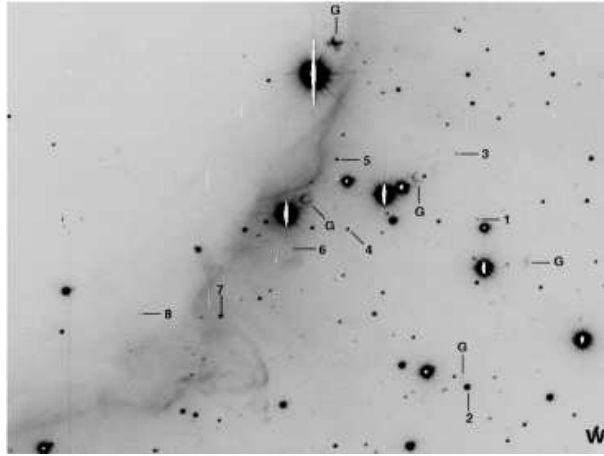


Figure 24. Finding chart for H $\alpha$  emission objects in S 140. G designate ghost images. (Ogura et al. 2002)

Tafalla et al. (1993) observed the dense gas in the L 1204/S 140 molecular complex using CS( $J = 1-0$ ) and NH $_3$ . The large-scale CS( $J = 1-0$ ) maps show that L 1204 is formed by three filamentary clouds, each being fragmented into cores of a few hundred solar masses and surrounded by low-level emission. The most prominent core is associated with S 140, the star-forming activity, however, is not restricted to the vicinity of the HII region, but extends throughout the complex; very red IRAS sources lie close to most of the cores, and molecular outflows have been detected in half of them. The ammonia observations reveal velocity shifts of about 0.5-0.8 km/s in the dense gas inside the cores with embedded stars. These velocity shifts, although small, are systematic and tend to divide the cores into two velocity regimes with little overlap. Fast rotation of the cores or the interaction between the bipolar outflows and the dense gas (or a combination of both) are the most likely causes for these velocity shifts. Minchin et al. (1996) studied the structure of the magnetic field by measuring the 800  $\mu$ m polarization at three positions towards S 140. Several studies reported detection of water maser emission toward the S 140 IRS region (e.g. Lekht et al. 1993; Tofani et al. 1995; Lekht & Sorochenko 2001; Trinidad et al. 2003).

Bally et al. (2002) carried out a wide field CCD survey of Herbig–Haro objects in the S 140 HII region and reported several new Herbig–Haro objects in the vicinity of S 140 (Table 16). They found two large bow shocks, HH 616 and HH 617. The northern shock, HH 617, is probably associated with the molecular hydrogen outflow from IRS 3, while the source of the larger velocity southern bow shock, HH 616, is still unclear. It appears to trace an outflow from an unknown source south of S 140.

Recently a survey using InfraRed Array Camera (IRAC) on board the *Spitzer Space Telescope* was carried out by Megeath et al. (2004). They used the IRAC color plane to identify 12 Class 0/I and 23 Class II objects (Table 17). The list of Megeath et al. (2004) contains 5 stars (1, 2, 4, 6, 7 in Table 15) with H $\alpha$  emission from Ogura et al. (2002).

Using H- and K $_s$ -band imaging polarimetry for S 140 and spectropolarimetry from 1.26 to 4.18  $\mu$ m for IRS 1, Yao et al. (1998) discovered two reflection nebulae, illuminated by IRS 1 and IRS 3, which seem to be physically connected. Based on the location

Table 17. List of Class II/I/0 objects in S 140 (Megeath et al. 2004)

RA (J2000)	Dec (J2000)	[3.6]	[4.5]	[5.8]	[8.0]	Class
22 18 21.6	+63 15 32	12.38	12.07	11.65	11.09	Class II
22 18 37.2	+63 13 01	12.91	12.49	12.20	11.65	Class II
22 18 48.5	+63 16 40	9.94	9.65	9.22	8.77	Class II
22 18 47.6	+63 18 17	13.03	12.82	12.26	11.38	Class II
22 18 58.8	+63 18 11	11.84	11.32	10.50	9.87	Class II
22 19 03.4	+63 18 00	12.10	11.78	10.99	10.13	Class II
22 19 24.5	+63 14 26	11.81	11.50	11.50	10.92	Class II
22 19 09.7	+63 17 20	11.97	11.62	11.32	10.62	Class II
22 19 28.3	+63 15 07	12.35	11.56	11.43	10.58	Class II
22 19 25.9	+63 18 24	11.70	10.90	10.23	9.50	Class II
22 19 20.4	+63 19 38	10.74	9.98	9.59	8.95	Class II
22 19 28.5	+63 18 49	11.92	11.32	10.51	9.54	Class II
22 19 27.1	+63 19 22	9.80	9.16	7.93	7.06	Class II
22 19 48.7	+63 16 41	11.37	11.22	11.23	10.46	Class II
22 19 29.1	+63 21 01	13.64	12.89	12.29	11.30	Class II
22 19 38.1	+63 19 32	12.85	12.56	11.78	10.83	Class II
22 20 19.2	+63 16 23	13.01	12.65	12.27	11.31	Class II
22 20 21.0	+63 16 14	13.09	12.62	11.81	10.90	Class II
22 20 07.5	+63 18 45	13.32	12.76	12.24	11.18	Class II
22 19 37.0	+63 25 31	12.54	12.36	11.63	10.65	Class II
22 20 27.3	+63 17 07	11.51	11.20	11.02	10.47	Class II
22 20 27.2	+63 17 58	12.31	11.58	11.10	10.34	Class II
22 19 37.9	+63 17 10	11.43	11.18	10.83	9.54	Class II
22 19 15.6	+63 19 33	11.29	9.75	8.90	7.87	Class 0/I
22 19 25.7	+63 18 49	10.61	9.56	8.74	8.12	Class 0/I
22 19 30.9	+63 18 32	11.16	10.13	9.19	8.54	Class 0/I
22 19 32.5	+63 19 24	9.96	8.38	6.24	4.83	Class 0/I
22 19 39.4	+63 19 03	11.94	10.92	10.43	9.70	Class 0/I
22 19 43.5	+63 20 08	11.91	11.18	10.57	9.30	Class 0/I
22 19 52.3	+63 19 01	14.73	12.78	11.86	11.00	Class 0/I
22 19 48.3	+63 20 27	14.24	12.42	11.62	10.86	Class 0/I
22 19 45.5	+63 21 21	14.59	13.01	12.39	11.47	Class 0/I
22 20 18.5	+63 18 57	12.12	10.73	10.07	8.91	Class 0/I
22 20 19.4	+63 19 05	13.90	12.75	11.90	11.05	Class 0/I
22 19 35.1	+63 20 26	14.80	13.40	12.43	12.14	Class 0/I

and orientation of the reflection lobes around IRS 1, Yao et al. (1998) suggest that S 140 IRS 1 may drive a quadrupolar outflow. Schertl et al. (2000) studied the structure of the envelope around the central protostar in IRS 1 using high resolution bispectrum speckle interferometry and speckle polarimetry. Their high resolution images showed bright emission which can be attributed to light reflected from the inner walls of a cavity in the circumstellar material around IRS 1. Given that the orientation of the evacuated cavity agrees with the direction of the molecular outflow they suggest that the cavity has been carved out by the strong outflow from IRS 1. Recently Hoare (2006) obtained multiepoch high-resolution radio continuum maps of IRS 1 using the full MERLIN array. The observations revealed a highly elongated source that changes over time and is perpendicular to the larger scale bipolar molecular outflow. He explained the phenomenon with an equatorial wind driven by radiation pressure from the central star and inner disk acting on the gas in the surface layer of the disk. Jiang et al. (2008) obtained K-band polarimetric images with the Coronagraphic Imager with Adaptive

Optics (CIAO) mounted on the Subaru telescope. They found that S140 IRS 1 shows well-defined outflow cavity walls and a polarization disk which matches the direction of previously observed equatorial disk wind (Hoare 2006), thus confirming that the polarization disk is actually the circumstellar disk. Preibisch et al. (2001) obtained a bispectrum speckle interferometric K-band image with a resolution of 150 mas and a seeing-limited molecular hydrogen line emission image of IRS 3. Their speckle image resolves IRS 3 into three point sources, a close binary with separation  $0''.63$  and a third component  $1''.3$  away. A rough assessment of the system stability suggests that the IRS 3 triple system is unstable. The speckle image also reveals extended diffuse emission of very complex morphology around IRS 3.

Trinidad et al. (2007) present results of 1.3 cm continuum and H<sub>2</sub>O maser emission observations made with the VLA in its A configuration toward IRS 1 and also present results of continuum observations at 7 mm and re-analyse observations at 2, 3.5 and 6 cm (previously published). IRS 1A is detected at all wavelengths, showing an elongated structure. Three water maser spots are detected along the major axis of the radio source IRS 1A. They have also detected a new continuum source at 3.5 cm (IRS 1C) located some  $0''.6$  northeast of IRS 1A. The presence of these two YSOs (IRS 1A and 1C) could explain the existence of the two bipolar molecular outflows observed in the region. In addition, they have also detected three continuum clumps (IRS 1B, 1D and 1E) located along the major axis of IRS 1A, and they discuss two possible models to explain the nature of IRS 1A: a thermal jet and an equatorial wind.

Several papers have studied the physical processes in photon dominated regions of S 140 using sub-mm and radio observations (see e.g. Li et al. 2002; Poelman & Spaans 2005, 2006; Rodríguez et al. 2007, and references therein). Ashby et al. (2000) detected H<sub>2</sub>O in S 140 using the Submillimeter Wave Astronomy Satellite. They used Monte Carlo simulation to model the radiative transport and to interpret the detected 557 GHz line profiles. Their model required significant bulk flow in order to explain the relatively single-peaked H<sub>2</sub>O line. However, they were not able to discriminate between infall and outflow.

#### 4.2. L 1188

L 1188 is one of the molecular clouds along the Cepheus Bubble. Abraham et al. (1995) mapped the cloud in <sup>13</sup>CO, and found a molecular mass of  $\sim 1800 M_{\odot}$  within a field of  $74' \times 44'$ . They selected 6 IRAS point sources as candidate YSOs in the field, and found 15 H $\alpha$  emission stars during a photographic objective prism survey. Figure 25 shows the 100  $\mu$ m optical depth image of the L 1188/L 1204 region, suggesting that these clouds are connected to each other, and the distribution of the candidate YSOs in and around L 1188. Könyves et al. (2004) studied the SEDs of the IRAS sources associated with L 1188 using 2MASS, MSX, IRAS, and ISOPHOT data.

#### 4.3. S 145

S 145 is an extended HII region, located at (l,b)=(107° 67, +5° 69), in the north-eastern part of the Cepheus Bubble. Both its distance and velocity suggest its relation to the bubble (Patel et al. 1998; Kiss et al. 2004). S 145 is associated with a bright rimmed cloud BRC 44 (Sugitani et al. 1991), in which Ogura et al. (2002) found 13 H $\alpha$  emission stars (Table 18, and Fig. 26).



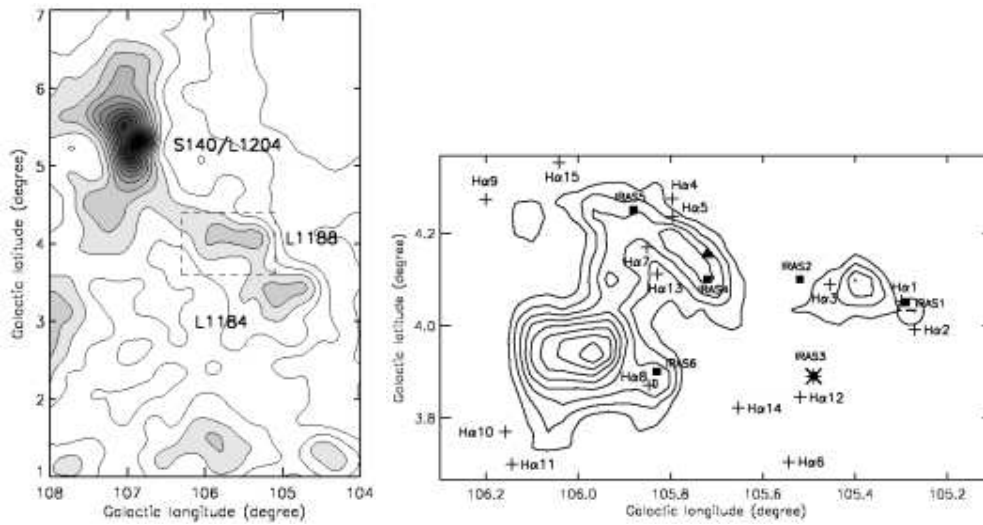


Figure 25. Left: 100  $\mu\text{m}$  optical depth image of the L 1188/L 1204 region. Right: Distribution of the molecular gas, IRAS point sources and H $\alpha$  emission stars in the region of L 1188 (From Ábrahám et al. 1995).

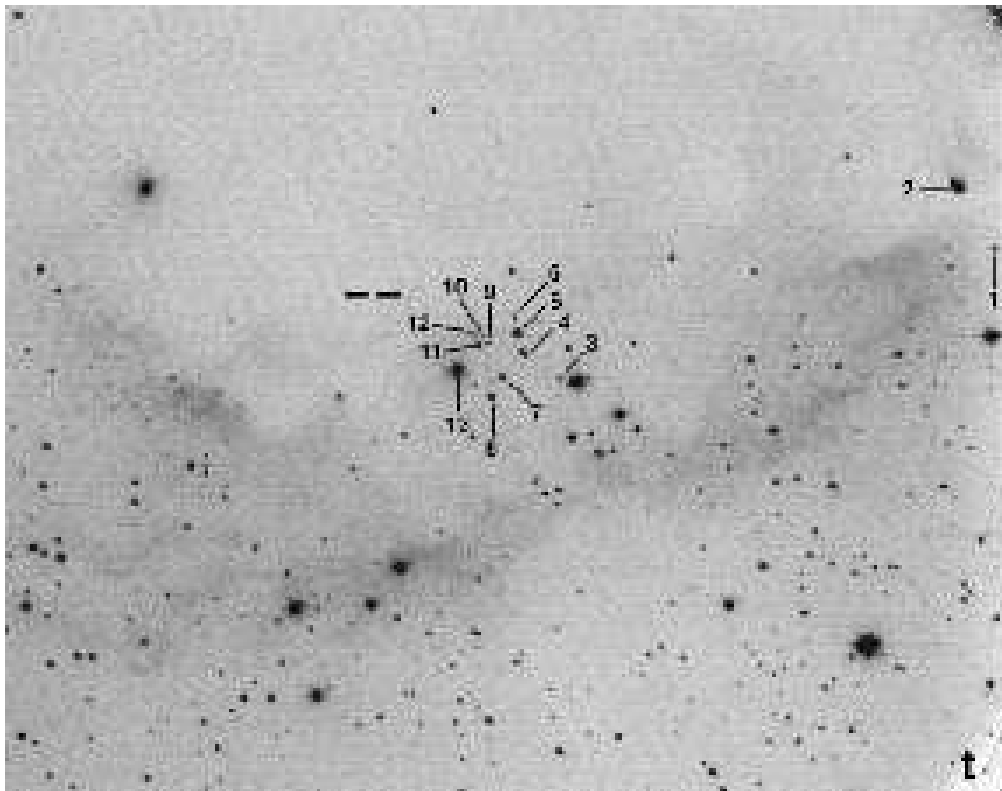


Figure 26. Finding chart for H $\alpha$  emission objects in BRC 44, a bright-rimmed dark cloud associated with S145 (Ogura et al. 2002).

Table 18.  $H\alpha$  emission stars associated with BRC 44 from Ogura et al. (2002) (EW-s and remarks revised by Ikeda et al. (2008) are shown.)

N	RA(J2000)	Dec(J2000)	EW ( $\text{\AA}$ )	Remarks
1	22 28 19.01	64 13 54.0	55.8	
2	22 28 21.00	64 14 13.2	4.2	reflection nebula ?
3	22 28 41.77	64 13 11.6	...	contam. from nearby star
4	22 28 43.54	64 13 19.1	...	double star
5	22 28 43.98	64 13 26.0	50.6	
6	22 28 44.12	64 13 31.2	20.1	very weak cont.
7	22 28 44.74	64 13 12.0	...	contam. from nearby stars
8	22 28 45.31	64 13 05.6	22.5	bad pix.
9	22 28 45.48	64 13 23.0	...	contam. from No. 11 star
10	22 28 45.77	64 13 24.9	...	contam. from Nos. 5 and 12 stars
11	22 28 45.96	64 13 22.1	53.5	contam. from No. 9 star
12	22 28 46.24	64 13 25.6	...	contam. from No. 5 star
13	22 28 47.12	64 13 14.3	9.5	

#### 4.4. S 134

Two star-forming molecular clouds, associated with this HII region, can be found in the literature. Yonekura et al. (1998) observed a head-tail structured molecular cloud and CO outflow associated with IRAS 22103+5828, whereas Dobashi & Uehara (2001) reported on a CO outflow and molecular cloud associated with IRAS 22134+5834. The latter source proved to be a high-mass protostar at a very early evolutionary stage (Sridharan et al. 2002). It is associated with  $H_2O$  maser emission (Cesaroni et al. 1988).

### 5. Star Formation in the Association Cep OB3

Blaauw, Hiltner & Johnson (1959) made the first detailed photometric investigation of the association Cep OB3. They found 40 early-type members at 725 pc. Blaauw (1964) found evidence for two subgroups, Cep OB3a and Cep OB3b, with ages of 8 and 4 Myr, respectively. The luminous stars of the younger subgroup, Cep OB3b, excite the HII region S 155. Garmany (1973) suggested an expansion age of 0.72 Myr, based on the relative motion of the two subgroups. Seventeen of the 40 Cep OB3 members compiled by Blaauw et al. are contained in the Hipparcos Catalog. However, de Zeeuw et al. (1999) could not identify Cep OB3 as a moving group using the Hipparcos data. Hoogerwerf et al. (2001) have shown that the parent association of the runaway star  $\lambda$  Cep is probably not Cep OB2, but Cep OB3.

Several photometric studies (Crawford & Barnes 1970; Garrison 1970; Jordi, Trullors & Galadí-Enríquez 1996) refined the Blaauw et al. membership list, and extended it to fainter stars. Moreno-Corral et al. (1993) performed  $JHK'LM$  photometry for the 40 luminous stars in Blaauw et al.'s list. A comprehensive summary of all previous membership studies was given by Jordi et al. (1996), who obtained ages of 7.5 and 5.5 Myr for the two subgroups.

Simonson & van Someren Greve (1976) found an expanding HI shell centered on the young subgroup in Cep OB3 but did not detect significant HI associated with the older subgroup.

Sargent (1977, 1979) mapped the vicinity of Cep OB3 in the J=1-0 transition of  $^{12}\text{CO}$ , and found a  $20\text{ pc} \times 60\text{ pc}$  molecular cloud complex at the average radial velocity of  $-10\text{ km s}^{-1}$ , close to the velocity range of the association members and S 155. Sargent's CO observations revealed several clumps in the Cep OB3 molecular cloud. She labeled them as *Cep A, B, C, D, E, F*, and concluded that some of them, especially Cep A, are sites of triggered star formation due to the interaction of the expanding HII region S 155 and the molecular cloud. Elmegreen & Lada (1977) considered Cep OB3 as one of the examples of sequential star formation. Felli et al. (1978) measured the thermal radio emission from Cep OB3 and S 155. Ammonia maps around the IRAS sources associated with the Cep A–Cep F clouds are presented in Harju, Walmsley & Wouterloot (1993). The distribution of the luminous stars of Cep OB3 and the associated molecular cloud as shown up in the extinction map of the region (Dobashi et al. 2005) is displayed in Fig. 27.

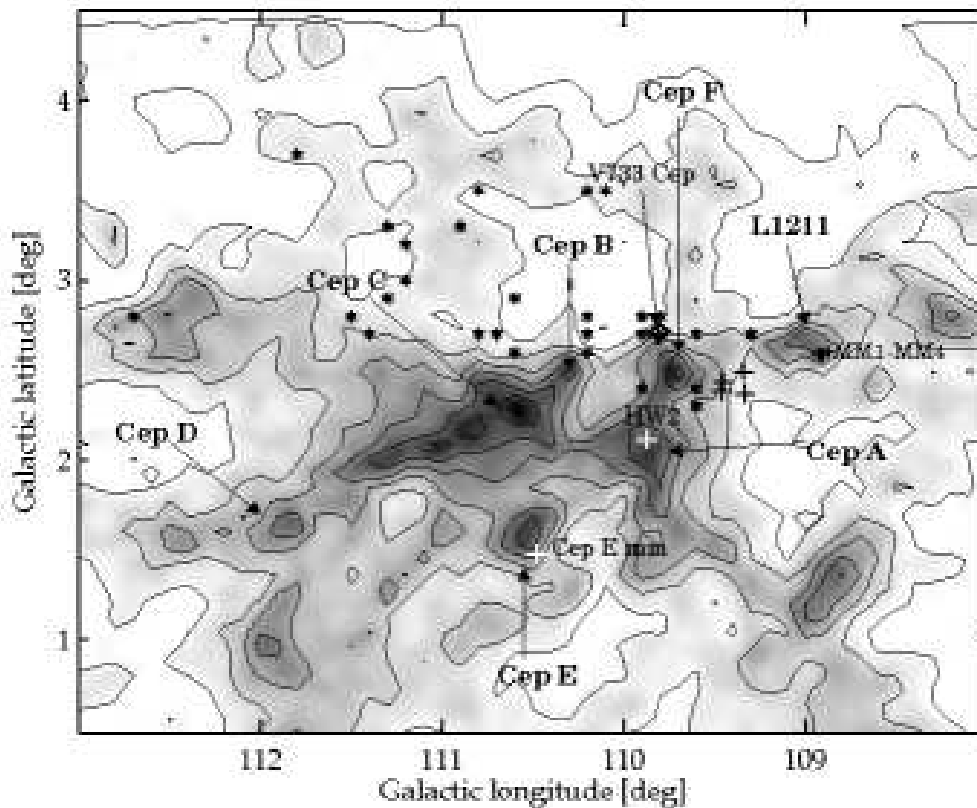


Figure 27. Distribution of the visual extinction (Dobashi et al. 2005) and the young, luminous stars in the region of Cep OB3b. The dense clumps Cep A–Cep F, identified in the distribution of CO by Sargent (1977), the dark cloud Lynds 1211, as well as the most prominent associated young stars are labeled. The lowest contour of the extinction is at  $A_V = 1$  mag, and the increment is 0.7 mag. Star symbols mark the luminous members of Cep OB3, listed by Garmany & Stencel (1992).

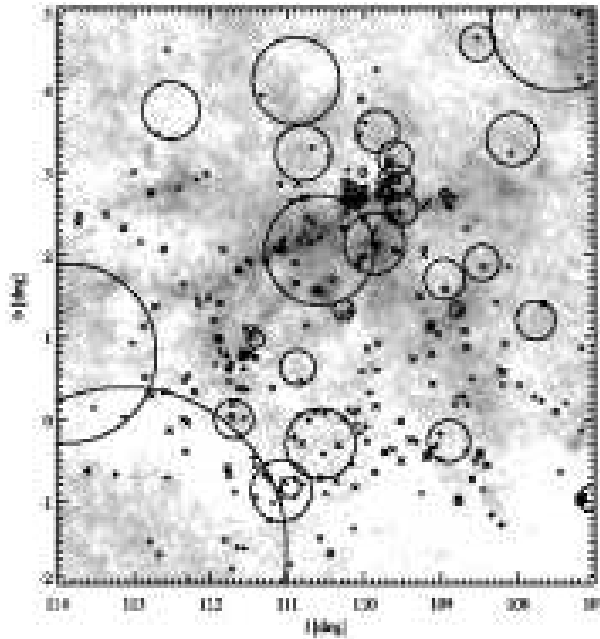


Figure 28. Pre-main sequence stars and candidates in the Cep OB3 region overlaid on the map of visual extinction, obtained from 2MASS data based on interstellar reddening using the NICER method (Lombardi & Alves 2001). Large circles denote the clouds from Table 1 associated with young stars. The meaning of the different symbols are as follows: Filled triangles - T Tauri stars; Filled squares - Herbig Ae/Be stars; Filled circles - Weak-line T Tauri stars; Open squares - Photometric candidate and possible PMS members; X -  $H\alpha$  emission stars; + - T Tauri candidates selected from 2MASS.

### 5.1. Pre-main Sequence Stars and Candidates in Cep OB3b

Naylor & Fabian (1999) discovered over 50 X-ray point sources in the region of Cep OB3 with ROSAT PSPC and HRI, the majority of which are probably T Tauri stars. Using the ratio of high-mass to low-mass stars to constrain the initial mass function, Naylor & Fabian (1999) found that it is consistent with that for field stars. Most of the T Tauri stars are close to, but outside the molecular cloud.

Pozzo et al. (2003) identified 10 T Tauri stars and 6 candidates using  $UBVI$  photometry and follow-up multi-fiber spectroscopy. Their optical survey covered an area of some 1300 arcmin<sup>2</sup>. The newly discovered pre-main sequence stars have masses in the range  $\sim 0.9 - 3.0 M_{\odot}$  and ages from  $< 1$  Myr to nearly 10 Myr. Out of the 10 definite TTS, four have a ROSAT X-ray counterpart in Naylor & Fabian (1999).

Mikami & Ogura (2001) presented a list and finding charts of  $H\alpha$  emission stars in the region of Cep OB3. Their objective prism survey covered an area of 36 square degrees. They found 108  $H\alpha$  emission stars, 68 of which are new. The surface distribution of the  $H\alpha$  emission stars outlines a ring-like area, which almost coincides with that of the heated dust shown by the IRAS images. The surveyed area is much larger than that occupied by the stars of Cep OB3, and extends to the south of the associated molecular cloud. It includes NGC 7419, a cluster at 2 kpc, and King 10, below the Galactic

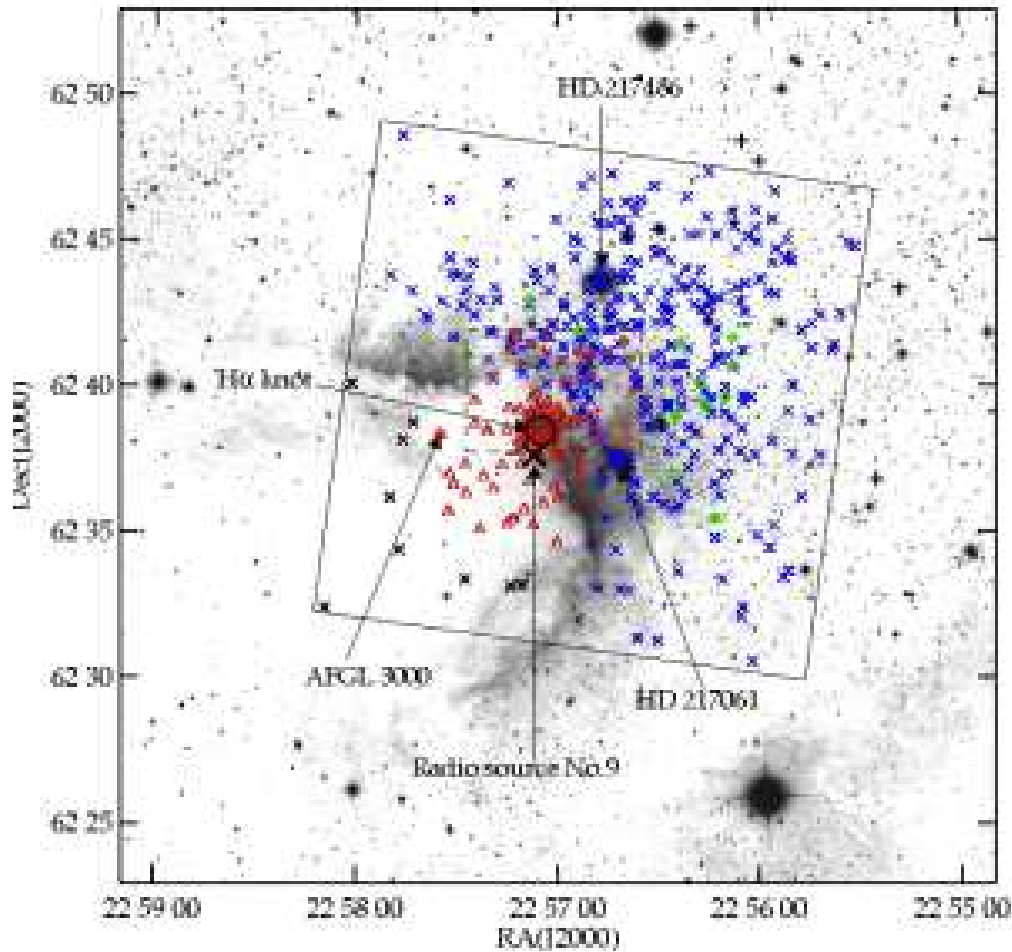


Figure 29. R-band image covering  $0^{\circ}5 \times 0^{\circ}5$  of the Cep B and Cep OB3b neighborhood from the Digitized Sky Survey (DSS). North is up, and east is to the left. The Chandra  $17' \times 17'$  ACIS-I field (Getman et al. 2006) is outlined by the square, and the dashed rectangle shows the region in which Ogura et al. (2002) searched for  $H\alpha$  emission stars. Cep B, the hottest component of the Cepheus molecular cloud, is at the bottom left corner of the Chandra field. To the north and west lies Cep OB3b, the younger of two subgroups of the Cep OB3 association. The interface between Cep B and Cep OB3 is delineated by the H II region S 155. The most massive and optically bright stars in the field, HD 217086 (O7n) and HD 217061 (B1V), are labeled. Black pluses indicate the T Tauri stars identified by Pozzo et al. (2003). Blue crosses show the X-ray sources which are probably members of a cluster belonging to Cep OB3b. Red triangles indicate the X-ray emitting members of an embedded cluster in the molecular cloud Cep B, whereas green diamonds show the X-ray sources whose 2MASS counterparts are indicative of K-band excess, originating from accretion disks. Small, thick red pluses within the dashed rectangle show the  $H\alpha$  emission stars found by Ogura et al. (2002). Black circle outlines the bright  $H\alpha$  knot on the ionization front, associated with a compact cluster and studied in detail by Moreno-Corral et al. (1993) and Testi et al. (1995). A star symbol shows the infrared source AFGL 3000, and a thick black cross is the bright radio continuum source No. 9 discovered by Felli et al. (1978).

plane. Further objects, not associated with Cep OB3 but included in the surveyed area and lying along the shell-like surface, are S 157, NGC 7654, and S 158.

A portion of the Cep OB3b and the molecular cloud Cepheus B have been observed with the ACIS detector on board the Chandra X-ray Observatory (Getman et al. 2006). The observations resulted in the discovery of two rich clusters of pre-main sequence stars. The cluster projected outside the molecular cloud is part of the association Cep OB3b. The X-ray observations detected 321 pre-main sequence members. This is the best census of the stellar population of the region. The results suggest that the X-ray luminosity function, and thus probably the IMF, of Cepheus OB3b differs from that of the Orion Nebula Cluster: more stars of  $M < 0.3M_{\odot}$  can be found in Cepheus OB3b than in Orion.

Figure 28 shows the distribution of pre-main sequence stars and catalogued clouds overlaid on the visual extinction in the Cep OB3 region (Dobashi et al. 2005). Figure 29 shows the field of view and the main results of the X-ray observations.

## 5.2. Star Formation in the Molecular Cloud associated with Cep OB3

*Cepheus A* is a very active high-mass star-forming region within the molecular cloud associated with Cep OB3. It shows strings of sources whose spectra suggest that some are thermal and some nonthermal (Hughes & Wouterloot 1984; Hughes 1985, 1988), several compact HII regions (Beichman et al. 1979; Rodríguez et al. 1980a), OH, H<sub>2</sub>O, and CH<sub>3</sub>OH masers (Blitz & Lada 1979; Wouterloot, Habing & Herman 1980; Lada et al. 1981; Cohen, Rowland & Blair 1984; Mehringer, Zhou & Dickel 1997; Patel et al. 2007), and strong infrared emission (Koppelaar et al. 1979; Beichman et al. 1979; Evans et al. 1981) within an area smaller than 1 arcmin. Cep A has been therefore an exciting target for high-resolution interferometric observations and has a huge literature.

A powerful molecular outflow was discovered by Rodríguez et al. (1980a) and studied in further detail by among others Richardson et al. (1987), Torrelles et al. (1987), Hayashi, Hasegawa & Kaifu (1988), Bally & Lane (1990), Torrelles et al. (1993), Narayanan & Walker (1996), and Froebrich et al. (2002). Water maser emission has been detected from several centers of activity (Torrelles et al. 1996), and numerous thermal and nonthermal radio sources (Garay et al. 1996; Hughes 2001). The HH object HH 168 (original name GGD 37), consisting of several knots (Hartigan & Lada 1985), lies about 2' west of Cep A. It was studied in detail by Hartigan & Lada (1985), Lenzen et al. (1984), Hartigan et al. (1986), Lenzen (1988), Garay et al. (1996), Wright et al. (1996), and Hartigan, Morse & Bally (2000). An apparent counter-flow of HH 168, HH 169 was discovered by Lenzen (1988) 2' northeast of Cep A. The objects are part of a larger, elliptical region containing several fainter HH objects (Corcoran, Ray & Mundt 1993). A comprehensive summary of the literature of HH 168 and 169 can be found in Reipurth (1999).

Hughes & Wouterloot (1982) mapped Cep A at 21 cm. The map has shown the presence of two sources, Cep A West and Cep A East, separated by  $\sim 1''.5$ . Cep A West is associated with optical nebulosities and an optically visible star at its peak contour level. It is named *HW object* (Hartigan & Lada 1985), and appears to be an HII region on the near side of the cloud. Hughes (1989) obtained radio maps of Cep A West, and found it to consist of two compact sources, W 1 and W 2. The first component is constant in time, while the second is variable, and there is a third, diffuse component, W 3. The HW object was found to be nonstellar, radiating mainly in H $\alpha$ , and suggested to be an HH object. Garay et al. (1996) studied in detail the three sources within Cep A

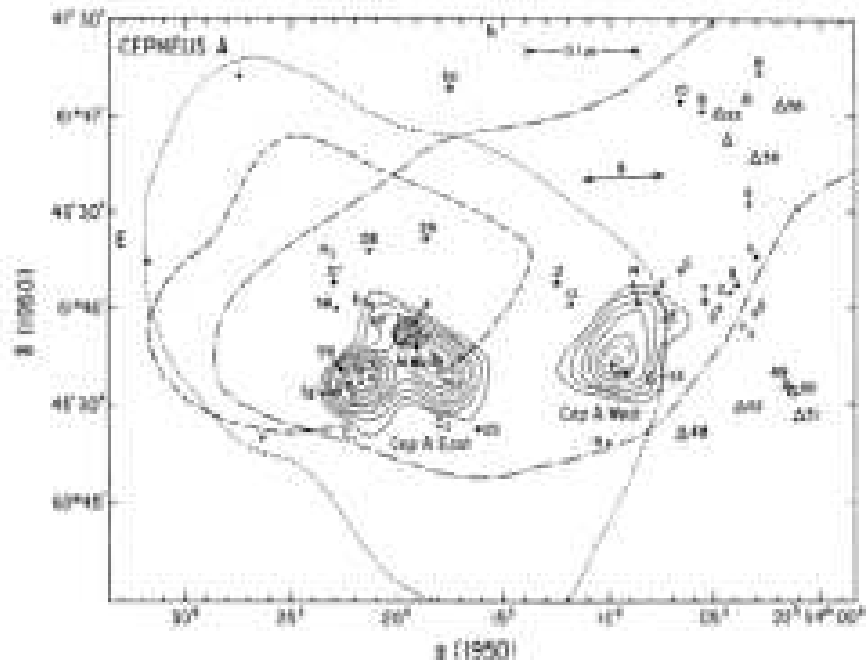


Figure 30. Structure of Cepheus A (Hartigan & Lada 1985). Solid lines show the 20 cm continuum contours (Rodríguez & Cantó 1983), dot-dash and long-dashed lines show the distribution of the redshifted and blueshifted CO, respectively (Rodríguez et al. 1980a), and a short-dashed line shows the extent of the  $\text{NH}_3$  emission (Ho, Moran & Rodríguez 1982). Triangles are reflection nebulae, plus signs indicate HH objects, and filled circles are visible stars. The hatched circular area is an extended 20  $\mu\text{m}$  emission area (Beichman et al. 1979). Small numbered open circles show the 6 cm continuum sources, detected by Hughes & Wouterloot (1984) and shown in more detail in Fig. 31.

West, and found that the energy source, powering the activity observed in Cep A West, is probably W 2, associated with a low-luminosity embedded pre-main sequence star, whereas emission of the shocked gas flowing from W 2 can be observed from the diffuse component W 3. Wright et al. (1996), based on observations by ISO SWS, studied the molecular hydrogen emission from the GGD 37 complex in Cep A West.

OH and  $\text{H}_2\text{O}$  maser sources are situated near the center of Cep A East, which appears younger and more heavily extinguished than Cep A West. Hughes & Wouterloot (1984) performed radio observations of Cep A East, with resolutions down to  $1''$  at 21 cm and 6 cm, using both the Westerbork Synthesis Radio Telescope and VLA. The maps have shown two strings of 14 compact radio sources, numbered as HW 1a, 1b, 2, 3a–d, 4, 5, 6, 7a–d, (see Fig. 31) which were interpreted as HII regions, being produced by about 14 stars, each of which mimics main-sequence B3 stars; the length of each string is about 0.1 pc. Hughes (1988; 1993) reported on the variability and high proper motion of some compact radio sources of Cep A East and discovered two new, highly variable compact radio sources (sources 8 and 9). He suggested that, contrary to the original interpretation, some of the compact sources are probably not HII regions, but Herbig–Haro objects. Garay et al. (1996), based on multifrequency, high resolution ra-

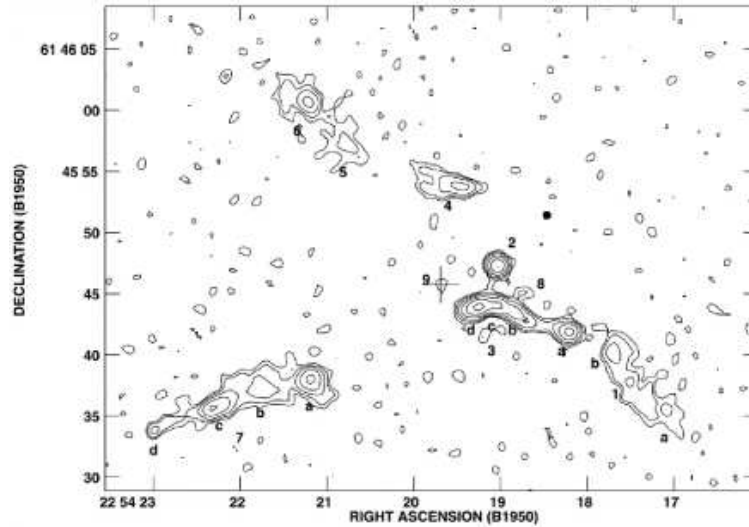


Figure 31. VLA map at 6 cm of Cep A East, observed by Hughes & Wouterloot (1984), displaying two chains of 14 compact sources.

dio continuum observations, classified the 16 compact sources into two groups: sources 2, 3a, 3c, 3d, 8, and 9 harbor an energy source, whereas sources 1a, 1b, 4, 5, 6, 7a, 7b, 7c, and 7d are excited by an external source of energy. Of the stellar sources, HW 2, 3c, and 3d are probably associated with high luminosity stars, while the variable sources 3a, 8, and 9 are probably low-mass pre-main sequence stars. The nature of source 3b remained uncertain. Torrelles et al. (1998) detected a new continuum source (Cep A:VLA 1) in an 1.3 cm VLA map. Goetz et al. (1998) present new infrared images, including near-infrared broadband (K, L', and M') and spectral line ([Fe II] emission line at  $1.644 \mu\text{m}$  and  $\text{H}_2$  1-0 S[1] line at  $2.122 \mu\text{m}$ ) observations of Cep A East. The images show two regions of shock-excited line emission from separate bipolar flows. Figure 30, adopted from Hartigan & Lada (1985), shows the schematic structure of the region of Cep A, and Fig. 31 shows the distribution of the radio continuum sources in Cep A East, discovered by Hughes & Wouterloot (1984).

Both the compact radio continuum and  $\text{H}_2\text{O}$  maser sources in Cep A exhibit remarkable variations on various time scales. Hughes (1985; 1988; 1993; 2001) reported on the variability of sources HW 2, 3c, and 3d, and pointed out that the strong variability results in appreciable changes in the spectra. Variations of  $\text{H}_2\text{O}$  maser emission have been detected by Mattila et al. (1985; 1988), Cohen & Brebner (1985), and Rowland & Cohen (1986).

Patel et al. (2007), using the Submillimeter Array (SMA), detected the 321.226 GHz,  $10_{29} - 9_{36}$  ortho- $\text{H}_2\text{O}$  maser emission from Cep A. The 22.235 GHz,  $6_{16} - 5_{23}$  water masers were also observed with the Very Large Array 43 days following the SMA observations. Three of the nine detected submillimeter maser spots are associated with the centimeter masers spatially as well as kinematically, while there are 36 22 GHz maser spots without corresponding submillimeter masers. The authors interpret the submillimeter masers in Cepheus A to be tracing significantly hotter regions (600-2000 K) than the centimeter masers.



Rodríguez et al. (1994) obtained multifrequency VLA radio continuum observations of HW 2, the most luminous radio continuum source of the region. They have shown HW 2 to be a powerful thermal radio jet, and suggest that it is responsible for at least part of the complex outflow and excitation phenomena observed in the region. HW 2 proved to be a complex object, consisting of several components (e.g. Gómez et al. 1999; Curiel et al. 2002, 2006; Jiménez-Serra et al. 2007; Brogan et al. 2007), including a hot core (Martín-Pintado et al. 2005). Torrelles et al. (2001) report three epochs of VLBA water maser observations toward HW 2. VLBA data show that some of the masers detected previously with the VLA (Torrelles et al. 1998) unfold into unexpected and remarkable linear/arcuate “microstructures,” revealing, in particular three filaments (R1, R2, R3) with length sizes  $\sim 3\text{--}25$  mas (2–18 AU) and unresolved in the perpendicular direction ( $\lesssim 0.1$  AU), an arcuate structure (R4-A) of  $\approx 20$  mas size (15 AU), and a curved chain of masers (R5) of  $\approx 100$  mas size ( $\approx 72$  AU). Some of these structures unfold into even smaller linear “building blocks” (down to scales of 0.4 AU) shaping the larger structures.

Jiménez-Serra et al. (2007) present VLA and PdBI subarcsecond images ( $0.15'' - 0.6''$ ) of the radio continuum emission at 7 mm and of the  $\text{SO}_2$   $J = 19_{2,18} - 18_{3,15}$  and  $J = 27_{8,20} - 28_{7,21}$  lines toward the Cep A HW 2 region. The  $\text{SO}_2$  images reveal the presence of a hot core internally heated by an intermediate-mass protostar, and a circumstellar rotating disk around the HW 2 radio jet of size  $600 \times 100$  AU and mass  $1 M_{\odot}$ . The high-sensitivity radio continuum image at 7 mm shows, in addition to the ionized jet, an extended emission to the west (and marginally to the south) of the HW2 jet, filling the southwest cavity of the HW 2 disk.

Torrelles et al. (2007) report SMA 335 GHz continuum observations with angular resolution of  $\sim 0''.3$ , together with VLA ammonia observations with  $\sim 1''$  resolution toward Cep A HW 2. The observations have shown a flattened disk structure of the dust emission of  $\sim 0''.6$  size (450 AU), peaking on HW 2. In addition, two ammonia cores were observed, one associated with a hot core previously reported and an elongated core with a double peak separated by  $\sim 1''.3$ , with signs of heating at the inner edges of the gas facing HW 2. The double-peaked ammonia structure, as well as the double-peaked  $\text{CH}_3\text{CN}$  structure reported previously (and proposed to be two independent hot cores), surround both the dust emission as well as the double-peaked  $\text{SO}_2$  disk structure found by Jiménez-Serra et al. (2007).

Pravdo & Tsuboi (2005) report the discovery of X-rays from both components of Cepheus A, East and West, with the XMM-Newton observatory. They detected prominent X-ray emission from the complex of compact radio sources and call this source HWX. Its hard X-ray spectrum and complex spatial distribution may arise from one or more protostars associated with the radio complex, the outflows, or a combination of the two. They also detected 102 X-ray sources, many presumed to be pre-main sequence stars on the basis of the reddening of their optical and IR counterparts.

Sonnentrucker et al. (2008) report the first fully sampled maps of the distribution of interstellar  $\text{CO}_2$  ices,  $\text{H}_2\text{O}$  ices and total hydrogen nuclei, as inferred from the  $9.7 \mu\text{m}$  silicate feature, toward Cepheus A East with the IRS instrument on board the Spitzer Space Telescope. They find that the column density distributions for these solid state features all peak at, and are distributed around, the location of HW2. A correlation between the column density distributions of  $\text{CO}_2$  and water ice with that of total hydrogen indicates that the solid state features mostly arise from the same molecular clumps along the probed sight lines.

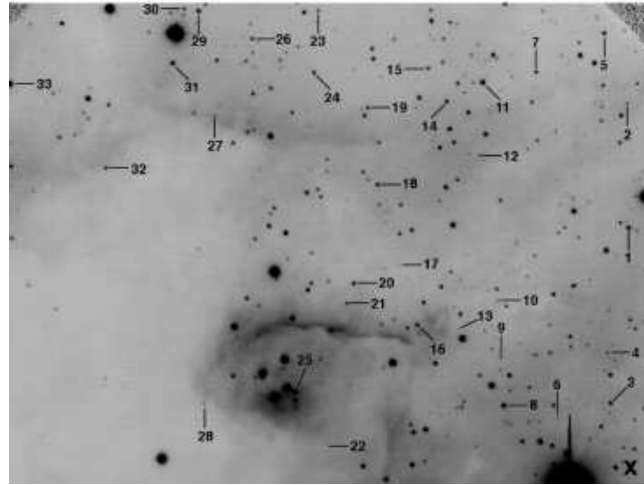


Figure 32.  $H\alpha$  emission stars in Cep B found by Ogura et al. (2002).

Comito et al. (2007) employed the Plateau de Bure Interferometer to acquire (sub-)arcsecond-resolution imaging of high-density and shock tracers, such as methyl cyanide ( $\text{CH}_3\text{CN}$ ) and silicon monoxide ( $\text{SiO}$ ), towards the HW2 position. They find that on the 1 arcsec ( $\sim 725$  AU) scale, the flattened distribution of molecular gas around HW2 appears to be due to the projected superposition, on the plane of the sky, of at least three protostellar objects, of which at least one is powering a molecular outflow at a small angle with respect to the line of sight. The presence of a protostellar disk around HW2 is not ruled out, but such structure is likely to be detected on a smaller spatial scale, or using different molecular tracers.

*Cepheus B* is located at the edge of the HII region S 155. Felli et al. (1978) and Panagia & Thum (1981) suggested that a younger subgroup of Cep OB3 originated from the Cep B/S 155 complex. Several features of the Cep B/S 155 interface indicate triggered star formation in Cep B, for instance a bright  $H\alpha$  nebula located near the ionization front, referred to as the  $H\alpha$  knot by Moreno-Corral et al. (1993) and Testi et al. (1995), a compact radio continuum source (source #9) detected by Felli et al. (1978), and the bright infrared source AFGL 3000.

Moreno-Corral et al. (1993) studied the S 155/Cep B interface with  $H\alpha$  and  $BV(RI)_C$  imaging, and identified a cluster of pre-main sequence stars in the  $H\alpha$  knot. Testi et al. (1995) performed radio and near infrared observations of the  $H\alpha$  knot. The unresolved radio source #9 lies on top of the diffuse emission. Far infrared and high resolution CO observations indicate that an embedded B1–B0.5 star is the source of heat for the molecular hot spot and the source of ionization of #9. More than 100 low luminosity stars have been found in an area of about  $3' \times 2'$ , and most of them lie above and to the right of the main sequence. Many of them are associated with reflection nebulosities. Testi et al. (1995) concluded that they are pre-main sequence stars. They identified new Herbig Ae/Be stars among the cluster members. Ogura et al. (2002) found 33  $H\alpha$  emission stars in Cep B. The list of these candidate pre-main sequence stars is given in Table 19, and the finding chart, adopted from Ogura et al. (2002) is displayed in Fig. 32. Getman et al. (2006) identified 64 members of the cluster embedded in Cep B, based on

deep X-ray observations with the Chandra Observatory (see Fig. 29). Mookerjea et al. (2006) studied the emission from the photon dominated regions in Cepheus B, based on  $15' \times 15'$  fully sampled maps of [C I] at 492 GHz and  $^{12}\text{CO}$  (4-3) observed at  $1'$  resolution. They estimated the column densities of neutral carbon in Cepheus B and studied the factors which determine the abundance of neutral carbon relative to CO.

Table 19.  $\text{H}\alpha$  emission stars associated with bright rimmed cloud Cep B (Ogura et al. 2002)

N	RA(J2000)	Dec(J2000)	EW*	Remarks*
1	22 56 37.97	62 39 51.1	69.7	
2	22 56 38.12	62 40 58.7	104.7	very weak cont.
3	22 56 39.33	62 38 15.5	80.1	
4	22 56 39.58	62 38 43.1	17.2	very weak cont.
5	22 56 39.93	62 41 37.1	14.6	M-star ?
6	22 56 43.54	62 38 07.5	...	invisible cont.
7	22 56 45.33	62 41 15.8	8.0	M-star ?
8	22 56 47.79	62 38 14.0	22.4	
9	22 56 48.02	62 38 40.2	125.6	very weak cont.
10	22 56 48.23	62 39 11.1	62.3	very weak cont.
11	22 56 49.54	62 41 10.0	21.4	
12	22 56 49.77	62 40 30.1	81.3	very weak cont.
13	22 56 51.41	62 38 55.8	...	invisible cont.
14	22 56 52.40	62 40 59.6	63.6	contam. from nearby star
15	22 56 53.87	62 41 17.7	19.0	
16	22 56 54.65	62 38 57.8	16.8	weak cont., contam. from bright rim
17	22 56 56.11	62 39 30.8	...	invisible cont.
18	22 56 57.83	62 40 14.0	59.8	
19	22 56 58.65	62 40 56.0	...	$\text{H}\alpha$ ?
20	22 56 59.68	62 39 20.2	76.4	
21	22 57 00.22	62 39 09.4	24.9	weak cont.
22	22 57 01.88	62 37 52.1	...	invisible cont.
23	22 57 02.63	62 41 48.7	...	contam. from nearby star
24	22 57 02.93	62 41 14.9	4.9	
25	22 57 04.31	62 38 21.1	...	contam. from neighboring stars
26	22 57 07.86	62 41 33.2	23.1	weak cont.
27	22 57 10.82	62 40 51.0	...	invisible cont., contam. from bright rim
28	22 57 11.48	62 38 14.1	39.6	very weak cont.
29	22 57 12.10	62 41 48.1	...	contam. from No. 30 star
30	22 57 13.26	62 41 49.3	...	contam. from No. 29 star
31	22 57 14.11	62 41 19.8	...	double star, both show $\text{H}\alpha$ emission
32	22 57 19.38	62 40 22.5	...	$\text{H}\alpha$ ?, contam. from bright. rim
33	22 57 27.04	62 41 07.9	6.4	
34N	22 57 04.93	62 38 23.2	14.2	
35N	22 57 05.91	62 38 18.4	10.1	
36N	22 56 36.14	62 36 45.9	...	invisible cont.
37N	22 56 35.29	62 39 07.8	8.1	

\*Column revised by Ikeda et al. (2008)

*Cepheus C* The mass of this clump, estimated from the formaldehyde observations obtained by Few & Cohen (1983) is  $\sim 3600 N_{\odot}$ , which ranks Cep C as the most massive clump of the Cep OB3 molecular cloud. The region contains a cluster of infrared sources (Hodapp 1994) and is associated with water maser emission (Wouterloot & Walmsley 1986) and an outflow (Fukui 1989). The Cep C cluster, first identified in a near-IR survey by Hodapp (1994), was included in the Young Stellar Cluster survey performed by the *Spitzer Space Telescope* (Megeath et al. 2004). In addition to the near-IR cluster,

the IRAC data show Class I and II sources distributed over a 3 pc diameter region. The molecular gas traced by the C<sup>18</sup>O is visible in the IRAC images as filamentary dark clouds obscuring a diffuse nebulosity extending across the entire mosaic. Two Class I objects appear outside the C<sup>18</sup>O emission; <sup>13</sup>CO emission is found toward both of these sources.

*Cepheus E* is the second most massive and dense clump ( $M \sim 2100 M_{\odot}$ ) of the Cep OB3 molecular cloud according to the H<sub>2</sub>CO map (Few & Cohen 1983). An outflow was identified in Cepheus E based on millimeter CO observations (Sargent 1977; Fukui 1989), followed by near-infrared and higher spatial resolution CO studies (Hodapp 1994; Eislöffel et al. 1996; Ladd & Hodapp 1997; Noriega-Crespo et al. 1998).

The outflow is quite compact, and driven by the source IRAS 23011+6126, also known as Cep E-mm. The outflow is deeply embedded in a clump of density  $10^5 \text{ cm}^{-3}$  and nearly invisible at optical wavelengths, with the exception of its southern lobe, which is breaking through the molecular cloud and is seen as HH 377 (Devine et al. 1997; Noriega-Crespo 1997; Noriega-Crespo & Garnavich 2001; Ayala et al. 2000). Lefloch, Eislöffel & Lazareff (1996) have shown that IRAS 23011+6126 is a Class 0 protostar. The properties of the outflow have been thoroughly analyzed by Eislöffel et al. (1996), Moro-Martin et al. (2001) and Smith et al. (2003). H<sub>2</sub> and [FeII] images obtained by Eislöffel et al. (1996) have shown two, almost perpendicular outflows emanating from Cep E, suggesting that the driving source is a Class 0 binary. Submillimeter and near-infrared line and continuum observations by Ladd & Hodapp (1997) led to a similar conclusion. With the assumption that the morphology of the jet results from precession, Terquem et al. (1999) inferred an orbital separation of 4–20 AU and disk radius of 1–10 AU for the binary.

Hot molecular bullets were detected in the outflow by Hatchell, Fuller & Ladd (1999). A comparative study of the Cep E-mm source, in the context of other well known Class 0/I sources, was carried out by Froebrich et al. (2003).

Submillimeter observations by Chini et al. (2001) and far-infrared photometry by Froebrich et al. (2003) resulted in  $L_{\text{submm}}/L_{\text{bol}} = 0.017 \pm 0.001$ , an envelope mass  $M_{\text{env}} = 7.0 M_{\odot}$ , an estimated age of  $3 \times 10^4$  yr, and an H<sub>2</sub> luminosity of  $0.07 L_{\odot}$ , which confirm that Cep E-mm belongs to the Class 0 objects. At a distance<sup>2</sup> of 730 pc, Cep E-mm is one of the brightest Class 0 protostars known and likely to become an intermediate-mass ( $3 M_{\odot}$ ) star (Moro-Martin et al. 2001; Froebrich et al. 2003).

The Cep E outflow and its protostellar source have been observed using the three instruments aboard the Spitzer Space Telescope (Noriega-Crespo et al. 2004). The new observations have shown that the morphology of the outflow in the mid-infrared is remarkably similar to that of the near-infrared observations. The Cep E-mm source or IRAS 23011+6126 was detected in all four IRAC channels. The IRAC and MIPS integrated fluxes of the Cep E-mm source are consistent with the Class 0 envelope models.

---

<sup>2</sup>Throughout the literature of Cep E, the distance of 730 pc is used. This value is not an independent estimate for this cloud, but rounded from the 725 pc derived by Blaauw et al. (1959) and Crawford & Barnes (1970) for Cep OB3 (see Ladd & Hodapp 1997).

*Cepheus F* (L 1216) contains V733 Cep (Persson’s star), the only known bona fide FUor in the star forming regions of Cepheus, located at the coordinates 22:53:33.3, +62:32:23 (J 2000). The brightening of this star was discovered by Persson (2004) by comparing the old and new Palomar Sky Survey plates. Reipurth et al. (2007) have shown that the optical spectrum of Persson’s star exhibits all the features characteristic of FU Ori type stars. They also identified a molecular outflow associated with the star. At an assumed distance of 800 pc the observed apparent magnitude  $R \sim 17.3$  mag, together with the extinction  $A_V \sim 8$  mag, estimated from the strength of the water vapor features in the infrared spectrum, corresponds to a luminosity of about  $135 L_{\odot}$ . The star erupted sometime between 1953 and 1984.

Reipurth et al. (2007) identified several nebulous near-infrared sources in L 1216 around IRAS 22151+6215 (Table 20, adopted from Reipurth et al. 2007). To the south of the aggregate of infrared sources containing Persson’s star there is an extended far-infrared source, Cep F(FIR) (Sargent et al. 1983), with a luminosity of about  $500 L_{\odot}$ . Several IRAS sources can be found around this object (see Table 21, adopted from Reipurth et al. 2007), which most probably form an embedded cluster containing a Herbig Ae/Be star. A compact HII region without an obvious IRAS counterpart, Cep F(HII), was discovered by Harten, Thum & Felli (1981) to the south of Cep F(FIR).

Table 20. Near-infrared sources in Cep F around IRAS 22151+6215 (Reipurth et al. 2007)

ID	RA(2000)	Dec(2000)	$K'$
IRS 1	22 53 40.7	62 32 02	16.3
IRS 2	22 53 41.1	62 31 56	13.7
IRS 3	22 53 40.9	62 31 49	18.1
IRS 4	22 53 41.0	62 31 48	17.4
IRS 5	22 53 41.2	62 31 48	15.6
IRS 6	22 53 43.3	62 31 46	14.2

Table 21. IRAS sources around Cep F(FIR) (Reipurth et al. 2007)

IRAS	RA(2000)	Dec(2000)	$12\mu\text{m}$	$25\mu\text{m}$	$60\mu\text{m}$	$100\mu\text{m}$	$L_{IRAS}$
22507+6208	22 50 47.9	62 08 16	0.54:	1.00	12.99:	53.98	18
22152+6201	22 51 14.1	62 01 23	1.61	4.86	13.11	<104.62	23
22518+6208	22 51 53.5	62 08 02	2.07	1.92:	34.53	210.21:	56
22521+6205	22 52 08.0	62 05 51	0.62	1.84	<21.48	257.23:	49

*L 1211* is a class 5 dark cloud (Lynds 1962) about  $1^{\circ}$  west of Cepheus A (see Fig. 27). The mass of this cloud, derived from  $^{13}\text{CO}$  measurements, is  $1900 M_{\odot}$  (Yonekura et al. 1997). Its angular proximity to the group of Cepheus A-F clouds and its similar LSR velocity suggest that it is related to the group, and therefore lies at a similar distance from the Sun (725 pc, see Blaauw et al. 1959; Crawford & Barnes 1970; Sargent 1977). Fukui (1989) has reported a bipolar outflow around the embedded source IRAS 22453+6146. Harju et al. (1993) have mapped the ammonia emission around this source, finding a dense molecular core, and Hodapp (1994) has imaged the region in the  $K'$  band, finding a small cluster of sources associated with diffuse emission.

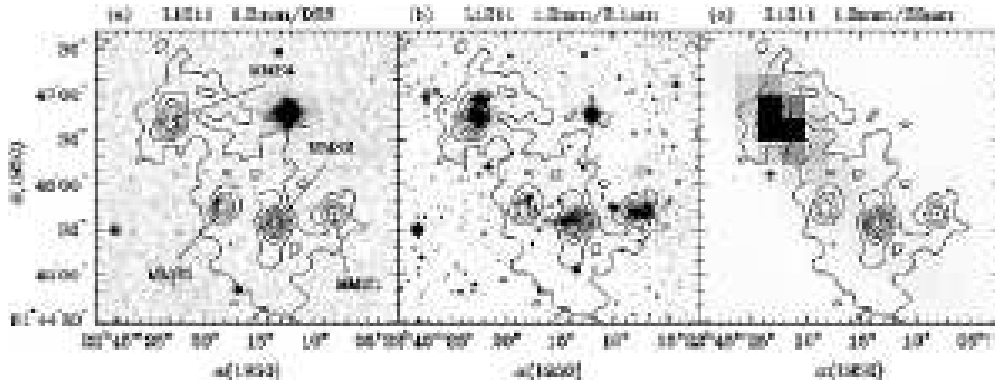


Figure 33. Distribution of 1.2 mm emission (contours) in L 1211 superimposed on images of emission at different wavelengths. (a) Optical DSS (red) image. (b)  $K'$  ( $2.1 \mu\text{m}$ ) image from Hodapp (1994). (c)  $25 \mu\text{m}$  IRAS HIRES image. Contours are at intervals of 25 mJy per beam starting at 25 mJy per beam. Adopted from Tafalla et al. (1999).

Tafalla et al. (1999) conducted millimeter continuum and line observations of a dense core in L 1211. They have found a small cluster of at least 4 millimeter sources with no optical counterparts, but each associated with near infrared diffuse emission. The strongest mm source has no NIR point-like counterpart, and constitutes a good candidate for a Class 0 object. The other mm objects appear associated with NIR sources and most likely belong to Class I, as also suggested by the spectral energy distributions derived from combining mm data with IRAS *HIRES* fluxes. As evidenced by mm line data, the mm sources are embedded in an elongated, turbulent core of about  $150 M_{\odot}$  of mass and 0.6 pc length. Two of the millimeter sources power bipolar molecular outflows, another signature of their extreme youth. These outflows are referred to as the L1211-MMS1 and L1211-MMS4 outflows. L 1211 is included in the far-infrared (ISOPHOT) photometric studies of embedded objects performed by Froebrich et al. (2003). Table 22 lists the coordinates, millimeter fluxes and estimated masses of the mm-sources in L 1211, and Fig. 33 shows their appearance at different wavelengths (adopted from Tafalla et al. 1999). Table 23 lists the Herbig–Haro objects in the Cepheus OB3 molecular cloud.

Table 22. L 1211 millimeter sources

Source	RA(2000)	Dec(2000)	Int. flux (mJy)	Mass* ( $M_{\odot}$ )
MMS 1	22 46 54.5	62 01 31	45	0.3
MMS 2	22 47 07.6	62 01 26	215	1.3
MMS 3	22 47 12.4	62 01 37	85	0.5
MMS 4	22 47 17.2	62 02 34	135	0.8

\* Assuming optically thin dust at 30 K with an opacity of  $0.01 \text{ cm}^2 \text{ g}^{-1}$

Table 23. Herbig–Haro objects in the Cepheus OB3 molecular clouds.

Name	RA(2000)	Dec(2000)	Source	Cloud	d	Reference
[H89] W3	22 56 08.8	+62 01 44		Cep A	700	2
HH 168	22 56 18.0	+62 01 47	HW 2	Cep A	700	1,5
HH 169	22 56 34.8	+62 02 36	HW 2	Cep A	700	3
HH 174	22 56 58.5	+62 01 42	HW 2	Cep A	700	4
HH 377	23 03 00.0	+61 42 00	IRAS 23011+6126	Cep E	700	6

References: 1 – Gyulbudaghian, Glushkov & Denisjuk (1978); 2 – Hughes (1989); 3 – Corcoran, Ray & Mundt (1993); 4 – Bally et al. (1999); 5 – Hartigan, Morse & Bally (2000); 6 – Devine et al. (1997).

## 6. Star Formation in Cepheus OB4

### 6.1. Structure of Cep OB4

Cep OB4 was discovered by Blanco & Williams (1959), who noticed the presence of 16 early-type stars in a small region around  $(l,b)=(118^\circ.4,+4^\circ.7)$ , including the cluster Berkeley 59. Cep OB4 is related to a dense, irregular dark cloud containing several emission regions, including the dense H II region S 171 (W 1) in the central part, and NGC 7822 to the north of S 171 (Lozinskaya, Sitnik & Toropova 1987), see Fig. 34. We note that in the original catalogs both W 1 (RA(J2000)=00 02 52; Dec(J2000)=+67 14, Westerhout 1958) and S 171 (RA(J2000)=00 04 40.3; Dec(J2000)=+67 09, Sharpless 1959) are associated with NGC 7822, situated about one degree north of the H II region, according to its catalog coordinates (RA(J2000)=00 03.6; Dec(J2000)=+68 37). The *Simbad* data server also associates these objects with each other. A detailed description of the association and related objects was given by MacConnell (1968). He identified 42 members earlier than B8 at 845 pc. MacConnell’s UVB photometric study of the luminous members of Cep OB4 revealed a correlation between the luminosity and reddening of the stars: the O and early B stars were found only within the cloud, whereas later B type stars are found only outside the cloud due to the incompleteness of their detection. Based on the absence of supergiants, an earliest spectral type of O7 V, and the gravitational contraction time of a B8 star, MacConnell estimated an age between 0.6 and 6 Myr.

Lozinskaya et al. (1987) studied the morphology and kinematics of the H II regions associated with Cep OB4 based on monochromatic images of the [OIII], [NII], [SII] and  $H\alpha$  lines, and found two expanding shells: one shell, of radius  $\sim 0.7$ , connects NGC 7822 and S 171. Most Cep OB4 members are located inside this shell; their energy input into the interstellar medium can account for its observed size and expansion velocity of  $10 \text{ km s}^{-1}$ . The other shell, of radius  $\sim 1.5$ , is centered on S 171 and has an expansion velocity of  $\sim 30\text{--}40 \text{ km s}^{-1}$ ; it may be the result of a supernova explosion or of the stellar wind of a massive star that so far has escaped detection.

Olano et al. (2006) found that the space distribution and kinematics of the interstellar matter in the region of Cep OB4 suggest the presence of a big expanding shell, centered on  $(l,b) \sim (122^\circ,+10^\circ)$ . Assuming a distance of 800 pc for the center they derived a radius of some 100 pc, expansion velocity of  $4 \text{ km s}^{-1}$ , and HI mass of  $9.9 \times 10^4 M_\odot$  for the Cepheus OB4 Shell, whose approximate position is plotted in Fig. 1.

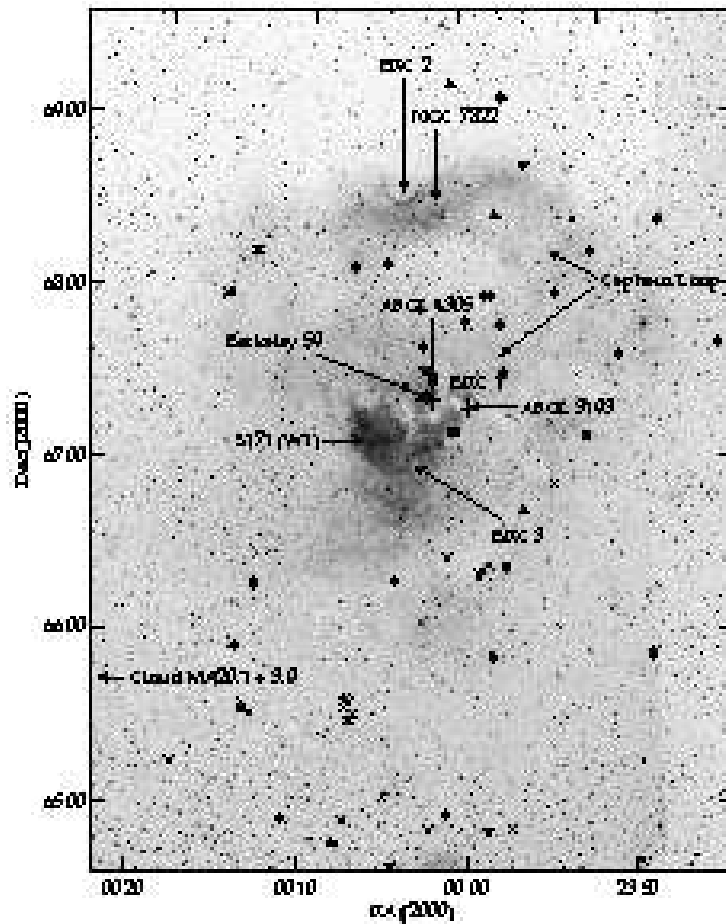


Figure 34. A large scale red photograph of the Cep OB4 region. The infrared sources and the radio continuum loop are indicated on the red DSS image. The HII region W1 is also known as S171. Star symbols show the luminous stars of Cep OB4 (Rossano et al. 1983), and crosses mark the  $H\alpha$  emission stars (MacConnell 1968).

Only 19 of the 42 classical members of Cep OB4 are listed in the Hipparcos Catalog (de Zeeuw et al. 1999). This may be caused by a combination of crowding effects and the large extinction toward Cep OB4,  $A_V > 3$  mag (MacConnell 1968). Based on their proper motions and parallaxes, three MacConnell stars (HIP 117724, 118192, 118194) are not associated with Cep OB4. De Zeeuw et al. (1999) found that the Hipparcos parallaxes of the other classical members are consistent with a distance of 800–1000 pc.

Rossano, Grayzeck & Angerhofer (1983) mapped the Cep OB4 region in the 6 cm transition of  $H_2CO$ , and detected neutral gas at the velocities  $-13$ ,  $-7$ , and  $-1$   $\text{km s}^{-1}$ . They established that Cep OB4 consisted of two kinematically distinct components, W1 west and W1 east, and a loop-shaped, optically thin, thermal shell, the Cep Loop. They modeled the observed morphology and kinematics as follows. The association Cep OB4 consists of two subgroups with differing ages and kinematic properties. The



older, dispersed, subgroup extends over an area about 4 degrees (60 pc) in diameter, clustered towards the Cep Loop. The younger subgroup, the young cluster Berkeley 59, extends over an area of 15' (about 4 pc) in diameter, located along the southern edge of the Cep Loop. The average velocity of the OB stars of the older subgroup is  $-6 \text{ km s}^{-1}$ . Thus Rossano et al. (1983) propose that the gas component at  $-7 \text{ km s}^{-1}$  represents the undisturbed gas associated with the star forming region. Beginning with a cloud complex having a velocity of  $-7 \text{ km s}^{-1}$ , star formation occurred near the center of what is now the Cep Loop. The Cep Loop was subsequently formed by this first generation of OB stars. Expansion of the Cep Loop into a cloud to the north resulted in collisional excitation of the HII region NGC 7822. In the south, expansion of the Cep Loop resulted in fragmentation of the remainder of the original dark complex producing clouds at  $-13$  and  $-1 \text{ km s}^{-1}$ . Berkeley 59 was formed in this environment. Ionization of the clouds surrounding Berkeley 59 has resulted in ionized gas at each velocity component. Ionization is now occurring most actively in a  $-1 \text{ km s}^{-1}$  cloud west of Be 59. Okada et al. (2003) studied the photodissociation region associated with S 171 using mid- to far-infrared spectroscopy using the ISO SWS, LWS, and PHT-S instruments. Gahm et al. (2006) investigated the structure and velocity of an elephant trunk associated with NGC 7822. Figure 34, based on Fig. 1 of Rossano et al. (1983), shows a large scale red photograph of the Cep OB4 region. The infrared sources and the radio continuum loop are indicated. Star symbols show the luminous stars of Cep OB4, and crosses mark the  $\text{H}\alpha$  emission stars.

## 6.2. Low and Intermediate Mass Star Formation in Cep OB4

MacConnell (1968) found 24  $\text{H}\alpha$  emission-line (named as MacCH1–H24) objects within the dark cloud in the region of Cep OB4, some of which may be T Tauri stars. Cohen & Kuhi (1976) obtained optical spectrophotometry and infrared photometry of some MacCH stars, determined their spectral types and luminosities, as well as masses and ages using Iben's (1965) pre-main sequence evolutionary tracks. They identified four new nebulous stars in the same field (MC 1–MC 4), three of which have shown  $\text{H}\alpha$  emission. Table 24 lists the  $\text{H}\alpha$  emission stars found by MacConnell, and nebulous  $\text{H}\alpha$  emission stars reported by Cohen & Kuhi (1976), supplemented by the spectral types determined by Cohen & Kuhi (1976).

Sharma et al. (2007) obtained slitless spectroscopy and JH photometry for Berkeley 59. They identified 9  $\text{H}\alpha$  emission stars, whose location in the  $J/J-H$  color-magnitude diagram indicates that they may be pre-main sequence stars. The age of the cluster was estimated from the turn-off and turn-on points and is found to lie between about 1 and 4 million years. Pandey et al. (2008) present  $UBVI_C$  CCD photometry of Be 59 with the aim to study the star formation scenario in the cluster. Using slitless spectroscopy, they have identified 48  $\text{H}\alpha$  emission stars in the region of Be 59. The ages of these YSOs range between  $<1$  and  $\sim 2$  Myr, whereas the mean age of the massive stars in the cluster region is found to be  $\sim 2$  Myr. They found evidence for second-generation star formation outside the boundary of the cluster, which may be triggered by massive stars in the cluster. The radial extent of the cluster is found to be  $\sim 10$  arcmin (2.9 pc). The interstellar extinction in the cluster region varies between  $E(B-V) = 1.4$  to 1.8 mag. The ratio of total-to-selective extinction in the cluster region is estimated as  $3.7 \pm 0.3$ . The distance of the cluster is found to be  $1.00 \pm 0.05$  kpc.

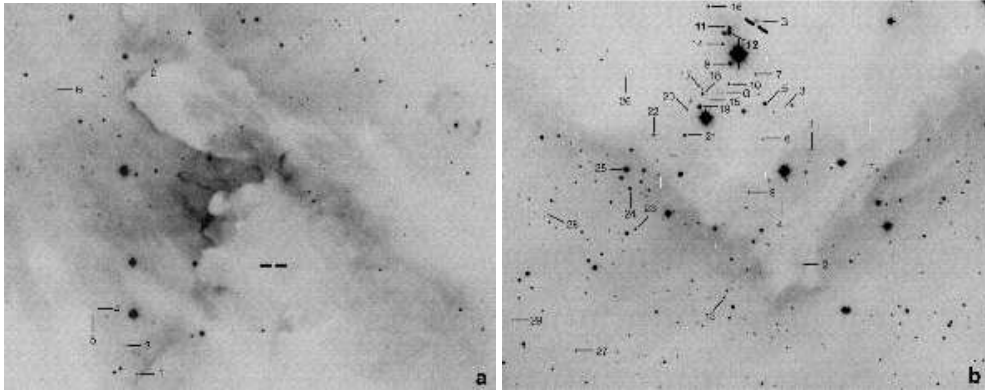


Figure 35.  $H\alpha$  emission stars discovered by Ogura et al. (2002) in BRC 1 (left) and BRC 2 (right) associated with S 171. The position of the IRAS source associated with the cloud is shown by a pair of thick tick marks.

Spectroscopic observations of the eclipsing binary system BD+66° 1673 by Majaess et al. (2008) revealed it to be an O5 V((f)n) star and the probable ionizing star of the Be 59/Cep OB4 complex.

Yang & Fukui (1992) discovered two dense molecular clumps near Be 59 and in the central region of S 171. They have shown that the clumps indicate the interaction between the HII region and the neighboring molecular cloud.

Sugitani et al. (1991) identified three bright rimmed clouds, BRC 1, BRC 2, and BRC 3, associated with S 171. We note that BRC 2 is actually associated with NGC 7822 (see Fig. 34). Ogura et al. (2002) found  $H\alpha$  emission stars in BRC 1 and BRC 2. Each cloud is included in the SCUBA survey of bright rimmed clouds by Morgan et al. (2008). Table 25 lists the coordinates and  $H\alpha$  equivalent widths (revised by Ikeda et al. 2008) of these stars, and Fig. 35 shows the finding charts.

The bright rimmed cloud BRC 2 contains a compact cluster of  $H\alpha$  emission stars. The *S171 cluster* was observed by the IRAC on board the *Spitzer Space Telescope* (Megeath et al. 2004). The cluster of young stars is situated near the edge of the cloud with a dense group of five Class I sources at the northern apex of the cluster. This morphology suggests that star formation is triggered by a photoevaporation-driven shock wave propagating into the cloud, as first proposed for this region by Sugitani et al. (1991). In addition to the stars in the cluster, *Spitzer* detected six Class II and two Class I objects spread throughout the molecular cloud. The presence of these stars suggests that a distributed mode of star formation is also occurring in the cloud.

A new generation of low mass stars has been born in the molecular clouds in the neighborhood of the young luminous stars. Yang et al. (1990) reported on the discovery of a molecular cloud in Cep OB4. The cloud M 120.1+3.0, appearing dense and filamentary, is composed of two parts. Each of the two parts has a size of  $6 \text{ pc} \times 1 \text{ pc}$ , and a mass of  $800 M_{\odot}$ . The cloud is associated with 12 low luminosity ( $L < 20 L_{\odot}$ ) IRAS sources, and the locations of the sources show remarkable coincidence with the distribution of the dense molecular gas. Two molecular outflows have been discovered towards two IRAS sources, IRAS 00213+6530 and IRAS 00259+6510. The results indicate that low-mass star formation took place recently in the cloud.

Table 24. Data for the H $\alpha$  emission stars found by MacConnell (1968) and Cohen & Kuhl (1976) in the region of Cep OB4

Name	Other name	RA(2000)	Dec(2000)	V	B-V	U-B	Type	Remarks
H1	HBC 742	23 52 33.0	68 25 55	14.97	1.47	+0.27	B8e $\alpha$	
H2		23 41 45.0	66 39 36	12.47	1.1	-0.09		1
H3	HBC 319, Blanco 1	23 54 26.6	66 54 17	14.50	1.09	-0.15	K2	2,20
H4	HBC 321n, Blanco 3	23 58 41.4	66 26 11	14.67	1.96:		A9e $\alpha$	3
H5	HBC 322, Blanco 4	23 59 20.2	66 23 10	15.80	1.75:		K5	4,20
H6		23 59 12.0	66 22 16	16.79			pT	
H7	Blanco 5	0 00 57.3	66 28 53	16.68	0.97		pT	5
H8	Blanco 11	0 15 21.6	65 45 32	17.33	0.60:		pT	6
H9	Blanco 10	0 13 29.1	65 35 59	14.96	1.28:	+0.72:	K4	7,20
H10	Blanco 9	0 12 54.4	65 34 09	14.72	1.51:	+0.52:	K4	8,20
H11	Blanco 7	0 07 06.1	65 40 15	16.83	0.92:		pT	
H12		0 07 03.1	65 38 37	16.23	1.12:		F:	9,20
H13	Blanco 8	0 07 18.4	65 36 42	16.77	0.87:		pT	10
H14		23 41 24.8	65 40 40	15.74				
H15	GG 179	0 17 35.0	65 16 08	12.12	1.04	-0.10		11
H16	Sh 118	0 07 20.2	64 57 21	13.79	1.17	-0.36		12
H17		0 04 52.2	65 05 49	13.49	0.83	-0.12		13
H18	HBC 323, Blanco 6	0 02 13.0	64 54 22	14.21	1.29:	+0.02:	K7	14,20
H19	HBC 320, Blanco 2	23 57 34.3	64 54 21	14.21	1.29:	+0.02:	K3	15,20
H20	GG 162	23 50 02.3	64 41 41	12.23				
H21		0 06 40.6	65 34 52	11.55	0.49	+0.32		16
H22	MWC 1085	23 52 12.4	67 10 07	9.96	0.53	-0.22	B3e	17
H23	AS 517	23 57 33.9	66 25 54	10.37	0.70	+0.01	B5e	18
H24	AS 2	0 12 58.9	66 19 19	10.68	0.77	+0.25	B5e	19
MC1		0 06 57.9	65 37 21	14.6			A5	20
MC2		0 35 57.5	66 19 15	14.1			A2	20
MC3		0 16 35.0	65 43 20	16.8			K5	20
MC4		0 16 42.0	65 44 20	14.4			K4	20
sH15		0 13 23.9	65 35 20	13.6			K1	20

Remarks: (1) Faint, blue continuum; could be Be. (2) Probable Ca II infrared emission; suspected var. in B. (3) LkHa 259; probably not T Tauri type. (4) Found independently by Herbig (unpublished); probable Ca II infrared emission; var. in B and V. (5) Found independently by Herbig (unpublished). (6) Suspected var. in B (no filter) and V. (8) Found independently by Herbig (unpublished); probable var. in V. (7) Found independently by Herbig (unpublished); probable var. in V. (8) Found independently by Herbig (unpublished); probable var. in V. (9) Near-red nebulosity; probable Ca II infrared emission; var. in V. (10) Var. in V. (11) Faint, blue continuum; could be Be. (12) Known planetary nebula, Sh 118. (13) Faint, blue continuum; could be Be. (14) Var. in U and V. (15) Var. in U and V. (16) New Be star; spectral type about B8, very broad Balmer lines, particularly H $\zeta$  and H $\eta$ . (17) Known Be star; No. 30 of MacConnell's Table 3. (18) Known Be star; No. 33 of MacConnell's Table 3. (19) Known Be star; No. 32 of MacConnell's Table 3. (20) Spectral type from Cohen & Kuhl (1976)

## 7. Cepheus OB6

The nearby association Cep OB6 first appeared in the literature in 1999. De Zeeuw et al. (1999) identified this moving group of 27 stars in the Hipparcos data base. The stars show a modest concentration at  $(l,b) \approx (104^\circ, -0^\circ.5)$ . The final sample contains 20 stars, 6 B, 7 A, 1 F, 2 G and 3 K type in the area  $110^\circ < l < 110^\circ$ , and  $-2^\circ < b < +2^\circ$ . The brightest member is the K1Ib supergiant  $\zeta$  Cep (HIP 109492). The color-magnitude diagram is very narrow, and strengthens the evidence that these stars form

Table 25. H $\alpha$  emission stars associated with bright rimmed clouds of S 171 and NGC 7822 (Ogura et al. 2002; Ikeda et al. 2008).

N	RA(J2000)	Dec(J2000)	EW(H $\alpha$ )	Remarks
BRC 1				
1	23 59 42.50	67 22 27.8	...	invisible cont., contam. from nearby star
2	23 59 43.72	67 25 50.0	26.6	weak cont.
3	23 59 43.99	67 22 46.8	...	invisible cont.
4	23 59 47.61	67 23 11.2	...	H $\alpha$ ?, invisible cont.
5	23 59 47.98	67 23 06.9	...	H $\alpha$ ?, weak cont.
6	23 59 52.75	67 25 37.5	32.6	weak cont.
BRC 2				
1	00 03 51.03	68 33 15.8	...	H $\alpha$ ?
2	00 03 52.32	68 31 58.8	...	invisible cont.
3	00 03 54.52	68 33 44.6	...	contam. from nearby stars
4	00 03 54.98	68 32 42.8	145.7	very weak cont.
5	00 03 57.12	68 33 46.7	15.6	
6	00 03 57.35	68 33 23.0	99.6	
7	00 03 58.33	68 34 06.5	13.1	
8	00 03 59.12	68 32 47.3	18.2	
9	00 04 01.70	68 34 13.8	2.8	
10	00 04 01.81	68 34 00.0	14.0	
11	00 04 01.80	68 34 37.4	5.5	
12	00 04 01.88	68 34 34.5	21.2	
13	00 04 02.32	68 31 36.2	...	H $\alpha$ ?
14	00 04 02.65	68 34 26.6	24.9	
15	00 04 04.69	68 33 49.3	25.8	weak cont.
16	00 04 04.59	68 34 52.2	23.0	
17	00 04 05.28	68 33 56.0	136.6	very weak cont.
18	00 04 05.26	68 33 53.1	50.4	
19	00 04 05.66	68 33 44.3	94.5	
20	00 04 07.33	68 33 42.3	...	invisible cont.
21	00 04 07.60	68 33 25.1	12.8	
22	00 04 11.66	68 33 25.4	46.7	
23	00 04 13.97	68 32 21.8	85.7	weak cont.
24	00 04 14.71	68 32 49.1	42.1	
25	00 04 15.18	68 33 02.0	16.1	
26	00 04 15.41	68 34 05.5	26.6	very weak cont.
27	00 04 21.66	68 30 59.6	...	H $\alpha$ ?
28	00 04 25.36	68 32 31.0	12.3	weak cont.
29	00 04 29.99	68 31 19.9	...	H $\alpha$ ?
30N	00 03 59.88	68 33 41.7	1.4	

a moving group, that is, an old OB association. The earliest spectral type is B5III, suggesting an age of some 50 million years. The mean distance of the association is  $270 \pm 12$  pc. The supergiant  $\delta$  Cephei, the archetype of Cepheid variables, also belongs to Cep OB6. Makarov (2007) during his study of the Galactic orbits of nearby stars found that a few members of the AB Dor moving group were in conjunction with the coeval Cepheus OB6 association 38 Myr ago. He proposed that the AB Dor nucleus formed 38 Myr ago during a close passage of, or encounter with, the Cepheus OB6 cloud, which may have triggered formation of the latter association as well. No younger subgroup of Cep OB 6 has been identified.

**Acknowledgments.** This work was supported by the Hungarian OTKA grant T049082. We are grateful to Jeong-Eun Lee for sending us the results on L 1251 B before publication, to Miklós RÁCZ for his help with some figures, to László Szabados

for a careful reading of the manuscript, and to Tom Megeath for the data in Table 17. We thank Giovanni Benintende, Richard Gilbert, John Bally, Robert Gendler, and Davide De Martin for the use of figures 6, 8, 10, 12, and 16, respectively. Bo Reipurth's referee report led to an enormous improvement of this chapter. We used the *Simbad* and *ADS* data bases throughout this work.

## References

- Ábrahám, P., Dobashi, K., Mizuno, A., & Fukui, Y. 1995, *A&A*, 300, 525
- Ábrahám, P., Balázs, L. G., & Kun, M. 2000, *A&A*, 354, 645
- Ábrahám, P., Leinert, Ch., Burkert, A., Henning, Th., & Lemke, D. 2000, *A&A*, 354, 965
- Alecian, E., Catala, C., Wade, G. A., Donati, J.-F., Petit, P., Landstreet, J. D., Böhm, T., Bouret, J.-C., Bagnulo, S., Folsom, C., Grunhut, J., & Silvester, J. 2008, *MNRAS*, 385, 391
- Altamore, A., Baratta, G. B., Cassatella, A., Grasdalen, G. L., Persi, P., & Viotti, R. 1980, *A&A*, 90, 290
- Alten, V. P., Bally, J., Devine, D., Miller, G. J. 1997, *Low Mass Star Formation - from Infall to Outflow*, poster proceedings of IAU 182, ed. F. Malbet & A. Castets, p.51
- Ambartsumian, V. A. 1949, *Dokl. Akad. Nauk. SSR*, 68, 22
- Amin, M. Y. 2001, *New Astr.*, 6, 393
- Anglada, G., Rodríguez, L. F., Cantó, J., Estalella, R., & Torrelles, J. M. 1992, *ApJ*, 395, 494
- Anglada, G., Sepúlveda, I., & Gómez, J. F. 1997, *A&AS*, 121, 255
- Arce, H. G. & Goodman, A. A. 2002, *ApJ*, 575, 911
- Arce, H. G. & Sargent A. I. 2004, *ApJ*, 612, 342
- Arce, H. G. & Sargent A. I. 2006, *ApJ*, 646, 1070
- Arce, H. G., Santiago-García, J., Jorgensen, J. K., Tafalla, M., & Bachiller, R. 2008, *ApJ*, 681, L21
- Armstrong, J. T. 1989, in *The Physics and Chemistry of Interstellar Molecular Clouds*, ed. G. Winnewisser & J. T. Armstrong (Berlin: Springer), p. 143
- Ashby, M. L. N., Plume, R., Carpenter, J. M., Neufeld, D. A. et al. 2000, *ApJ*, 539, L115
- Avery, L. W. & Chiao, M. 1996, *ApJ*, 463, 642
- Avila, R., Rodríguez, L. F., & Curiel, S. 2001, *RMxAA*, 37, 201
- Ayala, S., Noriega-Crespo, A., Garnavich, P., Curiel, S., Raga, A. C., & Böhm, K. H. 2000, *AJ*, 120, 909
- Baars, J. W. M. & Wendker, H. J. 1976, *A&A*, 49, 473
- Bachiller, R., Liehti, S., Walmsley, C. M., & Colomer, F. 1995, *A&A*, 295, 51
- Bachiller, R. & Pérez Gutiérrez, M. 1997, *ApJ*, 487, L93
- Bachiller, R., Pérez Gutiérrez, M., Kumar, M. S. N., & Tafalla, M. 2001, *A&A*, 372, 899
- Balázs, L. G., Ábrahám, P., Kun, M., Tóth, L. V., & Kelemen, J. 2004, *A&A*, 425, 133
- Balázs, L. G., Eisloffel, J., Holl, A., Kelemen, J., & Kun, M. 1992, *A&A*, 255, 281
- Balázs, L. G., Garibjanyan, A. T., Mirzoyan, L. V., Hambaryan, V. V., Kun, M., Frontó, A., & Kelemen, J. 1996, *A&A*, 311, 145
- Balázs, L.G. & Kun, M. 1989, *Astron. Nachr.*, 310, 192
- Bally, J., Devine, D., Fesen, R. A., & Lane, A. P. 1995, *ApJ*, 454, 345
- Bally, J., Reipurth, B., Lada, C. J., & Billawala, Y. 1999, *AJ*, 117, 410
- Bally, J. & Lane, A. P. 1990, *ASP Conf. Ser. 14, Astrophysics with Infrared Arrays*, ed. R. Elston, p. 273
- Bally, J. & Reipurth, B. 2001, *ApJ*, 552, L159
- Bally, J., Reipurth, B., Walawender, J., & Armond, T. 2002, *AJ*, 124, 2152
- Barnard, E.E. 1927, *Barnard's Catalogue of 349 Dark Objects in the Sky. A Photographic Atlas of Selected Regions of the Milky Way*, by Barnard, E.E., ed. Frost, E.B. and Calvert, M.R., Carnegie Institution of Washington  
see also <http://www.library.gatech.edu/barnard/>
- Bechis, K. P., Harvey, M. P. M., Campbell, M. F., & Hoffmann, W. F. 1978, *ApJ*, 226, 439
- Beichman, A., Becklin, E. E., & Wynn-Williams, C. G. 1979, *ApJ*, 232, L47

- Beichman, C. A., Myers, P. C., Emerson, J. P., et al. 1986, *ApJ*, 307, 337
- Beltrán, M. T., Estalella, R., Anglada, G., Rodríguez, L. F., & Torrelles, J. M. 2001, *AJ*, 121, 1156
- Beltrán, M. T., Girart, J. M., Estalella, R., Ho, P. T. P., & Palau, A. 2002, *ApJ*, 573, 246
- Beltrán, M. T., Gueth, F., Guilloteau, S., & Dutrey, A. 2004, *A&A*, 416, 631
- Benedettini, M., Viti, S., Codella, C., Bachiller, R., Gueth, F., Beltrán, M. T., Dutrey, A., & Guilloteau, S. 2007, *MNRAS*, 381, 1127
- Benson, P. J., Caselli, P., & Myers, P. C. 1998, *ApJ*, 506, 743
- Benson, P. J. & Myers, P. C. 1989, *ApJS*, 71, 89
- Berkhuijsen, E. M. 1973, *A&A*, 24, 143
- Berné, O., Joblin, C., Rapacioli, M., Thomas, J., Cuillandre, J.-C., & Deville, Y. 2008, *A&A*, 479, L41
- Bernes, C. 1977, *A&AS*, 29, 65
- Blaauw, A. 1964, *ARA&A*, 2, 213
- Blaauw, A., Hiltner, W. A., & Johnson, H. L. 1959, *ApJ*, 130, 69
- Blair, G. N., Evans, N. J., II, Vanden Bout, P. A., & Peters, W. L., III 1978, *ApJ*, 219, 896
- Blanco, V. M. & Williams, A. D. 1959, *ApJ*, 130, 482
- Blitz, L., Fich, M., & Stark, A. A. 1982, *ApJS*, 49, 183
- Blitz, L. & Lada, C. J. 1979, *ApJ*, 227, 152
- Brogan, C. L., Chandler, C. J., Hunter, T. R., Shirley, Y. L., & Sarma, A. P. 2007, *ApJ*, 660, L133
- Bronfman, L., Nyman, L.-A., & May, J. 1996, *A&AS*, 115, 81
- Brugel, E. W. & Fesen, R. A. 1990, *BAAS*, 22, 1258
- Brunt, C. M., Kerton, C. R., & Pomerleau, C., 2003, *ApJS*, 144, 47
- Cabrit, S., Lagage, P.-O., McCaughrean, M., & Olofsson, G. 1997, *A&A*, 321, 523
- Cederblad, S. 1946, *Lund Medd. Astron. Obs. Ser. II*, 119, 1
- Cesaroni, R., Palagi, F., Felli, M., Catarzi, M., Comoretto, G., di Franco S., Giovanardi, C., & Palla, F. 1988, *A&AS*, 76, 445
- Cesarsky, C. J., Cesarsky, D. A., Churchwell, E., & Lequeux, J. 1978, *A&A*, 68, 33
- Cesarsky, D., Lequeux, J., Ryter, C., & Gérin, M. 2000, *A&A*, 354, 87
- Chakraborty, A., Ge, J., & Mahadevan, S. 2004, *ApJ*, 606, L69
- Chini, R., Ward-Thompson, D., Kirk, J. M., et al. 2001, *A&A*, 369, 155
- Ciardi, D. R., Woodward, C. E., Clemens, D. P., Harker, D. E., & Rudy, R. J. 1998, *AJ*, 116, 349
- Ciardi, D. R., Woodward, C. E., Clemens, D. P., Harker, D. E., & Rudy, R. J. 2000, *AJ*, 120, 393
- Clayton, G. C. & Fitzpatrick, E. L. 1987, *AJ*, 92, 157
- Clemens, D. P. & Barvainis, R., 1988, *ApJS*, 68, 257
- Clemens, D. P., Yun, J. L., & Heyer, M. H. 1991, *ApJS*, 75, 877
- Codella, C., Bachiller, R., Nisini, B., Saraceno, P., & Testi, L. 2001, *A&A*, 376, 271
- Cohen, M. 1980, *AJ*, 85, 29
- Cohen, R. J. & Brebner, G. C. 1985, *MNRAS*, 216, 51
- Cohen, M. & Fuller, G. A. 1985, *ApJ*, 296, 620
- Cohen, M. & Kuhl, L. V. 1976, *ApJ*, 210, 365
- Cohen, M. & Kuhl, L. V. 1979, *ApJS*, 41, 743
- Cohen, M. & Schwartz, R. D. 1983, *ApJ*, 265, 877
- Cohen, M., Kuhl, L. V., & Harlan, E. A. 1977, *ApJ*, 215, L127
- Cohen, M., Kuhl, L. V., Spinrad, H., & Harlan, E. A. 1981, *ApJ*, 245, 920
- Cohen, R. J., Rowland, P. R., & Blair, M. M. 1984, *MNRAS*, 210, 425
- Comito, C., Schilke, P., Endesfelder, U., Jiménez-Serra, I., & Martín-Pintado, J. 2007, *A&A*, 469, 207
- Connelley, M. S., Reipurth, B., & Tokunaga, A. T. 2007, *AJ*, 133, 1528
- Contreras, M. E., Sicilia-Aguilar, A., Muzerolle, J., Calvet, N., Berlind, P., & Hartmann, L. 2002, *AJ*, 124, 1585
- Corcoran, D., Ray, T. P., & Mundt, R. 1993, *A&A*, 279, 206

- Corcoran, D. & Ray, T. P. 1997, A&A, 321, 189
- Crampton, D. & Fisher, W. A. 1974, Publ. Dom. Astrophys. Obs., 14, 283
- Crawford, D. L. & Barnes, J. V. 1970, AJ, 75, 952
- Curiel, S., Ho, P. T. P., Patel, N. A., Torrelles, J. M., Rodríguez, L. F., et al. 2006, ApJ, 638, 878
- Curiel, S., Trinidad, M. A., Cantó, J., Rodríguez, L. F., Torrelles, J. M., et al. 2002, ApJ, 564, L35
- Daflon, S., Cunha, K., & Becker, S. R. 1999, ApJ, 522, 950
- Davis, C. J. & Eislöffel, J. 1995, A&A, 330, 851
- de Gregorio-Monsalvo, I., Gómez, J. F., Suárez, O., Kuiper, T. B. H., Rodríguez, L. F., & Jiménez-Bailón, E. 2006, ApJ, 642, 319
- Devine, D., Reipurth, B., & Bally, J. 1997, *Low Mass Star Formation – from Infall to Outflow*, poster proceedings of IAU Symp. No. 182, eds. F. Malbet & A. Castets, p. 91
- de Vries, C. H., Narayanan, G., & Snell, R. L. 2002, ApJ, 577, 798
- de Zeeuw, P. T., Hoogerwerf, R., de Bruijne, J. H. J., Brown, A., & Blaauw, A. 1999, AJ, 114, 354
- Dinerstein, H. L., Lester, D. F., & Rank, D. M. 1979, ApJ, 227, L39
- Dobashi, K. & Uehara, H. 2001, PASJ, 53, 799
- Dobashi, K., Bernard, J. P., Yonekura, Y., & Fukui, Y. 1994, ApJS, 95, 419
- Dobashi, K., Uehara, H., Kandori, R., Sakurai, T., Kaiden, M., Umemoto, F., & Sato, F. 2005, PASJ, 57, S1
- Dorschner, J., & Gürtler, J. 1964, Astron. Nachr., 287, 257
- Draper, P. W., Warren-Smith, R. F., & Scarrott, S. M. 1984, MNRAS, 212, 5P
- Duvert, G., Cernicharo, J., Bachiller, R., & Gómez-González J. 1990, A&A, 233, 190
- Edwards, S., & Snell, R. L. 1983, ApJ, 270, 605
- Ehlerova, S. & Palous, J. 2005, A&A, 437, 101
- Eiroa, C., Gómez de Castro, A. I., & Miranda, L. F. 1992, A&AS, 92, 721
- Eiroa C., Lenzen R., Miranda L. F., Torrelles J. M., Anglada G., & Estalella, R. 1993, AJ, 106, 613
- Eiroa, C., Palacios, J., & Casali, M. M. 1998, A&A, 335, 243
- Eiroa, C., Torrelles, J. M., Miranda, L. F., Anglada, G., & Estalella R. 1994, A&AS, 108, 73
- Eislöffel, J. 2000, A&A, 345, 236
- Eislöffel, J., Smith, M. D., Davis, C. J., & Ray, T. P. 1996, AJ, 112, 2086
- Elmegreen, D. M. & Elmegreen, B. G. 1978, ApJ, 220, 510
- Elmegreen, B. G. & Lada, C. J. 1977, ApJ, 214, 725
- Eredics, M. & Kun, M. 2003, Comm. Konkoly Obs., 13, 27
- ESA 1997, The Hipparcos and Tycho Catalogues, ESA SP-1200
- Evans, N. J., II, Allen, L. E., Blake, G. A., Boogert, A. C. A., et al. 2003, PASP, 115, 965
- Evans, N. J. II, Kutner, M. L., & Mundy, L. G. 1987, ApJ, 323, 145
- Evans, N. J. II, Mundy, L. G., Kutner, M. L., & Depoy, D. L. 1989, ApJ, 346, 212
- Evans, N. J., II, Slovak, M. H., Becklin, E. E., Beichman, C., Gatley, I., Werner, M. W., Hildebrand, R. H., Keene, J. & Whitcomb S. E. 1981, ApJ, 244, 115
- Felli, M., Palagi, F., & Tofani, G. 1992, A&A, 255, 293
- Felli, M., Tofani, G., Harten, R. H., & Panagia, N. 1978, A&A, 69, 199
- Few, R. W. & Cohen, R. J. 1983, MNRAS, 203, 853
- Font, A. S., Mitchell, G. F., & Sandell, G. 2001, ApJ, 555, 950
- Froebrich, D., Smith, M. D., & Eislöffel, J. 2002, A&A, 385, 239
- Froebrich, D., & Scholz, A. 2003, A&A, 407, 207
- Froebrich, D., Scholz, A., Eislöffel, J., & Murphy, G. C. 2005, A&A, 432, 575
- Froebrich, D., Smith, M. D., Hodapp, K.-W., & Eislöffel, J. 2003, MNRAS, 346, 163
- Fuente, A. 2008, Ap&SS, 313, 135
- Fuente, A., Ceccarelli, C., Neri, R., Alonso-Albi, T., Caselli, P., Johnstone, D., van Dishoeck, E. F., & Wyrowski, F. 2007, A&A, 468, L37
- Fuente, A., Martín-Pintado, J., Rodríguez-Franco, A., & Moriarty-Schieven, G. D. 1998a, A&A, 339, 575
- Fuente, A., Martín-Pintado, J., Bachiller, R., Neri, R., & Palla, F. 1998b, A&A, 334, 253

- Fuente, A., Martín-Pintado, J., Rodríguez-Fernández, N. J., Cernicharo, J., & Gérin, M. 2000, *A&A*, 354, 1053
- Fuente, A., Neri, R., Martín-Pintado, J., Bachiller, R., Rodríguez-Franco, A., & Palla, F. 2001, *A&A*, 366, 873
- Fuente, A., Neri, R., & Caselli, P. 2005a, *A&A*, 444, 481
- Fuente, A., Rizzo, J. R., Caselli, P., Bachiller, R. & Henkel, C. 2005b, *A&A*, 433, 535
- Fukui, Y. 1989, *Low Mass Star Formation and Pre-Main Sequence Objects*, ed. B. Reipurth (Garching: ESO), p. 95
- Fuller, G. A. & Myers, P. C. 1992, *ApJ*, 384, 523
- Furusho, T., Yamasaki, N. Y., Ohashi, T., Saito, Y., & Voges, W. 2000, *PASJ*, 52, 677
- Furuya, R. S., Kitamura, Y., Wootten, A., Claussen, M. J., & Kawabe, R. 2003, *ApJS*, 144, 71
- Furuya, R. S., Kitamura, Y., & Shinnaga, H. 2006, *ApJ*, 653, 1369
- Furuya, R. S., Kitamura, Y., & Shinnaga, H. 2008, *PASJ*, 60, 421
- Gahm, G. F., Carlqvist, P., Johansson, L. E. B., & Nikolić, S. 2006, *A&A*, 454, 201
- Garay, G., Ramirez, S., Rodríguez, L. F., Curiel, S., & Torrelles, J. M. 1996, *ApJ*, 459, 193
- Garmany, C. D. 1973, *AJ*, 78, 185
- Garmany, C. D. & Stencel, R. E. 1992, *A&AS*, 94, 211
- Garrison, R. 1970, *AJ*, 75, 1001
- Garrison, R. F. & Kormendy, J. 1976, *PASP*, 88, 865
- Getman, K. V., Feigelson, E. D., Townsley, L., Broos, P., Garmire, G., & Tsujimoto, M. 2006, *ApJS*, 163, 306
- Getman, K. V., Feigelson, E. D., Garmire, G., Broos, P., & Wang, J. 2007, *ApJ*, 654, 316
- Giveon, U., Sternberg, A., Lutz, D., Feuchtgruber, H., & Pauldrach, A. W. A. 2002, *ApJ*, 566, 880
- Goetz, J. A., Pipher, J. L., Forrest, W. J., Watson, D. M., Raines, S. N., et al. 1998, *ApJ*, 504, 359
- Goicoechea, J. R., Berné, O., Gérin, M., Joblin, C., & Teyssier, D., 2008, *ApJ*, 680, 466
- Golynkin, A. A., & Konovalenko, A. A. 1991, *Sov. Astr. Lett.*, 17, 7
- Gómez, J. F., Sargent, A. I., Torrelles, J. M., Ho, P. T. P., Rodríguez, L. F., Cantó, J., & Garay, G. 1999, *ApJ*, 514, 287
- Gómez, M., Kenyon, S. J., & Whitney, B. A. 1997, *AJ*, 114, 265
- Gómez de Castro, A. I., Miranda, L. F., & Eiroa, C. 1993, *A&A*, 267, 559
- Gómez de Castro, A. I., & Robles, A. 1999, *A&A*, 344, 632
- Goodman, A. A. & Arce, H. G. 2004, *ApJ*, 608, 831
- Goodman, A. A., Benson, P. J., Fuller, G. A., & Myers, P. C. 1993, *ApJ*, 406, 528
- Greene, T. P. & Lada, C. J. 1996, *AJ*, 112, 2184
- Grenier, I. A., Lebrun, F., Arnaud, M., Dame, T. M., & Thaddeus, P. 1989, *ApJ*, 347, 231
- Gueth, F., Bachiller, R., & Tafalla, M. 2003, *A&A*, 401, L5
- Gueth, F., Guilloteau, S., & Bachiller, R. 1996, *A&A*, 307, 891
- Gueth, F., Guilloteau, S., & Bachiller, R. 1998, *A&A*, 333, 287
- Gueth, F., Guilloteau, S., Dutrey, A., & Bachiller, R. 1997, *A&A*, 323, 943
- Güsten, R. & Marcaide, J. M. 1986, *A&A*, 164, 342
- Gutermuth, R. A., Megeath, S. T., Muzerolle, J., Allen, L. A., Pipher, J. L., Myers, P. C., & Fazio, G. G. 2004, *ApJS*, 154, 374
- Gyulbudaghian, A. L. 1982, *Sov. Astr. Lett.*, 8, 123
- Gyulbudaghian, A. L. 1985, *Astrophysics*, 23, 538
- Gyulbudagyan, A. L., & Akopyan V. A. 1990, *Astrophysics*, 33, 528
- Gyulbudaghian, A. L., Glushkov, Yu. I., & Denisyuk, E. K. 1978, *ApJ*, 224, L137
- Gyulbudaghian, A. L., & Magakian, T. Yu. 1977, *Sov. Astr. Lett.* 3, 58
- Gyulbudaghian, A. L., Rodríguez, L. F., & Cantó, J. 1986, *Astrophysics*, 24, 119
- Gyulbudaghian, A. L., Rodríguez, L. F., & Mendoza-Torres, E. 1987, *RMxAA*, 15, 53
- Gyulbudaghian, A. L., Rodríguez, L. F., & Curiel, S. 1990, *RMxAA*, 20, 51
- Hackwell, J. A., Grasdalen, G. L., & Gehr, R. D. 1982, *ApJ*, 252, 250
- Haikala, L., & Dietrich, D. 1989, in *The Physics and Chemistry of Interstellar Molecular Clouds*, ed. G. Winnewisser & J. T. Armstrong (Berlin: Springer), p.236



- Haikala, L. & Laureijs, R. J. 1989, A&A, 223, 287  
 Hamann, F. & Persson, S. E. 1994, ApJS, 82, 285  
 Harju, J., Walmsley, C. W., & Wouterloot, J. G. A. 1993, A&AS, 98, 51  
 Harjunpää, P., & Mattila, K. 1991, A&A, 249, 493  
 Harker, D., Bregman, J., Tielens, A. G. G. M., Temi, P., & Rank, D. 1997, A&A, 324, 629  
 Harten, R. H., Thum, C., & Felli, M. 1981, A&A, 94, 231  
 Hartigan, P. & Lada, C.J. 1985, ApJS, 59, 383  
 Hartigan, P., Lada, C. J., Tapia, S., & Stocke, J. 1986, AJ, 92, 1155  
 Hartigan, P. Morse, J., & Bally, J. 2000, AJ, 120, 1436  
 Harvey, P. M., Wilking, B. A., & Joy, M. 1984, ApJ, 278, 156  
 Harvin, J. A. 2004, PASP, 116, 186  
 Hasegawa, T. I., Mitchell, G. F., & Henriksen, R. N. 1991, AJ, 102, 666  
 Hatchell, J., Fuller, G. A., & Ladd, E. F. 1999, A&A, 346, 278  
 Hayashi, M., & Murata, Y. 1992, PASJ, 44, 391  
 Hayashi, S. S., Hasegawa, T., & Kaifu, N. 1988, ApJ, 332, 354  
 Hayashi, M., Hasegawa, T., Omodaka, T., Hayashi, S. S., & Miyawaki, R. 1987 ApJ, 312, 327  
 Hayashi, M., Suzuki, S., Omodaka, T., & Hasegawa, T. 1985, ApJ, 288, 170  
 Heiles, C. 1967, ApJS, 15, 97  
 Herbig, G. H. 1960, ApJS, 4, 337  
 Herbig, G. H. 2008, AJ, 135, 637  
 Herbig, G.H. & Rao, N.K. 1972, ApJ, 174, 401  
 Herbig, G. H. & Bell, K. R. 1988, Lick Obs. Bull. No. 1111 (Santa Cruz: Lick Obs.)  
 Hernández, J., Calvet, N., Hartmann, L., & Berlind, P. 2004, AJ, 127, 1682  
 Heske, A., & Wendker, H. J. 1985, A&A, 149, 199  
 Hessman, F. V., Beckwith, S. V. W., Bender, R., Eisloffel, J., Goetz, W., & Guenther, E. 1995, A&A, 299, 464  
 Hillenbrand, L. A., Strom, S. E., Vrba, F. J., & Keene, J. 1992, ApJ, 397, 613  
 Hirano, N. & Taniguchi, Y. 2001, ApJ, 550, L219  
 Ho, P. T. P., Moran, J. M., & Rodríguez, L. F. 1982, ApJ, 262, 619  
 Hoare, M. G. 2006, ApJ, 649 856  
 Hodapp, K.-W. 1994, ApJS, 94, 615  
 Hogg, H. S. 1959, *Handbuch der Physik*, ed. S. Flugge (Berlin: Springer), 53, 194  
 Hoogerwerf, R., de Bruijne, J. H. J., & de Zeeuw, P. T. 2001, A&A, 365, 49  
 Hu, E. M. 1981, ApJ, 248, 119  
 Hubble, E. 1934, ApJ, 79, 8  
 Hughes, V. A. 1985, ApJ, 298, 830  
 Hughes, V. A. 1988, ApJ, 333, 788  
 Hughes, V. A. 1989, AJ, 97, 1114  
 Hughes, V. A. 1993, AJ, 105, 331  
 Hughes, V. A. 2001, ApJ, 563, 919  
 Hughes, V. A. & Wouterloot, J. G. A. 1982, A&A, 106, 171  
 Hughes, V. A. & Wouterloot, J. G. A. 1984, ApJ, 276, 204  
 Humphreys, R. M. 1978, ApJS, 38, 309  
 Iben, I. Jr. 1965, ApJ, 142, 1447  
 Ikeda, H., Sugitani, K., Watanabe, M., Fukuda, N., Tamura, M., Nakajima, Y., Pickles, A. J., et al. 2008, AJ, 135, 2323  
 Indrani, C. & Sridharan, T. K. 1994, JApA, 15, 157  
 Jessop, N. E. & Ward-Thompson, D. 2000, MNRAS, 311, 63  
 Jiang, Z., Tamura, M., Hoare, M. G., Yao, Y., Ishii, M., Fang, M., & Yang, J. 2008, ApJ, 673, L175  
 Jiménez-Serra, I., Martín-Pintado, J., Rodríguez-Franco, A., Chandler, C., Comito, C., & Schilke, P. 2007, ApJ, 661, L187  
 Jones, T. J. 2003, AJ, 125, 3208  
 Jordi, C., Trullors, E., & Galadí-Enríquez, D. 1996, A&A, 312, 499  
 Joyce, R. R., & Simon, T. 1986, AJ, 91, 113

- Kallas, E. & Reich, W. 1980, A&AS, 42, 227
- Kandori, R., Dobashi, K., Uehara, H., Sato, F., & Yanagisawa, K. 2003, AJ, 126, 1888
- Kauffmann, J., Bertoldi, F., Evans, N. J. II, & the C2D Collaboration 2005, Astron. Nachr., 326, 878
- Kawabe, R., Suzuki, M., Hirano, N., Akabane, K., Barsony, M., Najita, J. R., Kameya, O., & Ishiguro, M. 1992, PASJ, 44, 435
- Keene, J., Blake, G. A., Phillips, T. G., Huggins, P. J., & Beichman, C. A. 1985, ApJ, 299, 967
- Kerber, F., Lercher, G., & Weinberger, R. 1996, A&AS, 119, 423
- Kiss, Cs., Moór, A., & Tóth, L. V. 2004, A&A, 418, 131
- Kiss, Z. T., Tóth, L. V., Krause, O., Kun, M., & Stickel, M. 2006, A&A, 453, 923
- Koppelaar, K., van Duinen, R. J., Aalders, J. W. G., Sargent, A. I., & Nordh, L. 1979, A&A, 75, L1
- Könyves, V., Moór, A., Kiss, Cs., & Ábrahám, P. 2004, Balt. Astr., 13, 470
- Kronberger, M., Teutsch, P., Alessi, B., Steine, M., Ferrero, L., et al. 2006, A&A, 447, 921
- Kuchar, T. A. & Clark, F. O. 1997, ApJ, 488, 224
- Kun, M. 1986, Ap&SS, 125, 13
- Kun, M. 1998, ApJS, 115, 59
- Kun, M. 2007, *Triggered Star Formation in a Turbulent ISM*, Ed. B. G. Elmegreen and J. Palous. Proc. of the IAU Symp. 237, Cambridge Univ. Press, p.119
- Kun, M., Balázs, L.G., & Tóth, I. 1987, Ap&SS, 134, 211
- Kun, M. & Pásztor, L. 1990, Ap&SS, 174, 13
- Kun, M. & Prusti T. 1993, A&A, 272, 235
- Kun, M., Vinkó, J., & Szabados, L. 2000, MNRAS, 319, 777
- Lada, C. J. 1985, ARA&A, 23, 267
- Lada, C. J., Blitz, L., Reid, M. J., & Moran, J. M. 1981, ApJ, 243, 769
- Ladd, E. F. & Hodapp, K. W. 1997, ApJ, 474, 749
- Laureijs, R. J., Acosta-Pulido, J., Ábrahám, P., Kinkel, U., Klaas, U., et al. 1996, A&A, 315, L313
- Lebrun, F. 1986, ApJ, 306, 16
- Lee, C.-F. & Ho, P. T. P. 2005, ApJ, 632, 964
- Lee, C. W. & Myers, P. C. 1999, ApJS, 123, 233
- Lee, C.-F., Mundy, L. G., Stone, J. M., & Ostriker, E. C. 2002, ApJ, 576, 294
- Lee, J. E., Di Francesco, J., Lai, S. P., Bourke, T. L., Evans, N. J., II., et al. 2006, ApJ, 648, 491
- Lee, J.-E., Di Francesco, J., Bourke, T. L., Evans, N. J., II., & Wu, J. 2007, ApJ, 671, 1748
- Lefloch, B., Eisloffel, J., & Lazareff, B. 1996, A&A, 313, L17
- Leisawitz, D., Bash, N. F., & Thaddeus, P. 1989, ApJS, 70, 731
- Lekht, E. E. & Sorochenko, R. L. 2001, Astronomy Reports, 45, 113
- Lekht, E. E., Likhachev, S. F., Sorochenko, R. L., & Strel'nitskii, V. S. 1993, Astronomy Reports, 37, 367
- Lenzen, R. 1988, A&A, 190, 269
- Lenzen, R., Hodapp, K.-W., & Solf, J. 1984, A&A, 137, 202
- Lester, D. F., Harvey, P. M., Joy, M., & Ellis, H. B., Jr. 1986, ApJ, 309, 80
- Levreault, R. M. 1984, ApJ, 277, 634
- Levreault, R. M. 1985, Ph.D. thesis, Univ. Texas, Austin
- Levreault, R. M. 1988, ApJS, 67, 283
- Levreault, R. M. & Opal, C. B. 1987, AJ, 93, 669
- Li, W., Evans, N. J., II, Jaffe, D. T., van Dishoeck, E. F., & Thi, W. F. 2002, ApJ, 568, 242
- Liseau, R. & Sandell, G. 1983, RMxAA, 7, 199
- Little, L. T., Brown, A. T., MacDonald, G. H., Riley, P. W., & Matheson, D. N. 1980, MNRAS, 193, 115
- Lombardi, M., & Alves, J. 2001, A&A, 377, 1023
- Looney, L. W., Tobin, J. J., & Kwon, W. 2007, ApJ, 670, L131
- Loren, R. B., Peters, W. L., & Vanden Bout, P. A. 1975, ApJ, 195, 75
- Lozinskaya, T. A., Sitnik, T. G., & Toropova, M. S. 1987, Soviet Ast., 31, 493
- Lynds, B. T. 1962, ApJS, 7, 1

- MacConnell, D. J. 1968, ApJS, 16, 275
- Magakian, T. Yu. 2003, A&A, 399, 141
- Magakian, T. Yu., & Movsessian, T. A. 2001, Astrophysics, 44, 419
- Magakian, T. Yu., Movsessian, T. A., & Nikogossian, E. H. 2004, Astrophysics, 47, 519
- Magnani, L., Blitz, L., & Mundy, L. 1985, ApJ, 295, 402
- Majaess, D. J., Turner, D. G., Lane, D. J., & Moncrieff, K. E. 2008, JAVSO.tmp., 74
- Makarov, V. V. 2007, ApJS, 169, 105
- Mardones, D., Myers, P. C., Tafalla, M., Wilner, D. J., Bachiller, R., & Garay, G. 1997, ApJ, 489, 719
- Marschall, L. A., Karshner, G. B., & Comins, N. F. 1990, AJ, 99, 1536
- Marschall, L. A. & van Altena, W. F. 1987, AJ, 94, 71
- Martin, A. H. M. 1973, MNRAS, 163, 141
- Martín-Pintado, J., Jiménez-Serra, I., Rodríguez-Franco, A., Martín, S., & Thum, C. 2005, ApJ, 628, L61
- Marvel, K. B. 2005, AJ, 130, 2732
- Matthews, H. E., Purton, C. R., Roger, R. S., Dewdney, P. E., & Mitchell, G. F. 2003, ApJ, 592, 176
- Mattila, K., Holsti, N., Toriseva, M., Anttila, R., & Malkamaki, L. 1985, A&A, 145, 192
- Mattila, K., Toriseva, M., Liljeström, T., Anttila, R., & Malkamaki, L. 1988, A&AS, 73, 209
- McGroarty, F., Ray, T. P., & Bally, J. 2004, A&A, 415, 189
- Meehan, L. S. G., Wilking, B. A., Claussen, M. J., Mundy, L. G., & Wootten, A. 1998, AJ, 115, 1599
- Megeath, S. T., Allen, L. E., Gutermuth, R. A., et al. 2004, ApJS, 154, 367
- Mehring, D. M., Zhou, S., & Dickel, H. R. 1997, ApJ, 475, 57
- Mezger, P. G. 1994, Ap&SS, 212, 197
- Miesch, M. S. & Bally, J. 1994, ApJ, 429, 645
- Mikami, T., Umemoto, T., Yamamoto, S., & Saito, S. 1992, ApJ, 392, L87
- Mikami, T. & Ogura, K. 2001, Ap&SS, 275, 441
- Minchin, N. R., Bonifacio, V. H. R., & Murray, A. G. 1996, A&A, 315, L5
- Minchin, N. R., White, G. J., & Ward-Thompson, D. 1995a, A&A, 301, 894
- Minchin, N. R., Ward-Thompson, D., & White, G. J. 1995b, Ap&SS, 224, 203
- Minchin, N. R., Krause, D., Stutzki, J., & White, G. J. 1995c, in: *The Physics and Chemistry of Interstellar Molecular Clouds*, Ed. G. Winnewisser & G. C. Pelz. Springer, p. 210
- Minchin, N. R., White, G. J., & Padman, R. 1993, A&A, 277, 595
- Minkowski, R. 1947, PASP, 59, 257
- Miranda, L. F., Eiroa, C., & Birkle, K. 1994, A&A, 289, L7
- Miranda, L. F., Eiroa, C., & Gómez de Castro, A. I. 1993, A&A, 271, 564
- Miroshnichenko, A. S., Bergner, Y. K., & Kuratov, K. S. 1997, Astron. Letters, 23, 97
- Miskolczi, B., Tothill, N. F. H., Mitchell, G. F., & Matthews, H. E. 2001, ApJ, 560, 841
- Mitchell, G. F. & Matthews, H. E. 1994, ApJ, 423, L55
- Mookerjee, B., Kramer, C., Röllig, M., & Masur, M. 2006, A&A, 456, 235
- Mora, A., Merín, B., Solano, E., Montesinos, B., de Winter, D., et al. 2001, A&A, 378, 116
- Morbidelli, L., Patriarchi, P., Perinotto, M., Barbaro, G., & di Bartolomeo, A. 1997, A&A, 327, 125
- Moreno-Corral, M. A., Chavarría-K., C., de Lara, E., & Wagner, S. 1993, A&A, 273, 619
- Moreno-Corral, M. A., Chavarría-K., C., & de Lara, E. 1995, RMxAC, 3, 121
- Morgan, L. K., Thompson, M. A., Urquhart, J. S., & White, G. J. 2008, A&A, 477, 557
- Moriarty-Schieven, G. H., Xie, T., & Patel, N. A. 1996, ApJ, 463, L105
- Moro-Martin, A., Noriega-Crespo, A., Molinari, S., Testi, L., Cernicharo, J., & Sargent, A. I. 2001, ApJ, 555, 146
- Morris, P. W., Noriega-Crespo, A., Marleau, F. R., Teplitz, H. I., Uchida, K. I., & Armus, L. 2004, ApJS, 154, 339
- Movsessian, T. A. & Magakian, T. Yu. 2004, Astron. Rep., 48, 988
- Movsessian, T. A., Magakian, T. Yu., Boulesteix, J., & Amram, T. 2004, A&A, 413, 203

- Muzerolle, J., Megeath, S. T., Gutermuth, R. A., Allen, L. E., Pipher, J. L., et al. 2004, ApJS, 154, 379
- Myers P. C. & Benson P. J. 1983, ApJ, 266, 309
- Myers, P. C., Fuller, G. A., Goodman, A. A., & Benson, P. J. 1991, ApJ, 376, 561
- Myers, P. C., Linke, R., & Benson, P. J. 1983, ApJ, 264, 517
- Myers, P. C., Heyer, M., Snell, R. L., & Goldsmith, P. F. 1988, ApJ, 324, 907
- Nakano, M., Tomita, Y., Ohtani, H., Ogura, K., & Sofue, Y. 1989, PASJ, 41, 1073
- Narayanan, G. & Walker, C. K. 1996, ApJ, 466, 844
- Naylor, T. & Fabian, A. C. 1999, MNRAS, 302, 714
- Neckel, T. & Staude, H. J. 1984, A&A, 131, 200
- Neckel, T., Staude, H. J., Sarcander, M., Birkle, K. 1987, A&A, 175, 231
- Neri, R., Fuente, A., Ceccarelli, C., Caselli, P., Johnstone, D., van Dishoeck, E. F., et al. 2007, A&A, 468, L33
- Nikolić, S., Johansson, L. E. B., & Harju, J. 2003, A&A, 409, 941
- Nikolić, S., & Kun, M., 2004, Balt. Astr., 13, 487
- Nisini, B., Massi, F., Vitali, F., Giannini, T., et al. 2001, A&A, 376, 553
- Noriega-Crespo, A. 1997, in IAU Symp. 182, *Herbig-Haro Flows and the Birth of Low Mass Stars*, ed. B. Reipurth & C. Bertout (Dordrecht: Kluwer), 103
- Noriega-Crespo, A., & Garnavich, P. M. 2001, AJ, 122, 3317
- Noriega-Crespo, A., Garnavich, P. M., & Molinari, S. 1998, AJ, 116, 1388
- Noriega-Crespo, A., Moro-Martin, A., Carey, S., Morris, P. W., Padgett, D. L., Latter, W. B., & Muzerolle, J. 2004, ApJS, 154, 402
- Ogura, K., Chauhan, N., Pandey, A.K., Bhatt, B. C., Ojha, D., & Itoh, Y. 2007, PASJ, 59, 199
- Ogura, K. & Sato, F. 1990, PASJ, 42, 583
- Ogura, K., Sugitani, K., & Pickles, A. 2002, AJ, 123, 2597
- Okada, Y., Onaka, T., Shibai, H., & Doi, Y. 2003, A&A, 412, 199
- Olano, C. A., Meschin, P. I., & Niemela, V. S. 2006, MNRAS, 369, 867
- Padgett, D. L., Rebull, L. M., Noriega-Crespo, A., Carey, S. J., Stapelfeldt, K. R., et al. 2004, ApJS, 154, 433
- Pan, K., Federman, S. R., Cunha, K., Smith, V. V., & Welty, D. E. 2004, ApJS, 151, 313
- Pan, K., Federman, S. R., Sheffer, Y., & Andersson, B. G. 2005, ApJ, 633, 986
- Panagia, N., & Thum, C. 1981, A&A, 98, 295
- Pandey, A. K., Sharma, S., Ogura, K., Ojha, D. K., Chen, W. P., Bhatt, B. C., & Ghosh, S. K. 2008, MNRAS, 383, 1241
- Park, Y. & Minh, Y. 1995, Journal of Korean Astron. Soc., 28, 255
- Parker, N. D., Padman, R., & Scott, P. F. 1991, MNRAS, 252, 442
- Parker, N. D., Padman, R., Scott, P. F., & Hills, R. E. 1988, MNRAS, 234, 67P
- Parsamian E. S. & Petrosian V. M. 1979, Byurakan Soobs., 51, 3
- Patel, N. A., Curiel, S., Zhang, Q., Sridharan, T. K., Ho, P. T. P., & Torrelles, J. M. 2007, ApJ, 658, L55
- Patel, N. A., Goldsmith, P. F., Heyer, M. H., Snell, R. L., & Pratap, P. 1998, ApJ, 507, 241
- Patel, N. A., Goldsmith, P. F., Snell, R. L., Hezel, T., & Xie, T. 1995, ApJ, 447, 721
- Persi, P., Ferrari-Toniolo, M., Marenzi, A. R., Busso, M., Corcione, L., Marengo, M., & Tapia, M. 1995, Ap&SS, 224, 535
- Persson, R. 2004, IAUC 8441
- Petrossian, V. M. 1985, Astrofizika, 22, 423
- Plume, R., Jaffe, D. T., & Keene, J. 1994, ApJ, 425, L49
- Poelman, D. R. & Spaans, M. 2005, A&A, 440, 559
- Poelman, D. R. & Spaans, M. 2006, A&A, 453, 615
- Pogodin, M. A., Miroshnichenko, A. S., Tarasov, A. E., Mitskevich, M. P., Chountonov, G. A., et al. 2004, A&A, 417, 715
- Poidevin, F. & Bastien, P. 2006, ApJ, 650, 945
- Porras, A., Christopher, M., Allen, L., Di Francesco, J., Megeath, S. T., & Myers, P. C. 2003, AJ, 126, 1916
- Pottasch, S. 1956, Bull. Astron. Inst. Netherlands, 13, 77

- Pozzo, M., Naylor, T., Jeffries, R. D., & Drew, J. E. 2003, MNRAS, 341, 805
- Pravdo, S. H. & Tsuboi, Y. 2005, ApJ, 626, 272
- Preibisch, T. & Smith, M. D. 2002, A&A, 383, 540
- Preibisch, T., Balega, Y. Y., Schertl, D., Smith, M. D., & Weigelt, G. 2001, A&A, 378, 539
- Racine, R. 1968, AJ, 73, 233
- Ray, T. P., Poetzel, R., Solf, J., & Mundt, R. 1990, ApJ, 357, L45
- Reach, W. T., Rho, J., Young, E., Muzerolle, J., Fajardo-Acosta, S., et al. 2004, ApJS, 154, 385
- Reipurth, B. 1999, *A General Catalogue of Herbig-Haro Objects*, 2. Edition, (<http://casa.colorado.edu/hhcat/>)
- Reipurth, B., Armond, T., Raga, A., & Bally, J. 2003, ApJ, 593, 47
- Reipurth, B. & Aspin, C. 1997, AJ, 114, 2700
- Reipurth, B. & Bally, J. 2001, ARA&A, 39, 403
- Reipurth, B., Aspin, C., Beck, T., Brogan, C., Connelley, M. C., & Herbig, G. H. 2007, AJ, 133, 1000
- Reipurth, B., Bally, J., & Devine, D. 1997, AJ, 114, 2708
- Reipurth, B., Rodríguez, L. F., Anglada, G., & Bally, J. 2004, AJ, 127, 1736
- Reipurth, B., Yu, K. C., Heathcote, S., & Bally, J. 2000, AJ, 120, 1449
- Richardson, K. J., White, G. J., Avery, L. W., Woodsworth, A. W. 1987, A&A, 174, 197
- Ridge, N. A., Wilson, T. L., Megeath, S. T., Allen, L. E., & Myers, P. C. 2003, AJ, 126, 286
- Rodríguez, L. F. & Cantó, J. 1983, RMxAA, 8, 163
- Rodríguez, L. F., Garay, G., Curiel, S., Ramirez, S., Torrelles, J. M., Gómez, Y., & Velazquez, A. 1994, ApJ, 430, L65
- Rodríguez, L. F., Ho, P. T. P., & Moran, J. M. 1980, ApJ, 240, L149
- Rodríguez, L. F., Moran, J. M., Ho, P. T. P., & Gottlieb, E. W. 1980, ApJ, 235, 845
- Rodríguez, L. F. & Reipurth, B. 1996, RMxAA, 32, 27
- Rodríguez, L. F. & Reipurth, B. 1998, RMxAA, 34, 13
- Rodríguez, M. I., Wiklind, T., Allen, R. J., Escalante, V., & Loinard, L. 2007, ApJ, 663, 824
- Rogers, C., Heyer, M. H., & Dewdney, P. E. 1995, ApJ, 442, 694
- Rosino, L. & Romano, G. 1962, Asiago Contrib. 127
- Rossano, G. S., Grayzeck, E. J., & Angerhofer, P. E. 1983, AJ, 88, 1835
- Rosvick, J. M. & Davidge, T. J. 1995, PASP, 107, 49
- Roth, M. 1988, MNRAS, 233, 773
- Rouan, D., Lena, P. J., Puget, J. L., de Boer, K. S., & Wijnbergen, J. J. 1977, ApJ, 213, L35
- Rowland, P. R. & Cohen, R. J. 1986, MNRAS, 220, 233
- Sandell, G. & Olofsson, H. 1981, A&A, 99, 80
- Saraceno, P., Ceccarelli, C., Clegg, P., Correia, C., di Giorgio, A., et al. 1996, A&A, 315, L293
- Sargent, A. I. 1977, ApJ, 218, 736
- Sargent, A. I. 1979, AJ, 88, 1236
- Sargent, A. I., van Duinen, R. J., Nordh, H. L., Fridlund, C. V. M., Aalders, J. W. G., & Beintema, D. 1983, AJ, 88, 1236
- Sato, F. & Fukui, Y. 1989, ApJ, 343, 773
- Sato, F., Mizuno, A., Nagahama, T., Onishi, T., Yonekura, Y., & Fukui, Y. 1994, ApJ, 435, 279
- Scarrott, S. M., Rolph, C. D., & Tadhunter, C. N. 1991a, MNRAS, 249, 131
- Scarrott, S. M., Rolph, C. D., & Tadhunter, C. N. 1991b, MNRAS, 250, 111
- Schertl, D., Balega, Y., Hannemann, T., Hofmann, K.-H., Preibisch, T., & Weigelt, G. 2000, A&A, 361, L29
- Schneider, N., Madden, S., Stutzki, J., Block, D., & Winnewisser, G. 1995, in *The Physics and Chemistry of Interstellar Molecular Clouds*, ed. G. Winnewisser & J. T. Armstrong (Berlin: Springer), p. 128
- Schulz, N. S., Berghöfer, T. W., & Zinnecker, H. 1997, A&A, 325, 1001
- Schultz, A. S. B., Rank, D., Temi, P. & Harker, D. 1995, Ap&SS, 233, 71
- Schwartz, P. R. 1989, ApJ, 338, L25
- Schwartz, P. R., Snell, R. L., & Schloerb, F. P. 1989, ApJ, 336, 519
- Schwartz, R. D., Wilking, B. A., & Gyulbudaghian, A. L. 1991, ApJ, 370, 263
- Schneider, S. & Elmegreen, B. G. 1979, ApJS, 41, 87

- Semkov, E. H. 2003, *IBVS*, 5406  
 Semkov, E. H. 2004, *Balt. Astr.* 13, 538  
 Serabyn, E., Güsten, R., & Mundy, L. 1993, *ApJ*, 404, 247  
 Sharma, S., Ogura, K., Pandey, A. K., Ojha, D. K., & Bhatt, B. C. 2007, *Bull. Astron. Soc. India*, 35, 53  
 Sharpless, S., 1959, *ApJS*, 4, 257  
 Shevchenko, V. S., Grankin, K. N., Ibragimov, M. A., Mel'nikov, S. Y., Yakubov, S. D. & Melikyan, N. D. 1991, *IBVS*, 3628  
 Shevchenko, V. S., Ibragimov, M. A., & Yakubov, S. D. 1989, *Soviet Ast.*, 33, 487  
 Shevchenko, V. S., & Yakubov, S. D. 1989, *Soviet Ast.*, 33, 370  
 Shirley, Y. L., Evans, N. J., Rawlings, J. M. C., & Gregersen, E. M. 2000, *ApJS*, 131, 249  
 Sicilia-Aguilar, A., Hartmann, L. W., Briceño, C., Muzerolle, J., & Calvet, N. 2004, *AJ*, 128, 805  
 Sicilia-Aguilar, A., Hartmann, L., Hernández, J., Briceño, C., & Calvet, N. 2005, *AJ*, 130, 188  
 Sicilia-Aguilar, A., Hartmann, L. W., Calvet, N., Megeath, S. T., Muzerolle, J., et al. 2006a, *ApJ*, 638, 897  
 Sicilia-Aguilar, A., Hartmann, L. W., Fűrész, G., Henning, T., Dullemond, C., & Brandner, W. 2006b, *AJ*, 132, 2135  
 Sicilia-Aguilar, A., Hartmann, L. W., Watson, D., Bohac, C., Henning, T., & Bouwman, J. 2007, *ApJ*, 659, 1637  
 Sicilia-Aguilar, A., Merín, B., Hormuth, F., Abraham, P., Henning, T., Kun, M., Patel, N., Juhász, A., Brandner, W., Hartmann, L., Csizmadia, Sz., Moór, A. 2008, *ApJ*, 673, 382  
 Simon, T. 2006, *AJ*, 131, 501  
 Simonson, S. C. 1968, *ApJ*, 154, 923  
 Simonson, S. C. & van Someren Greve, H. W. 1976, *A&A*, 49, 343  
 Slipher, V. M. 1918, *PASP*, 30, 63  
 Slysh, V. I., Dzura, A. M., Val'ts, I. E., & Gerard, E. 1997, *A&AS*, 124, 85  
 Smirnov, G. T., Sorochenko, R. L., & Kitaev, V. V. 1992, *Sov. Astr. Lett.*, 18, 192  
 Smith, M. D., Froebrich, D., & Eislöffel, J. 2003, *ApJ*, 592, 245  
 Snell, R. L., 1981, *ApJS*, 45, 121  
 Sonnentrucker, P., Neufeld, D. A., Gerakines, P. A., Bergin, E. A., Melnick, G. J., Forrest, W. J., Pipher, J. L., & Whittet, D. C. B. 2008, *ApJ*, 672, 361  
 Sridharan, T. K., Beuther, H., Schilke, P., Menten, K. M., & Wyrowski, F. 2002, *ApJ*, 566, 945  
 Staude, H. J., 1986, *Ap&SS*, 128, 179  
 Stecklum, B., Meusinger, H., & Froebrich, D. 2007, *Ap&SS*, 311, 63  
 Stoerzer, H., Stutzki, J., & Sternberg, A. 1995, *A&A*, 296, L9  
 Straizys, V., Cernis, K., Kazlauskas, A., & Meistas, E. 1992, *Balt. Astr.*, 1, 149  
 Strom, S. E., Vrba, F. J., & Strom, K. M. 1976, *AJ*, 81, 638  
 Sugitani, K., Fukui, Y., & Ogura, K. 1991, *ApJS*, 77, 59  
 Sugitani, K., Matsuo, H., Nakano, M., Tamura, M., & Ogura, K. 2000, *AJ*, 119, 323  
 Sugitani, K., Morita, K., Nakano, M., Tamura, M., & Ogura, K. 1997, *ApJ*, 486, L141  
 Tachihara, K., Neuhäuser, R., Kun, M., & Fukui, Y. 2005, *A&A*, 437, 919  
 Tafalla, M. & Bachiller, R. 1995, *ApJ*, 443, L37  
 Tafalla, M. & Myers, P. C. 1997, *ApJ*, 491, 653  
 Tafalla, M., Bachiller, R., & Martín-Pintado, J. 1993, *ApJ*, 403, 175  
 Tafalla, M., Myers, P. C., Mardones, D., & Bachiller, R. 1999, *A&A*, 348, 479  
 Tapia, M., Persi, P., Bohigas, J., & Ferrari-Toniolo, M. 1997, *AJ*, 113, 1769  
 Taylor, D. K., Dickman, R. L., & Scoville, N. Z. 1987, *ApJ*, 315, 104  
 Terebey, S., Vogel, S. N., & Myers, P. C. 1989, *ApJ*, 340, 472  
 Terquem, C., Eislöffel, J., Papaloizou, J. C. B., & Nelson, R. P. 1999, *ApJ*, 512, L131  
 Testi, L., Olmi, L., Hunt, L., Felli, M., & Goldsmith, P. 1995, *A&A*, 303, 881  
 Thronson, H. A., Jr., Lada, C. J., Smith, H. A., Glaccum, W., Harper, D. A., Schwartz, P. R., & Knowles, S. H. 1983, *ApJ*, 271, 625  
 Tofani, G., Felli, M., Taylor, G. B., & Hunter, T. R. 1995, *ApJS*, 112, 299  
 Tokunaga, A. T., Erickson, E. F., Caroff, L. J., & Dana, R. A. 1978, *ApJ*, 224, L19

- Tommasi, E., Lorenzetti, D., Giannini, T., Nisini, B., & Palla, F. 1999, *Ap&SS*, 291, 187
- Torrelles, J. M., Gómez, J. F., Garay, G., Rodríguez, L. F., Curiel, S., Cohen, R. J., & Ho, P. T. P. 1998, *ApJ*, 509, 262
- Torrelles, J. M., Gómez, J. F., Rodríguez, L. F., Curiel, S., Ho, P. T. P., & Garay, G. 1996, *ApJ*, 457, L107
- Torrelles, J. M., Ho, P. T. P., Moran, J. M., Rodríguez, L. F., & Cantó, J. 1987, *ApJ*, 321, 884
- Torrelles, J. M., Ho, P. T. P., Rodríguez, L. F., & Cantó, J. 1985, *ApJ*, 288, 595
- Torrelles, J. M., Patel, N. A., Curiel, S., Ho, P. T. P., Garay, G., & Rodríguez, L. F. 2007, *ApJ*, 666, L37
- Torrelles, J. M., Patel, N. A., Gómez, J. F., Ho, P. T. P., Rodríguez, L. F., Anglada, G., Garay, G., Greenhill, L., Curiel, S., & Cantó, J. 2001, *ApJ*, 560, 853
- Torrelles, J. M., Rodríguez, L. F., Cantó, J., Carral, P., Marcaide, J., Moran, J. M., & Ho, P. T. P. 1983, *ApJ*, 274, 214
- Torrelles, J. M., Verdes-Montenegro, L., Ho, P. T. P., Rodríguez, L. F., & Cantó, J. 1993, *ApJ*, 410, 202
- Tóth, L. V. & Walmsley, C. M. 1996, *A&A*, 311, 981
- Trinidad, M. A., Curiel, S., Torrelles, J. M., Rodríguez, L. F., Cantó, J., Gómez, J. F., Patel, N., & Ho, P. T. P. 2004, *ApJ*, 613, 416
- Trinidad, M. A., Rojas, V., Plascencia, J. C., Ricalde, A., Curiel, S., & Rodríguez, L. F. 2003, *RMxAA*, 39, 311
- Trinidad, M. A., Torrelles, J. M., Rodríguez, L. F., & Curiel, S. 2007, *AJ*, 134, 1870
- Umemoto, T., Hirano, N., Kameya, O., Fukui, Y., Kuno, N., & Takakubo, K. 1991, *ApJ*, 377, 510
- Umemoto, T., Iwata, T., Fukui, Y., Mikami, H., Yamamoto, S., Kameya, O., & Hirano, N. 1992, *ApJ*, 392, 83
- Umemoto, T., Mikami, H., Yamamoto, S., & Hirano, N. 1999, *ApJ*, 525, L105
- Ungerechts, H. & Thaddeus, P. 1989, in *The Physics and Chemistry of Interstellar Molecular Clouds*, ed. G. Winnewisser & J. T. Armstrong (Berlin: Springer), 213
- Ungerechts, H., Winnewisser, G., & Walmsley, C. M. 1986, *A&A*, 157, 207
- Valdettaro, R., Palla, F., Brand, J., & Cesaroni, R. 2005, *A&A*, 443, 535
- Valdettaro, R., Migenes, V., Trinidad, M. A., Brand, J., & Palla, F. 2008, *ApJ*, 675, 1352
- van den Ancker, M., De Winter, D., & Tjin A Dje, H. R. E. 1998, *A&A*, 330, 145
- Velusamy, T., Langer, W. D., & Goldsmith, P. F. 2002, *ApJ*, 565, L43
- Viotti, R., 1969, *Mem. Soc. Astr. It.*, 40, 75
- Visser, A. E., Richer, J. S. & Chandler, C. J. 2002, *AJ*, 124, 2756
- Wang, Y., Evans, N. J., Zhou, S., & Clemens, D. P. 1995, *ApJ*, 454, 217
- Wang, S. & Looney, L. W. 2007, *ApJ*, 659, 1360
- Watt, G. D., Burton, W. B., Choe, S.-U., & Liszt, H. S. 1986, *A&A*, 163, 194
- Weigelt, G., Balega, Y. Y., Preibisch, T., Schertl, D., & Smith, M. D. 2002, *A&A*, 381, 905
- Weikard, H., Wouterloot, J. G. A., Castets, A., Winnewisser, G., & Sugitani, K. 1996, *A&A*, 309, 581
- Weintraub, D. A., Kastner, J. H., & Mahesh, A. 1994, *ApJ*, 420, L87
- Weintraub, D. A., Kastner, J. H., Gatley, I., & Merrill, K. M. 1996, *ApJ*, 468, L45
- Wendker, H. J. & Baars, W. M. 1980, *A&A*, 89, 180
- Werner, M. V., Uchida, K. I., Sellgren, K., Marengo, M., Gordon, K. D., Morris, P. W., Houck, J. R., & Stansberry, J. A. 2004, *ApJS*, 154, 309
- Westerhout, G. 1958, *Bull. Astron. Inst. Netherlands*, 14, 215
- Weston, E. B. 1953, *AJ*, 58, 48
- Wiesemeyer, H., Cox, P., Güsten, R., & Zylka, R. 1999, *The Universe as seen by ISO*, Eds. P. Cox & M. F. Kessler, ESA SP-427, p. 533
- Wiesemeyer, H., Güsten, R., Cox, P., Zylka, R., & Wright, M. C. H. 1998, *Star Formation with the Infrared Space Observatory*, ed. by J. L. Yun and R. Liseau, ASP Conf. Ser. 132, p. 189
- Wiesemeyer, H., Güsten, R., & Wright, M. C. H. 1997, *Low Mass Star Formation - from Infall to Outflow*, Poster proceedings of IAU Symposium No. 182, ed. F. Malbet and A. Castets,

p. 260

- Wilking, B. A., Mundy, L. G., & Schwartz, R. D. 1986, ApJ, 303, L61  
 Wilking, B. A., Schwartz, R. D., Mundy, L. G., & Schultz, A. S. B. 1990, AJ, 99, 344  
 Wilner, D. J. & Welch, W. J. 1994, ApJ, 427, 898  
 Wink, J. E., Altenhoff, W. J., & Mezger, P. G. 1982, A&A, 108, 227  
 Witt, A. N. & Cottrell, M. J. 1980, AJ, 85, 22  
 Witt, A. N., Walker, G. A. H., Bohlin, R. C., & Stecher, T. P. 1982, ApJ, 261, 492  
 Wolf, S., Launhardt, R., & Henning, T. 2003, ApJ, 592, 233  
 Wood, D. O. S. & Churchwell, E. 1989, ApJS, 69, 831  
 Wouterloot, J. G. A. & Brand, J. 1989, A&A, 80, 149  
 Wouterloot, J. G. A., Brand, J., & Fiegle, K. 1993, A&AS, 98, 589  
 Wouterloot, J. G. A., Habing, H. J., & Herman, J. 1980, A&A, 81, 11  
 Wouterloot, J. G. A. & Walmsley, C. M. 1986, A&A, 168, 237  
 Wright, C. M., Drapatz, S., Timmermann, R., van der Werf, P. P., Katterloher, R., & de Graauw, T. 1996, A&A, 315, 301  
 Wu, Y., Zhou, S., & Evans, N. J. II 1992, ApJ, 394, 196  
 Wu, J.-W., Wu, Y.-F., Wang, J.-Z., & Cai K. 2002, ChJAA, 2, 33  
 Wu, Y., Wei, Y., Zhao, M., Shi, Y., Yu, W., Qin, S., & Huang, M. 2004, A&A, 426, 503  
 Wu, J., Dunham, M. M., Evans, N. J. II, Bourke, T. L., & Young, C. H. 2007, AJ, 133, 1560  
 Yang, J. 1990, Ph.D. thesis, Nagoya Univ.  
 Yang, J., Fukui, Y., Umemoto, T., Ogawa, H., & Chen, H. 1990, ApJ, 362, 538  
 Yang, J. & Fukui, Y. 1992, ApJ, 386, 618  
 Yao, Y., Ishii, M., Nagata, T., Ogawa, Y., Sato, S., Watanabe, M., & Yamashita, T. 1998, ApJ, 500, 320  
 Yonekura, Y., Dobashi, K., Hayashi, Y., Sato, F., Ogawa, H., & Fukui, Y. 1998, AJ, 115, 2009  
 Yonekura, Y., Dobashi, K., Mizuno, A., Ogawa, H., & Fukui, Y. 1997, ApJS, 110, 21  
 Young, C. H., Bourke, T. L., Young, K. E., Evans II, N. J., Jorgensen, J. K., Shirley, Y. L., van Dishoeck, E. F., & Hogerheide, M. 2006, AJ, 132, 1998  
 Yu, Z., Nagahama, T., & Fukui, Y. 1996, ApJ, 471, 867  
 Yun, J. L. 1996, AJ, 111, 930  
 Yun, J. L. & Clemens, D. P. 1992, ApJ, 385, L21  
 Yun, J. L. & Clemens, D. P. 1994, ApJS, 92, 145  
 Zeng, Q., Yang, J., Cao, Y. Q., Lou, G. F., & Fukui, Y. 1991, Ap&SS, 180, 151  
 Zhang, Q., Ho, P. T. P., Wright, M. C. H., & Wilner, D. J. 1995, ApJ, 451, L71  
 Zhang, Q., Ho, P. T. P., & Wright, M. C. H. 2000, AJ, 119, 134  
 Zhou, S., Butner, H. M., Evans, N. J., II, Güsten, R., Kutner, M. L., & Mundy, L. G. 1994, ApJ, 428, 219  
 Zhou, S., Evans, N. J., II, Mundy, L. G., & Kutner, M. L. 1993, ApJ, 417, 613  
 Zhou, J. J., Zhang, X. Z., Zhang, H. B., Esimbek, J., Zhang, J. Y., & Ju, B. G. 2006, New Astron., 12, 111